INFORMATION TO USERS

This material was produced from a microfilm copy of the original document. While the most advanced technological means to photograph and reproduce this document have been used, the quality is heavily dependent upon the quality of the original submitted.

The following explanation of techniques is provided to help you understand markings or patterns which may appear on this reproduction.

1. The sign or "target" for pages apparently lacking from the document photographed is "Missing Page(s)". If it was possible to obtain the missing page(s) or section, they are spliced into the film along with adjacent pages. This may have necessitated cutting thru an image and duplicating adjacent pages to insure you complete continuity.

2. When an image on the film is obliterated with a large round black mark, it is an indication that the photographer suspected that the copy may have moved during exposure and thus cause a blurred image. You will find a good image of the page in the adjacent frame.

3. When a map, drawing or chart, etc., was part of the material being photographed the photographer followed a definite method in "sectioning" the material. It is customary to begin photoing at the upper left hand corner of a large sheet and to continue photoing from left to right in equal sections with a small overlap. If necessary, sectioning is continued again — beginning below the first row and continuing on until complete.

4. The majority of users indicate that the textual content is of greatest value, however, a somewhat higher quality reproduction could be made from "photographs" if essential to the understanding of the dissertation. Silver prints of "photographs" may be ordered at additional charge by writing the Order Department, giving the catalog number, title, author and specific pages you wish reproduced.

5. PLEASE NOTE: Some pages may have indistinct print. Filmed as received.

Xerox University Microfilms
300 North Zeeb Road
Ann Arbor, Michigan 48106

Reproduced with permission of the copyright owner. Further reproduction prohibited without permission.

75-16,410

LUKASZEK, Wieslaw A., 1946-
CONDUCTION MECHANISMS IN LOW BREAKDOWN VOLTAGE SILICON P-N JUNCTIONS.

The University of Florida, Ph.D., 1974
Engineering, electrical

Xerox University Microfilms, Ann Arbor, Michigan 48106

Reproduced with permission of the copyright owner. Further reproduction prohibited without permission.

CONDUCTION MECHANISMS IN LOW BREAKDOWN VOLTAGE SILICON P-N JUNCTIONS

By

Wieslaw A. Lukaszek

A DISSERTATION PRESENTED TO THE GRADUATE COUNCIL OF
THE UNIVERSITY OF FLORIDA
IN PARTIAL FULFILLMENT OF THE REQUIREMENTS FOR THE
DEGREE OF DOCTOR OF PHILOSOPHY

UNIVERSITY OF FLORIDA
1974

Reproduced with permission of the copyright owner. Further reproduction prohibited without permission.

ACKNOWLEDGMENTS

I am indebted to Dr. Aldert van der Ziel, my most inspiring teacher, for his generous assistance and encouragement as my advisor. I also thank Dr. Eugene R. Chenette for his encouragement and Dr. Karel M. van Vliet for his friendly advice and many helpful discussions during the final stages of this work. The friendly help of Dr. Charles V. Shaffer and Dr. Samuel B. Trickey is also most warmly appreciated.

The aid of Mr. Don Estreich of Teledyne who supplied the diode samples and data, and of Mr. Sam Weaver of Texas Instruments who supplied the low noise JFET's employed in this study, is gratefully appreciated.

Finally, my deepest thanks go to my parents, Antoni and Stefania, and my brother, John, whose encouragement and countless sacrifices I shall never be able to repay.

Reproduced with permission of the copyright owner. Further reproduction prohibited without permission.

TABLE OF CONTENTS

		Page
ACKNOWLEDGMENTS		ii
ABSTRACT		iv
CHAPTER I	INTRODUCTION	1
CHAPTER II	EXPERIMENTAL METHODS	5
CHAPTER III	DISCUSSION OF EXPERIMENTAL RESULTS	11
CHAPTER IV	DETAILED ANALYSIS OF NOISE DATA	28
CHAPTER V	CALCULATION OF DC MULTIPLICATION	47
CHAPTER VI	CONCLUSIONS	58
CHAPTER VII	RECOMMENDATIONS FOR FURTHER STUDY	62
APPENDIX A	MULTIPLICATION NOISE RESULTING FROM NO MORE THAN ONE IONIZATION PER CARRIER TRANSIT ACROSS DIODE SPACE CHARGE REGION	66
APPENDIX B	MULTIPLICATION NOISE RESULTING FROM NO MORE THAN TWO IONIZATIONS PER CARRIER TRANSIT ACROSS DIODE SPACE CHARGE REGION	73
APPENDIX C	DC MULTIPLICATION SIMULATION PROGRAM	87
BIBLIOGRAPHY		154
BIOGRAPHICAL SKETCH		157

Reproduced with permission of the copyright owner. Further reproduction prohibited without permission.

Abstract of Dissertation Presented to the
Graduate Council of the University of Florida in Partial
Fulfillment of the Requirements for the
Degree of Doctor of Philosophy

CONDUCTION MECHANISMS IN LOW BREAKDOWN VOLTAGE SILICON P-N JUNCTIONS

By

Wieslaw A. Lukaszek

August, 1974

Chairman: Aldert van der Ziel
Co-Chairman: Eugene R. Chenette
Major Department: Electrical Engineering

White noise spectra of diodes 1N746 to 1N752 have been used to investigate the reverse conduction mechanisms in silicon junctions breaking down by a combination of tunneling and impact ionization multiplication. The reverse voltages at the onset of multiplication noise indicate that, regardless of junction field strengths, carrier multiplication sets in only when the carrier energies exceed the threshold energies for ionization. Further examination of noise data yields their values, indicating that the multiplication process is dominated by the effects of the threshold energies for ionization. When they are taken into account, it becomes clear why Tager's

Reproduced with permission of the copyright owner. Further reproduction prohibited without permission.

and McIntyre's theories of noise in avalanche diodes, and the conventional DC multiplication calculations, are not applicable to low breakdown voltage diodes. Consequently, a new method of performing DC multiplication calculations as well as a new theory of noise in low breakdown voltage diodes is developed.

Reproduced with permission of the copyright owner. Further reproduction prohibited without permission.

CHAPTER I

INTRODUCTION

As the reverse bias across a p-n junction is increased, the junction eventually begins to pass appreciable current. Typical voltage-current characteristics for commercially available diodes are shown in Figure 1. It is evident that the reverse current characteristics are considerably different for p-n junctions which "break down" at different voltages.

The type of breakdown typified by Figure 1a is characterized by (i) temperature sensitive pre-breakdown (saturation) current which approximately doubles for each 10°C rise in temperature, (ii) a well-defined breakdown voltage, V_B, and (iii) a unique, positive, breakdown voltage temperature coefficient, B, defined by

$$V_B = V_{BO}[1+B(T-T_O)]$$

where V_{BO} is the breakdown voltage at room temperature, T_O. This type of breakdown, characteristic of relatively wide p-n junctions with V_B>14 volts, is commonly known as "avalanche" breakdown since it can be understood in terms of an impact ionization mechanism resembling an avalanche (Tyagi, 1968).

Reproduced with permission of the copyright owner. Further reproduction prohibited without permission.

Reverse conduction of the type shown in Figure 1c is characterized by (i) temperature insensitive reverse current -- temperature change of 200°C changes the current by a factor of two or three, (ii) lack of well-defined breakdown voltage, and (iii) a negative temperature coefficient whose magnitude depends on temperature and reverse voltage. This type of breakdown, characteristic of narrow p-n junctions capable of passing considerable current densities at reverse voltages smaller than about 2.5 volts, can be understood in terms of internal field emission of valence band electrons, also known as Zener tunneling (Chynoweth et al., 1960; Tyagi, 1968).

P-n junctions which break down between about 2.5 to 14 volts do so as a result of the combined effect of internal field emission and impact ionization multiplication (Tyagi, 1968). Since most of the measurements which formed the basis for the understanding of p-n junction breakdown were DC measurements, this range of breakdown voltages has never been carefully investigated. The reason for it was the severe difficulty encountered in distinguishing the contributions of each of the two mechanisms.

The aim of this study was to investigate the reverse conduction mechanisms in diodes breaking down in this range of voltages. The difficulty which previous workers encountered in distinguishing the tunneling current from the impact ionization multiplied current was overcome

Reproduced with permission of the copyright owner. Further reproduction prohibited without permission.

by using noise as a diagnostic tool, the idea being that noise would more closely reflect the basic microscopic conduction mechanisms. This technique was first employed by Lauritzen (1966) in determining the onset of carrier multiplication in low breakdown voltage silicon diodes. Interest in avalanche diodes as photodetectors, microwave signal sources, and amplifiers has already led to extensive experimental (Haitz, 1965, 1966; Haitz and Voltmer, 1968; Baertsch, 1966, 1967; Kumo et al., 1968) and theoretical (Tager, 1965; McIntyre, 1966; Hines, 1966; Gummel and Blue, 1967) studies of noise in these diodes at low and high frequencies.

Because noise measurements provide the experimental foundation of this study, Chapter II is primarily devoted to the experimental considerations and techniques involved in collecting the noise data. DC and capacitance measurements are discussed there also.

A general discussion of the data is undertaken in Chapter III. It is found that Tager's (1965) and McIntyre's (1966) theories of noise in avalanche diodes are incapable of explaining the data. The reason for this becomes clear when the mechanism of the onset of carrier multiplication is inferred from the noise data. It is then also apparent that the conventional method of calculating DC multiplication is not applicable to low breakdown voltage diodes.

Reproduced with permission of the copyright owner. Further reproduction prohibited without permission.

When a new definition of the DC multiplication factor, and a new functional form of the expression for noise are introduced in Chapter IV, the noise data reveal in detail the influence of the threshold energies for ionization on the multiplication process. On basis of the inferences made in this and the preceding chapter, new theories of noise in low breakdown voltage diodes are developed and compared with experimental results.

The details of the multiplication process inferred in Chapters III and IV are incorporated in Chapter V, which discusses a simulation program implementing a new method of performing DC multiplication calculations in low breakdown voltage junctions. The results of the conventional and the new calculations are then compared with data.

Chapter VI summarizes the highlights.

Chapter VII suggests topics for further study.

Reproduced with permission of the copyright owner. Further reproduction prohibited without permission.

CHAPTER II

EXPERIMENTAL METHODS

The p-n junctions investigated in this study are commercially available diodes, types 1N746 to 1N752, manufactured by alloying small aluminum buttons onto n-type silicon. The raised appearance of the aluminum buttons, shown in a vertical cross-section of the diode in Figure 2, is the result of acid etch used to delineate the junction geometry and eliminate surface effects around the button periphery.

The samples chosen for study were those which exhibited very little flicker noise. In final samples, flicker noise was not noticeable at frequencies greater than 300 Hz. This selection criterion presumably eliminated from consideration those diodes in which surface or edge effects might have had significant influence on the reverse conduction mechanisms of the junctions. All final samples, whose DC V-I characteristics are shown in Figure 3, came from Continental Device Corporation, now Teledyne Semiconductor.

In this study the reverse conduction mechanisms were inferred from two sets of diode terminal measurements: the DC V-I characteristics and noise. The DC characteristics provided information on the average behavior of carriers in the junctions, whereas the noise measurements provided

Reproduced with permission of the copyright owner. Further reproduction prohibited without permission.

statistical information on the transient, or microscopic, details of the conduction process. The noise measurements thus provided the groundwork details for the conduction model, which will be discussed in the following chapter.

The noise measurements, which form the experimental foundation of this study, were performed with the aid of the noise measurement system shown in Figure 4. The GR 1381 Random Noise Generator coupled to the HP 350-D 600 Ω attenuator supplied a 2 Hz to 50 KHz white noise calibration signal. The 600 Ω resistor following the attenuator provided the proper impedance match for the attenuator, while the 1 μf capacitor in series with the 200 KΩ resistor provided DC and impedance isolation from the rest of the circuit. The impedance isolation was necessary to maintain a constant impedance level at the attenuator terminals regardless of the impedance levels existing in the diode bias network, and to convert the noise calibration network into a high impedance, current-like source to prevent excessive loading of the diode. The diode bias network consisted of a large number of wire wound resistors, R_b. When used to adjust the diode reverse current, they were chosen so that R_b was more than ten times greater than the diode dynamic resistance, R_d.

The low noise preamplifier used for its first stage a preselected sample of a Texas Instruments low noise JFET, the SFB 8558. The schematic diagram of the preamplifier is given in Figure 5, and the preamplifier's equivalent noise resistance

Reproduced with permission of the copyright owner. Further reproduction prohibited without permission.

referred to the input, R_n, as a function of frequency, is given in Figure 6. The preamplifier was followed by a selectable gain amplifier which amplified the noise signal to a level suitable for processing by the GR 1925-1926 Real Time Spectrum Analyzer. The oscilloscope was used for visual observation of the noise waveforms.

The GR 1925-1926 Real Time Spectrum Analyzer contains a bank of 45 third-octave filters, ranging in center frequencies from 3.15 Hz to 80 KHz. The output of each filter is sampled for up to 32 seconds and the dB of the RMS voltage of each filter is computed and displayed on the GR 1926, or is printed out by the MDS 800 tape printer.

The measurements were performed as follows. First, the noise calibration signal, provided by the GR 1381 and the 600 Ω attenuator, was removed by disconnecting the attenuator from the circuit and replacing it with a 600 Ω resistor placed in parallel with the 600 Ω attenuator termination resistor. The diode bias resistor, R_b, was then chosen to obtain the desired value of diode reverse current, and five, 32 second, diode noise data sets were recorded. Next, the 600 Ω resistor in parallel with the attenuator termination resistor was removed, and the attenuator returned to the circuit. The attenuation level was then adjusted to obtain a calibration plus diode noise output about 20 dB higher than the diode noise output alone, and a second set of five, 32 second, readings was recorded. Given the system noise equivalent input circuit of Figure 7, it is a trivial matter

Reproduced with permission of the copyright owner. Further reproduction prohibited without permission.

to determine that the diode noise current spectral density, S_{id}, is then given by

$$S_{id} = \frac{S'_{ig}}{[10^{(\frac{\Delta dB}{10})} - 1]} - \frac{S_{va}}{|Z_t|^2} - S_{ir} - S_{ib} \tag{2.1}$$

and

$$S'_{ig} = (\frac{1}{200K\Omega})^2 (10^{\frac{-dB_{att}}{10}}) S_{vg} \tag{2.2}$$

$$S_{va} = 4KTR_n \tag{2.3}$$

$$S_{ir} = 4kT(\frac{1}{200K\Omega} + \frac{1}{200K\Omega}) \tag{2.4}$$

$$S_{ib} = \frac{4kT}{R_b} \tag{2.5}$$

$$|Z_t|^2 = R_b^2 (\frac{1}{1+\omega^2 C_t^2 R_t^2}) \tag{2.6}$$

$$R_t = \frac{1}{(\frac{1}{200K\Omega} + \frac{1}{200K\Omega} + \frac{1}{R_d} + \frac{1}{R_b})} \tag{2.7}$$

where S_{vg} is the spectral density of the noise generator output voltage, R_n is the equivalent noise resistance of the low noise preamplifier, R_d is the diode dynamic resistance, R_b is the bias resistance, C_t is the total input capacitance, dB_{att} is the attenuator setting, and ΔdB is the difference in dB between the calibration plus diode noise level, and the diode noise level alone. This calculation was carried out for each filter, and the final results were averaged over all filters processing a white noise spectrum. Typically,

Reproduced with permission of the copyright owner. Further reproduction prohibited without permission.

this resulted in averaging over the 25 filters of center frequencies greater than 250 Hz.

The system accuracy was verified by measuring the thermal noise of resistors. When resistors of 200 Ω to 2 MΩ were inserted in place of a diode, and the above measurement procedure was repeated, the resistance values predicted from noise measurements agreed to better than 2% with values obtained from precision bridge measurements.

Since the low noise preamplifier employed a JFET for the first stage, it sensed the voltage, rather than the current, at its input terminals. Consequently, the diode noise current was converted to a noise voltage by the diode dynamic impedance before the noise signal was amplified. The diode dynamic impedance, therefore, had to be determined, and was measured using the diode bias network, capacitively coupled to a Wayne Kerr B601 Radio Frequency Bridge utilizing a Wayne Kerr SR 268 Source & Detector, as shown in Figure 8. The 100 KHz signal applied by the bridge to the diode was adjusted until further signal level reduction produced no difference in the measured RC values. This typically occurred for applied signal levels of less than 40 mV RMS. The parallel equivalent RC values of the diode and its bias network were thus determined to an accuracy of ±1%.

The capacitance values determined above were also employed in the C-V plots used in estimating the junction doping profiles and doping densities. The diode areas were obtained from junction photographs taken after the aluminum

Reproduced with permission of the copyright owner. Further reproduction prohibited without permission.

button was etched away in phosphoric acid. The error in determining the junction area in this manner was estimated to be about 15%.

A typical junction surface is shown in Figure 9. Although the surface is full of ridges, it is assumed that the junctions are very nearly planar because they are extremely thin. On the scale of the several hundred angstrom thin space charge regions (SCR), the ridge contours should appear as gentle undulations in the junction topology.

The DC V-I measurements were made using the test setup shown in Figure 10. It consisted of the diode bias network, a Keithley Model 615 Digital Electrometer operating as an ammeter, and a Fluke Model 801B Differential Voltmeter. The accuracy of the DC measurements was ±0.5% for currents greater than 10^{-7} amperes, and ±2% for currents between 10^{-7} and 10^{-9} amperes. Voltage measurements were accurate to ±0.05%.

All measurements were taken at room temperature, 22±2°C.

Reproduced with permission of the copyright owner. Further reproduction prohibited without permission.

CHAPTER III

DISCUSSION OF EXPERIMENTAL RESULTS

In order to make the forthcoming discussions of noise and DC V-I measurements meaningful, it is necessary to know the junction properties and parameters. Some of them can be inferred from the $\frac{1}{C^2}$ vs. V_r plots for the four most important diodes, the 1N749 to 1N752, shown in Figures 11 to 14.

Since the $\frac{1}{C^2}$ vs. V_r plots do not yield straight lines over the entire range of reverse voltages, it appears that the junctions are not abrupt. Unfortunately, $\frac{1}{C^3}$ vs. V_r plots do not yield straight lines, either. Consequently, it seems that the junction profiles are composite of linearly graded and abrupt. If it is assumed, however, that to a first order approximation the diodes can be treated as step junctions (provided that the doping densities are evaluated from $\frac{1}{C^2}$ vs. V_r slopes obtained for large reverse biases, where the doping densities are most likely to be representative of the bulk doping densities) the results of Table I are obtained.

The calculated doping densities on the n-side of the junctions are seen to lie within the range of doping densities predicted from the starting resistivities of

Reproduced with permission of the copyright owner. Further reproduction prohibited without permission.

Reproduced with permission of the copyright owner. Further reproduction prohibited without permission.

TABLE I

DIODE PARAMETERS

DIODE TYPE	DOPING DENSITY ON P-SIDE (a)	RESISTIVITY OF N-TYPE WAFER (b)	DOPING DENSITY ON N-SIDE	CALCULATED DOPING DENSITY ON N-SIDE (c)	BUILT-IN POTENTIAL (d)	BUILT-IN POTENTIAL (e)	PEAK ELECTRIC FIELD (f)	JUNCTION WIDTH (g)	JUNCTION WIDTH (h)
1N749	9	0.012 - 0.014	2.8 - 3.6	2.85	1.0	1.02	1.35	483	448
1N750	9	0.014 - 0.016	2.2 - 2.8	2.12	1.0	1.01	1.26	558	490
1N751	9	0.016 - 0.018	1.75 - 2.2	2.02	1.04	1.01	1.24	556	500
1N752	9	0.018 - 0.021	1.3 - 1.75	1.75	1.0	1.01	1.17	580	526
	$x10^{18} cm^{-3}$	ohm-cm	$x10^{18} cm^{-3}$	$x10^{18} cm^{-3}$	volts		$x10^{6}$ volt/cm	Å	

(a) Logan (1969)

(b) Don Estreich, Teledyne Semiconductor, personal communication

(c) from $\frac{1}{C^2}$ vs. V_r plots and depletion approximation

(d) from $\frac{1}{C^2}$ vs. V_r intercept

(e) calculated from doping densities

(f) calculated for step junction @ $V_r = 2.0$ volts

(g) calculated from capacitance data @ $V_r = 2.0$ volts

(h) calculated for step junction @ $V_r = 2.0$ volts

the n-type wafers. This seems to indicate that for reverse voltages greater than about 1.5 to 2 volts, the doping densities at the junction edges attain the bulk doping densities, and the junctions should begin to assume step junction characteristics. The changes in the $\frac{1}{C^2}$ vs. V_r slopes for smaller reverse biases are caused by the extreme thinness of the diode SCR's: as the reverse biases decrease, the SCR's narrow and enter the diode metallurgical transition regions where the doping densities are no longer constant.

However, demonstrating that the doping densities at junction edges reach bulk doping densities does not conclusively prove that for V_r greater than 1.5 to 2 volts the junctions may be approximated by step junctions. Another piece of evidence which strengthens this contention, though, will be obtained when the DC V-I characteristics are examined. This discussion will be most meaningful after the noise measurements are examined.

The typical noise data obtained for diodes 1N746 to 1N752 are shown in Figures 15 to 21. The diode noise current spectral density, S_{id}, has been normalized with respect to the noise current spectral density of a saturated thermionic diode conducting a DC current equal to the p-n junction reverse current. The noise ratio, NR, is, therefore, given by

Reproduced with permission of the copyright owner. Further reproduction prohibited without permission.

$$NR = \frac{S_{id}}{2qI_r} \tag{3.1}$$

where I_r is the p-n junction reverse current.

Since the noise current of a saturated thermionic diode arises from the reception at the anode of all individually, and randomly emitted, thermally excited cathode electrons, a noise ratio of unity indicates that the p-n diode reverse current is also due to collection of randomly and singly generated carriers, or carrier pairs. This is precisely what happens when the p-n junction reverse current arises from internal field emission in which thermally excited valence band electrons tunnel to the conduction band. The noise measurements thus furnish a foolproof method of determining the range of reverse voltages for which the diode reverse conduction arises from a single step tunneling process. (A few samples exhibiting multi-step tunneling were also observed. They are characterized by a noise ratio less than unity (van der Ziel, personal communication), as shown in Figures 21a and 21b. These samples, however, exhibited substantially greater $\frac{1}{f}$ noise than the remaining samples and, therefore, were excluded from further study.)

An independent method of verifying that over the range of reverse voltages for which the noise ratio is unity the reverse current arises from single step tunneling is obtained from the laws of internal field emission.

Reproduced with permission of the copyright owner. Further reproduction prohibited without permission.

Chynoweth et al. (1960) and Tyagi (1968) found that for a phonon-assisted tunneling process the diode reverse current is given by

$$I_r = AV_r^{\eta}E^n e^{-\left(\frac{\gamma E_g^{3/2}}{E}\right)} \quad ; \quad \gamma = \frac{4\sqrt{2m_e^*}}{3q\hbar} \tag{3.2}$$

where I_r is the diode reverse current, V_r is the diode reverse voltage, A is a constant for a given temperature, E is the electric field, E_g is the band gap energy, m_e^* is the effective mass of tunneling electrons, q is the electronic charge, $\hbar = \frac{h}{2\pi}$, where h is the Planck constant, and η and n are constants. The factor $e^{-\left(\frac{\gamma E_g^{3/2}}{E}\right)}$ represents the phonon-assisted tunneling probability, E^n accounts for image fields or Coulombic forces corrections included in the theory, and V_r^{η} takes into account, in an empirical way, the effect of electron tunneling from the conduction band back to the valence band so that for zero reverse bias the net current, I_r, is also zero. For abrupt junctions Tyagi claims $\eta \simeq 1$, $n \simeq 1.5$.

Compared to $e^{-\left(\frac{\gamma E_g^{3/2}}{E}\right)}$, $AV_r^{\eta}E^n$ is a slow varying function of the reverse voltage so that the reverse current may be written as

$$I_r = I_0 e^{-\frac{s'}{E}} \tag{3.3}$$

Reproduced with permission of the copyright owner. Further reproduction prohibited without permission.

where I_o and s' are considered constant provided $V_r \neq 0$, and $\bar{E}$ is an "effective" electric field such that

$$e^{-\frac{s'}{\bar{E}}} = \int_o^w e^{-\frac{s'}{E(x)}} dx \qquad (3.4)$$

where the integration extends over the entire width of the diode space charge region, w. For an abrupt junction the main contribution to the integral comes from electric field values close to the maximum electric field value, E_m. Thus, little error is made in assuming that the "effective" electric field is given by E_m. Consequently, for an abrupt junction

$$I_r = I_0 e^{\frac{-s}{\sqrt{V_r+\phi}}} \qquad (3.5)$$

where s is a constant and ϕ is the built-in potential of the junction. Thus, if a junction is indeed abrupt and the reverse current is due to tunneling, log I_r vs. $\frac{1}{\sqrt{V_r+\phi}}$ should give a straight line.

Inspection of Figures 22 to 28, which show log I_r vs. $\frac{1}{\sqrt{V_r+\phi}}$ for diodes 1N746 to 1N752, reveals that over the range of reverse voltages for which the noise ratio is unity, log I_r vs. $\frac{1}{\sqrt{V_r+\phi}}$ is, indeed, a straight line. The DC V-I data and the noise data are, therefore, consistent, and the contention that the junctions may, to a first order approximation, be considered abrupt is further strengthened.

Reproduced with permission of the copyright owner. Further reproduction prohibited without permission.

If the randomly emitted tunneling electrons undergo multiplication due to impact ionization, the randomness of the multiplication process generates additional noise, and the noise ratio becomes greater than unity. Comparison of Figures 15 to 21 with Figures 22 to 28 reveals that over the range of voltages for which the noise ratio increases from unity, log I_r increasingly departs from the straight line it followed at lower reverse voltages. This suggests that the failure of the reverse current to obey the tunneling relation is due to impact ionization multiplication of the tunneling current.

If this contention is indeed correct, then it should be possible to verify it quantitatively with the help of noise theories of Tager (1965) or McIntyre (1966) relating the spectral density of noise current generated in impact ionization multiplication to the terminal DC current flowing through the diode. According to Tager, the low frequency spectral density of noise current produced in an impact ionization multiplication process in which the electrons and holes have the same ionization coefficients, is given by

$$S_i = 2qI_t(M')^3 \tag{3.6}$$

where I_t is the current initiating the multiplication process, which in this case is the tunneling current, and M' is the DC current multiplication factor, defined by

Reproduced with permission of the copyright owner. Further reproduction prohibited without permission.

$$M' = \frac{I_r}{I_t} \tag{3.7}$$

where I_r is the terminal reverse current flowing through the diode. Thus, if it is assumed that the expression for tunneling current remains valid in the presence of impact ionization multiplication (which, in light of the current densities encountered, is a very reasonable assumption) then M' is simply the ratio of the measured value of reverse current to the extrapolated value of the tunneling current.

Thus, if

$$\log \frac{S_{id}}{2qI_t} = \log\left[\frac{2qI_t M'(NR)}{2qI_t}\right] = \log[M'(NR)] \tag{3.8}$$

is plotted vs. log M', as done in Figures 29 to 32 for diodes 1N749 to 1N752, a straight line with a slope of three should be obtained. It is clear that, with the exception of the 1N752 diode for which the agreement between experimental results and theory is reasonable, considerable discrepancies exist. Moreover, the discrepancies are serious because the measured values of $\frac{S_{id}}{2qI_t}$ are larger than the theoretical one, which represents the upper limit attainable in impact ionization multiplication for which electrons and holes have the same ionization coefficient. In addition, at low values of multiplication the rate of increase of $\frac{S_{id}}{2qI_t}$ also exceeds the

Reproduced with permission of the copyright owner. Further reproduction prohibited without permission.

theoretical, and, therefore,the upper limit value.

At this point it might be argued that these discrepancies arise from the unequal ionization rates of electrons and holes in silicon. However, if the latest ionization rate data of van Overstraeten and de Man (1970), shown in Figure 33,are extrapolated to the field strengths encountered in diodes used in this study, the extrapolated electron ionization rates are not substantially greater than the extrapolated hole ionization rates.

For the sake of completeness, however, the noise data was also analyzed in terms of McIntyre's (1966) theory of noise current spectral density for impact ionization multiplication in diodes for which the electron and hole ionization rates are not equal. According to McIntyre, if the carriers initiating the multiplication are electrons, the low frequency noise current spectral density is given by

$$S_i = 2qI_t(M')^3\left[1-(1-k)\left(\frac{M'-1}{M}\right)^2\right] \qquad (3.9)$$

where I_t is the electron current initiating the multiplication, which in this case is the tunneling current, $k=\frac{\beta}{\alpha}$ is the ratio of the hole ionization rate, β, to the electron ionization rate, α, and M' is the DC current multiplication factor, $M'=\frac{I_r}{I_t}$. Since β and α depend strongly on the electric field, this equation is strictly correct only if an appropriate "average" value of k is used (McIntyre, 1973).

Reproduced with permission of the copyright owner. Further reproduction prohibited without permission.

However, for the purposes of this discussion this is not an important consideration.

According to McIntyre's (1966) theory, $\frac{S_i}{2qI_t}$ is given by

$$\frac{S_i}{2qI_t} = (M')^3\left[1-(1-k)\left(\frac{M'-1}{M'}\right)^2\right] \qquad (3.10)$$

which is plotted for several values of k in Figure 34. Comparison of Figure 34 with the experimental values of $\frac{S_{id}}{2qI_t}$ of Figures 29 to 31 indicates that a closer agreement between theory and experiment could be obtained only if the hole ionization rate were substantially larger than the electron ionization rate. In light of the measured and extrapolated values of ionization rates of Figure 33 this, however, does not seem very likely.

Moreover, it will be shown in Chapter V that if the measured and extrapolated values of ionization rates of Figure 33 are used in the conventional calculations of DC multiplication, the results obtained indicate that multiplication should occur for any non-zero value of reverse bias. This implies that the noise ratio should be greater than unity for all non-zero values of reverse voltage, which is in direct contradiction with the experimental data of Figures 15 to 21.

The existing theories are, therefore, in serious difficulty: they either fail to correctly predict the

Reproduced with permission of the copyright owner. Further reproduction prohibited without permission.

magnitude and functional dependence of $\frac{S_{id}}{2qI_t}$ on M', or require an unreasonable ratio of ionization rates to possibly achieve an acceptable agreement of theory and experiment; they fail to correctly predict the magnitude of the experimentally observed DC multiplication; and they completely fail to predict the existence of a reverse voltage threshold for the onset of impact ionization multiplication. Any theory of reverse breakdown transition from tunneling to impact ionization multiplication must be able to eliminate all of these discrepancies, while remaining consistent with all other observations of breakdown phenomena in silicon p-n junctions.

One of these observations, made by many workers investigating carrier multiplication in semiconductors, is the existence of an energy threshold for pair production (Shockley, 1961; Moll and van Overstraeten, 1963): the agent attempting to generate a carrier pair must be capable of supplying at least a certain minimum amount of energy if it is to succeed in producing a hole-electron pair. The latest values of threshold energies for impact ionization in silicon, as determined in ionization rate measurements and first reported by Moll and van Overstraeten (1963), are 1.8±0.1 eV for electrons and 2.4±0.1 eV for holes.

Since the noise data of Figures 15 to 21 indicate that carrier multiplication, as judged from the departure

Reproduced with permission of the copyright owner. Further reproduction prohibited without permission.

of the noise ratio from unity, always sets in at a well-defined value of reverse voltage that is almost independent of the diode breakdown voltage (if the breakdown voltage is defined as that value of reverse bias which gives rise to some constant value of reverse current density), the author contends that the onset of multiplication is governed by the magnitude of the threshold energy for ionization.

To substantiate this contention quantitatively, the following multiplication threshold model, described in terms of Figure 35, which shows the electric field and energy band diagrams for a reverse biased abrupt p-n junction, is proposed. Since the tunneling probability is strongly dependent on the electric field, most of the tunneling current originates at x=0. At $x=x_1$ the tunneling electrons become free carriers, absorbing $1.12 \pm E_r$ eV, where $\pm E_r$ corresponds to the emission or absorption of one phonon whose energy may be 17.9 meV (TA), 43.7 meV (LA), 53.2 meV (LO), or 58.5 meV (TO), (Logan, 1969). Continuing towards x_2 the electrons acquire energy from the electric field, and at x_2 those which have made the fewest number of collisions with the lattice are sufficiently energetic to participate in ionizing collisions. The onset of impact ionization multiplication, therefore, occurs when $x_2=x_n$. Denoting the reverse voltage at which this occurs by V_{rth}, the abrupt junction approximation yields

Reproduced with permission of the copyright owner. Further reproduction prohibited without permission.

$$\frac{x_n}{x_n+x_p} = \frac{(1.12\pm E_r)+(1.8\pm 0.1)}{V_{rth}+\phi} \qquad (3.11)$$

where

$$\frac{x_n}{x_n+x_p} = \frac{N_A-N_D}{N_A} \quad . \qquad (3.12)$$

Consequently,

$$V_{rth} = [(1.12\pm E_r)+(1.8\pm 0.1)]\left(\frac{N_A}{N_A-N_D}\right)-\phi \quad . \qquad (3.13)$$

Table II compares the reverse threshold voltages, V_{rth}, computed using the doping densities of Table I and E_r=0.06 eV, with the reverse threshold voltages obtained from Figures 18 to 21. In light of the approximations made and the experimental uncertainties involved in determining the doping densities, they are in good agreement.

The holes produced in ionizing collisions between x_2 and x_n travel in opposite direction, but they, too, ionize only after they have acquired at least the necessary threshold energy for ionization. The electrons produced in hole ionizing collisions then travel towards x_n, and after acquiring at least 1.8±0.1 eV participate in more ionizing collisions. This process repeats itself, but since the number of ionizing collisions decreases with each successive set of ionizations, the process converges to a finite value of DC multiplication.

Reproduced with permission of the copyright owner. Further reproduction prohibited without permission.

TABLE II

REVERSE VOLTAGES AT THE ONSET OF IMPACT IONIZATION MULTIPLICATION: COMPARISON OF DATA WITH THEORY

DIODE TYPE	EXPERIMENTAL REVERSE THRESHOLD VOLTAGE	COMPUTED REVERSE THRESHOLD VOLTAGE
1N749	2.65±0.1 V	2.99 - 3.45 V
1N750	2.7±0.15 V	2.39 - 2.78 V
1N751	2.7±0.15 V	2.31 - 2.71 V
1N752	2.7±0.15 V	2.27 - 2.65 V

Reproduced with permission of the copyright owner. Further reproduction prohibited without permission.

In light of this model it is not difficult to see why the existing theories could not explain the experimental data: none of the theories take the influence of the threshold energies for ionization explicitly into account. The DC multiplication, which will be discussed in more detail in Chapter V, has conventionally been calculated by integrating the ionization rates $\alpha(x)$ and $\beta(x)$ over the junction SCR in accordance with the solution of the differential equation

$$-\frac{dJ_p(x)}{dx} = \frac{dJ_n(x)}{dx} = \alpha(x)J_n(x)+\beta(x)J_p(x) \qquad (3.14)$$

modeling the process (Moll and van Overstraeten, 1963; Lee et al., 1964; van Overstraeten and de Man, 1970). $J_n(x)$ and $J_p(x)$ denote, respectively, the electron and hole current densities as a function of position in the junction SCR. This equation does not explicitly consider the effect of threshold energies on the multiplication process because it claims that the differential increase in current densities at point x is proportional to the current densities at point x, which does not take into account a "distance delay" over which the carriers are incapable of ionizing because they are acquiring the necessary threshold energy. For diodes which break down at several hundred volts of reverse bias this "distance delay" is very small in comparison to the width of the

Reproduced with permission of the copyright owner. Further reproduction prohibited without permission.

junction SCR, and the approximation involved in neglecting it is very good. For diodes breaking down at several volts of reverse bias, on the other hand, the "distance delay" could constitute the entire width of the diode SCR. The approximation of neglecting it in such cases and employing equation 3.14 is totally unacceptable - it leads to calculation of finite DC multiplication when no multiplication is experimentally observed.

Application of conventional calculations of DC multiplication to very low breakdown voltage diodes thus leads to the conclusion that multiplication must be taking place in these junctions because the electric fields in them are very strong. The author, on the other hand, contends that if the electric fields in these junctions are very strong, multiplication will occur, but only if the carrier energies exceed the threshold energies for ionization. This is precisely why no impact ionization multiplication occurs in tunnel diodes, in spite of the extremely strong electric fields existing in these junctions.

Because McIntyre's theory of noise in avalanche diodes employs equation 3.14 in its derivation, it is now clear why his theory is not capable of predicting the multiplication noise in diodes employed in this study. Moreover, Tager's theory is also unacceptable because it does not incorporate in its derivation an upper limit on the number of ionizing collisions a carrier can undergo

Reproduced with permission of the copyright owner. Further reproduction prohibited without permission.

in its transit across the diode SCR. Such a limit must be imposed if threshold energies for ionization are taken into account.

Not explicitly incorporating the influence of the threshold energies for ionization in the existing theories of noise and DC multiplication, therefore, renders them inapplicable to the diodes employed in this study. The next two chapters will attempt to resolve these difficulties.

Reproduced with permission of the copyright owner. Further reproduction prohibited without permission.

CHAPTER IV

DETAILED ANALYSIS OF NOISE DATA

Figures 29 to 32 indicate that if the DC multiplication factor, M', is defined conventionally by

$$M' = \frac{I_r}{I_t} \tag{4.1}$$

it is impossible to obtain a unique slope which would define the exponent, x, in Tager's (1965) expression for the low frequency noise current spectral density

$$S_i = 2qI_t(M')^x \quad . \tag{4.2}$$

The author suspected that this difficulty arose because the DC multiplication factor was not appropriately defined. This can be seen most clearly when $M' = 1$, which is perfectly acceptable mathematically, but is physically meaningless, for a multiplication factor of unity means that there is no carrier multiplication. Thus, it was the author's contention that the DC multiplication factor should be defined by

$$I_r = I_t + MI_t \quad , \text{ or} \tag{4.3}$$

$$M = \frac{I_r}{I_t} - 1 \quad . \tag{4.4}$$

Reproduced with permission of the copyright owner. Further reproduction prohibited without permission.

This definition reduces to the conventional one for large values of M, but is more appealing physically for it allows M to go to zero when there is no carrier multiplication. However, if M is defined by $M = (I_r/I_t)-1$, the expression for the noise current spectral density has to be reformulated, for consistency, to

$$S_i = 2qI_t[1+f(M)] \qquad (4.5)$$

where f(M) goes to zero when M goes to zero.

The results of plotting f(M) vs. M for diodes 1N749 to 1N752 are shown in Figures 36 to 39. These graphs contain several interesting features. First, even though all data points do not lie on one straight line, it is possible to fit most of them along two or three straight lines, the slopes of which increase monotonically with increasing reverse voltages. Second, the departures of data points from lines of lower slopes to lines of higher slopes occur for all diodes at roughly the same (although somewhat increasing) value of reverse voltage. The values of reverse voltages at which these transitions set in, as defined, whenever possible, by the intersection of the two slopes, are:

Diode type	Onset of 1st transition	Onset of 2nd transition
1N749	3.95 V	4.35 V
1N750	4.1 V	4.65 V
1N751	4.4 V	4.95 V
1N752	4.7 V	5.1 V

Reproduced with permission of the copyright owner. Further reproduction prohibited without permission.

Finally, even though the slope of any line tangent to the data points does not exceed its maximum allowed value of three, as did the tangents to the data points of Figures 36 to 39, it is now possible to draw tangent lines whose slopes approach unity -- which appears to contradict the established results that, according to the old definitions, the values of the slopes should never be less than two.

All of these observations can be understood in terms of the conduction model incorporating the carrier threshold energy for ionization, as proposed in the preceding chapter. Since the amount of noise produced in impact ionization multiplication increases as the maximum number of ionizing collisions per carrier transit across the SCR increases, and eventually approaches the upper limit value given by Tager's (1965) expression for the case of unlimited number of ionizing collisions on a carrier transit across the SCR, the breaks in the straight lines in Figures 36 to 39 and the monotonic increase in slopes are indicative of transitions from a lower to a higher maximum number of ionizing collisions that a carrier can undergo in a transit across the diode SCR. In particular, if the built-in voltage of the junctions is taken into account, and an electron threshold energy of 1.8±0.1 eV is assumed, as given by Moll and van Overstraeten (1963), then it becomes clear that the onset of the first break in the slopes of Figures 36 to 39 is due to a transition from a maximum of two to a maximum of

Reproduced with permission of the copyright owner. Further reproduction prohibited without permission.

three ionizing collisions per electron transit across the diode SCR. This is easily verified by dividing 1.8±0.1 eV into the total diode potential, the sum of the built-in potential listed in Table 1, and the potential at the onset of the first slope transition, listed above. The results are:

Diode type	Total potential divided by 1.8±0.1 eV
1N749	2.92 - 2.62
1N750	3.01 - 2.69
1N751	3.19 - 2.85
1N752	3.36 - 3.01

When the procedure is reversed and the total potential at the onset of the first slope transition is divided by three, the following electron threshold energies for ionization are obtained:

Diode type	Electron threshold energy for ionization
1N749	1.66 eV
1n750	1.7 eV
1N751	1.8 eV
1N752	1.9 eV

This is in excellent agreement with Moll and van Overstraeten's (1963) value of 1.8±0.1 eV. The apparent increase in the threshold energy for ionization with increasing diode breakdown voltage is also reasonable. Both Moll and van Overstraeten's (1963) and these values include the "intrinsic" threshold energy as well as energy lost in

Reproduced with permission of the copyright owner. Further reproduction prohibited without permission.

phonon collisions. Since the rate of energy acquisition with distance is smaller in higher voltage breakdown diodes (the electric fields are weaker), but the rate of energy losses is the same (because it depends on mean free path between phonon collisions, which, presumably, is not strongly dependent on field strength), it can be expected that an increasingly larger number of phonon collisions would occur between successive ionizations, resulting in increasingly higher observed threshold energies in higher breakdown voltage diodes.

An analogous analysis can be made for the second slope transition in Figures 36 to 39. Since the threshold energy for ionization for holes is, according to Moll and van Overstraeten (1963), greater than the threshold energy for ionization for electrons, the second slope transition may be suspected to arise from a transition from a maximum of two to a maximum of three ionizing collisions per hole transit across the diode SCR. When the total potential at the onset of the second slope transition is divided by three, the following values of threshold energy for ionization for holes are obtained:

Diode type	Hole threshold energy for ionization
1N749	1.79 eV
1N750	1.89 eV
1N751	1.99 eV
1N752	2.04 eV

Reproduced with permission of the copyright owner. Further reproduction prohibited without permission.

These values are considerably smaller then the 2.4±0.1 eV obtained by Moll and van Overstraeten (1963). Thus it may be suspected that the second slope transition is due to a transition from a maximum of one to a maximum of two ionizing collisions per hole transit across the SCR. This, however, results in hole threshold energies that are substantially higher than those given by Moll and van Overstraeten (1963):

Diode type	Hole threshold energy for ionization (assuming transition from a maximum of one to a maximum of two ionizations per transit)
1N749	2.69 eV
1N750	2.84 eV
1N751	2.99 eV
1N752	3.06 eV

Moreover, if the hole threshold energies obtained under this assumption are used in the simulation of DC multiplication, a serious difficulty arises which does not occur when the hole threshold energy of 1.9±0.15 eV is used. As a consequence, it is suggested that the value of 2.4±0.1 eV is probably too high.

An immediate application of this interpretation of noise data can be made in conjunction with the conduction model proposed in the preceding chapter and the $\frac{1}{C^2}$ vs. V data to compute the doping densities on the n and p sides of the junctions. With the help of Figure 35, the analysis proceeds as follows. At the onset of impact ionization multiplication

Reproduced with permission of the copyright owner. Further reproduction prohibited without permission.

$$\frac{V_g+V_e}{V_{rth}} = \frac{N_A-N_D}{N_A} \tag{4.6}$$

where $V_g = E_g/q$, $V_e = E_e/q$ and E_g is the bandgap energy and E_e is the electron threshold energy for ionization. Moreover, from $\frac{1}{C^2}$ vs. V data

$$\frac{(N_A-N_D)N_D}{N_A} = \frac{2}{\varepsilon_r \varepsilon_o q}\left(\frac{\Delta V_r}{\Delta \frac{1}{C^2}}\right) = P \quad . \tag{4.7}$$

Therefore,

$$N_D = \frac{PV_{rth}}{V_g+V_e} \quad . \tag{4.8}$$

Moreover,

$$N_A = \frac{N_D^2}{N_D-P} \quad , \text{ or} \tag{4.9}$$

$$N_A = \frac{PV_{rth}^2}{V_{rth}(V_g+V_e)-(V_g+V_e)^2} \quad . \tag{4.10}$$

Since $\frac{\Delta V_r}{\Delta \frac{1}{C^2}}$ and, therefore, P, can be determined from the $\frac{1}{C^2}$ vs. V data, and V_{rth} and V_e can be determined from the noise data, N_D and N_A can be calculated. A comparison of N_D and N_A obtained in this manner with the values of N_D and N_A given in Table I is shown in Table III. The agreement is quite good, which lends further credence to the proposed conduction model and the subsequent interpretation of noise data.

Reproduced with permission of the copyright owner. Further reproduction prohibited without permission.

TABLE III

COMPARISON OF DOPING DENSITIES DETERMINED FROM NOISE DATA WITH DOPING DENSITIES OBTAINED UNDER THE ASSUMPTION OF $N_A = 9 \times 10^{18} cm^{-3}$

DIODE TYPE	N_D FROM WAFER RESISTIVITY *	DOPING DENSITIES FROM NOISE DATA N_A	N_D	N_D ASSUMING $N_A = 9 \times 10^{18} cm^{-3}$ **
1N749	2.8 - 3.6	10.14	2.63	2.85
1N750	2.2 - 2.8	8.91	2.13	2.12
1N751	1.75 - 2.2	9.37	1.99	2.02
1N752	1.3 - 1.75	9.34	1.73	1.75
	$\times 10^{18} cm^{-3}$	$\times 10^{18} cm^{-3}$		$\times 10^{18} cm^{-3}$

*Don Estreich, Teledyne Semiconductor, personal communication

**Logan (1969)

Reproduced with permission of the copyright owner. Further reproduction prohibited without permission.

Moreover, if the proposed conduction model is truly valid, then a suitable derivation incorporating the essential features of the model should yield expressions for the magnitude of the noise current spectral density which should be in good agreement with experimentally observed results. From the point of view of noise as a statistical fluctuation phenomenon, the most important feature of the proposed conduction model is the limit it imposes on the maximum number of ionizing collisions a carrier can experience in one transit across the diode SCR. Consequently, any derivation of the noise current spectral density must incorporate this constraint. This complicates the problem considerably for it requires that the multiplication process be examined on basis of individual, successive transits of carriers across the diode SCR, rather than on monitoring the end product of the multiplication process at the device terminals, as was done by Tager (1965) and McIntyre (1966).

To obtain some insight into how the analysis of multiple ionizing collisions might be carried out, the author began by considering the limiting case of a maximum of one ionizing collision per carrier transit across the diode SCR. This is more than just an exercise. According to the author's interpretation of Figures 36 to 38, about half of the data points correspond to multiplication resulting from no more than two ionizing collisions per carrier transit across the SCR. Moreover, even when up to two ionizing collisions are energetically possible, the probability of

Reproduced with permission of the copyright owner. Further reproduction prohibited without permission.

the second collision will be considerably smaller then the probability of the first collision because the space charge regions of the diodes examined in this study are very narrow, whereas the mean free path between ionizing collisions, as quoted by previous workers (Moll and van Overstraeten, 1963; Lee et al., 1964) is relatively large. Thus the approximation of no more than one ionizing collision per carrier transit across the diode SCR should yield reasonable results, especially for the case of the diode with the narrowest SCR, the 1N749.

The analysis of the noise current spectral density is best carried out by referring to Figure 35. The tunneling electrons, originating at x=0 at the rate of n_0 per second, are accelerated from $x=x_1$ to $x=x_2$, and undergo ionizing collisions from $x=x_2$ to $x=x_n$, producing n_1 electron-hole pairs. The n_0 tunneling electrons and the n_1 ionization produced electrons are swept to the right and out of the SCR. The n_1 holes travel to the left and, after acquiring the necessary threshold energy, undergo ionizing collisions, producing n_2 electron-hole pairs. The (n_1+n_2) holes are then swept to the left and out of the SCR, while the n_2 electrons travel to the right and, after acquiring the necessary threshold energy, ionize, producing n_3 electron-hole pairs. This process continues, so that the total number of carriers, N, collected at the device terminals becomes

Reproduced with permission of the copyright owner. Further reproduction prohibited without permission.

$$N = \sum_{i=0}^{\infty} n_i \quad . \tag{4.11}$$

Letting $\bar{n}_1=\bar{a}_1\bar{n}_0$, $\bar{n}_2=\bar{b}_2\bar{n}_1=\bar{b}_2\bar{a}_1\bar{n}_0$, $\bar{n}_3=\bar{a}_3\bar{n}_2=\bar{a}_3\bar{b}_2\bar{a}_1\bar{n}_0$, etc., where the $\bar{}$ denotes averages and $\bar{a}_i$ and $\bar{b}_i$ represent the probability of ionization for electrons and holes, respectively, on the i-th transit across the diode SCR,

$$\bar{N} = \bar{n}_0 \sum_{i=0}^{\infty} \prod_{j=0}^{i} \bar{a}_j \text{ odd} \bar{b}_j \text{ even} \; ; \; \bar{a}_0 \equiv 1, \; \bar{b}_0 \equiv 1 \; . \tag{4.12}$$

This converges to a finite number because $\bar{a}_i<1$ and $b_i<1$ since no more than one ionizing collision per carrier transit across the SCR is allowed. A reasonable simplification which can be made at this point is that $\bar{a}_i=\bar{a}$ and $\bar{b}_i=\bar{b}$. This means that the probabilty of ionization differs for holes and electrons, but remains the same on all transits. In this case,

$$\bar{N} = \bar{n}_0(1+\bar{a}+\bar{a}\bar{b}+\bar{a}^2\bar{b}+\bar{a}^2\bar{b}^2+ \ldots)$$

$$= \bar{n}_0\left(\frac{1+\bar{a}}{1-\bar{a}\bar{b}}\right) \tag{4.13}$$

and the DC multiplication factor, $M = \frac{\bar{N}}{\bar{n}_0} - 1$, becomes

$$M = \frac{\bar{a}(1+\bar{b})}{1-\bar{a}\bar{b}} \quad . \tag{4.14}$$

The low frequency spectrum of the current fluctuations resulting from the multiplication process can be obtained from

$$S_N = 2\text{var } N \tag{4.15}$$

Reproduced with permission of the copyright owner. Further reproduction prohibited without permission.

where S_N denotes the magnitude of the spectrum of N, the number of events occurring during a unit time interval (van der Ziel, 1970). Since the diode current, I_r, is given by $\bar{I}_r = qN$,

$$S_{I_r} = 2q^2 \text{var } N \tag{4.16}$$

where

$$\text{var } N = \overline{N^2} - \bar{N}^2$$

$$= \overline{\left(\sum_{i=0}^{\infty} n_i\right)^2} - \left(\overline{\sum_{i=0}^{\infty} n_i}\right)^2$$

$$= \sum_{i=0}^{\infty} \sum_{j=0}^{\infty} (\overline{n_i n_j} - \bar{n}_i \bar{n}_j) \quad . \tag{4.17}$$

In order to evaluate S_{I_r} it, therefore, remains to evaluate $\overline{n_i n_j}$. This is accomplished by representing n_i by

$$n_i = \sum_{r=1}^{n_0} a_{1r} b_{2r} a_{3r} b_{4r} \cdots \begin{cases} b_{ir}; & \text{i even} \\ a_{ir}; & \text{i odd} \end{cases} \tag{4.18}$$

where a_{jr} and b_{mr} are either 1 or 0 (depending on whether or not an electron or hole ionizes on the j-th or m-th transit across the SCR) and ensemble averaging over the products $n_i n_j$. This analysis is discussed in detail in Appendix A. The resulting expression for var N is given by

$$\text{var } N = n_0 \left\{ \frac{1 + 3\bar{a} + 3\bar{a}\bar{b} + \bar{a}^2\bar{b}}{(1 - \bar{a}\bar{b})^2} \right\} \tag{4.19}$$

Reproduced with permission of the copyright owner. Further reproduction prohibited without permission.

and, therefore,

$$S_{I_r} = 2q\bar{n}_0\left\{\frac{1+3\bar{a}+3\bar{a}\bar{b}+\bar{a}^2\bar{b}}{(1-\bar{a}\bar{b})^2}\right\}$$

$$= 2qI_t\left\{\frac{1+3\bar{a}+3\bar{a}\bar{b}+\bar{a}^2\bar{b}}{(1-\bar{a}\bar{b})^2}\right\} \quad . \tag{4.20}$$

If, for the moment, it is assumed that the probability of ionization is the same for holes as it is for electrons, $\bar{a}=\bar{b}$, then

$$M = \frac{\bar{a}}{1-\bar{a}} \tag{4.21}$$

and

$$S_{I_r} = 2qI_t\frac{(1+\bar{a})}{(1-\bar{a})^2} \quad . \tag{4.22}$$

Eliminating $\bar{a}$,

$$S_{I_r} = 2qI_t(1+3M+2M^2) \tag{4.23}$$

which is, indeed, in the previously postulated form

$$S_{I_r} = 2qI_t[1+f(M)] \quad . \tag{4.24}$$

This result provides a more formal justification of the previously proposed redefinitions of the DC multiplication factor and the functional form of S_i, and lends greater credence to the interpretation of noise data based on the new definitions.

Reproduced with permission of the copyright owner. Further reproduction prohibited without permission.

When equation 4.20 is rewritten in the form

$$S_{I_r} = 2qI_t[1+f(\bar{a},\bar{b})] \tag{4.25}$$

and $f(\bar{a},\bar{b})$ is plotted as a function of M for various values of $k=\frac{\bar{b}}{\bar{a}}$, Figure 40 is obtained, which contains the somewhat surprising result that $f(\bar{a},\bar{b})$ is rather weakly dependent on k. This result is exploited in the derivation of the magnitude of the noise current spectral density for the case of up to two ionizations per carrier transit across the diode SCR. Moreover, since

$$S_{I_r} = 2qI_t[1+f(\bar{a},\bar{b})] \simeq 2qI_t(1+3M+2M^2) \tag{4.26}$$

over a fairly wide range of $k=\frac{\bar{b}}{\bar{a}}$ for low values of M, it demonstrates that the slope of f(M) vs. M can, indeed, approach unity, as it does for the data of Figure 36.

To compare the results of this analysis with experiment, Figure 41 shows, along with $f(M)=3M+2M^2$ plotted versus M, the experimental data for the 1N749 diode. Although the theoretical curve shows the same functional dependence on M as do the experimental data, it is about a factor of three too low. However, in view of the fact that the derivation of the theory is strictly statistical, taking no account of any junction parameters, this result was most encouraging.

At this point the author suspected that the discrepancy between theory and data resulted from dismissing the possibility

Reproduced with permission of the copyright owner. Further reproduction prohibited without permission.

of the second and third ionizations, and proceeded to extend the theory to more than one ionization per carrier transit across the SCR. Although this is easily done in principle, it becomes extremely tedious algebraically because the analysis must take into account the various branching possibilities, and the correlation between the branches. In fact, the extension of the theory to the case of up to two ionizations per carrier transit across the SCR is a composite of an infinite number of the up-to-one-ionization analyses. In order to restrict the algebraic details to manageable size, the author chose to analyze the case of up to two ionizations per carrier transit under the additional restriction that the probability of the second ionization is much smaller than the probability of the first ionization, and, therefore, that terms containing $\bar{a}_2^2$, where $\bar{a}_2$ is the probability of the second ionization, could be neglected. It was felt that this would be a reasonable approximation for the noise data of Figures 36 to 39 below the first slope transition.

The analysis of this case under the additional approximation that the electron and hole ionization probabilities are the same (as justified by DC calculations of Chapter V and by the relative insensitivity of the results of Figure 40 to $k=\frac{\bar{b}}{\bar{a}}$) is given in Appendix B. The algebraically tedious results, evaluated for $\frac{\bar{a}_2}{\bar{a}_1} = 0.3$, which is the highest ratio

Reproduced with permission of the copyright owner. Further reproduction prohibited without permission.

of the probability of the second ionization to the probability of the first ionization that the author felt could be assumed under the approximation that $\bar{a}_2 << \bar{a}_1$, are compared in Figure 42 with the results of the up to one ionization per transit theory, evaluated for $k=\frac{\bar{b}}{\bar{a}}=1$. Although the two curves intersect giving rise to a slope transition, in accordance with the previous interpretation of the slope transitions in the experimental data, the results are somewhat disappointing in that $f(\bar{a}_1,\bar{a}_2)$ is not sufficiently larger to give substantially better agreement between theory and the noise data of Figures 36 to 39.

A careful examination of the various assumptions and approximations made in the theoretical analysis revealed that the source of the final discrepancy between the theoretical results and the experimental data lay in the simplifying approximation that the carrier ionization probability is the same on all transits. A typical plot of the number of carriers generated on a given transit per one tunneling electron, obtained from DC calculations for the 1N752 diode operating at reverse bias of 5.2 volts, and shown in Figure 43, demonstrates that the ionization probability for electrons on the first transit across the diode SCR is considerably smaller than the ionization probability for carriers traversing the SCR on succeeding transits. This may be deduced by comparing the ratio of consecutive

Reproduced with permission of the copyright owner. Further reproduction prohibited without permission.

terms for transit numbers greater than about five which, in the case of Figure 42 is 0.88, with the value of the first term,0.516. If the ionization probability were identical for all transits, the value of the first term would have been 0.88. In retrospect, it is easy to see why the ionization probability on the first transit is less than on succeeding transits. The electrons undergoing ionizations on the first transit come from tunneling, which, in terms of Figure 35, means that they do not become free carriers until $x=x_1$. Consequently, they ionize over a much smaller portion of the SCR than do the succeeding holes or electrons originating as free carriers closer to the edges of the SCR.

To determine what effect the smaller ionization probability on the first transit would have on the noise theory, the derivation of the up-to-one-ionization-per-SCR-transit theory was repeated for the case of $\bar{a}=\bar{b}$, $\frac{\bar{a}_1}{\bar{a}}=r<1$, where $\bar{a}_1$ is the ionization probability on the first transit. The result, derived in detail in Appendix A, is given by

$$S_i = 2qI_t(1+3M+2M^2/r) \qquad (4.27)$$

clearly indicating that theoretically predicted noise output will increase for $r<1$.

This analysis was also repeated for the up to two ionizations per SCR transit theory. Indeed, this is the

Reproduced with permission of the copyright owner. Further reproduction prohibited without permission.

derivation that appears in Appendix B. Because the results are algebraically tedious, they are evaluated numerically once the values of $\bar{a}_{11}$, $\bar{a}_1$, and $\bar{a}_2$ have been determined. Here, $\bar{a}_{11}$ denotes the probability of the first ionization on the first transit, and $\bar{a}_1$ and $\bar{a}_2$ are the first and second ionization probabilities on succeeding transits. For the range of voltages where the up to two ionizations theory is valid, the probability of second ionization on the first transit is zero. The details of evaluating $\bar{a}_{11}$, $\bar{a}_1$ and $\bar{a}_2$ from the DC multiplication program are discussed in Appendix C.

The final results of the up to two ionizations per SCR transit theory for the case of $\bar{a}_{11}<\bar{a}_1$ are compared with the experimental data for the 1N749 to 1N751 diodes in Figures 44 to 46. In view of the many approximations made in the derivation of the theory, the agreement is quite good, even for those values of M where the probability of a third ionization is no longer zero. In the case of the 1N751 diode, where at low values of M the theory predicts a larger noise output than appears to have been observed, the discrepancy is probably due to incorrect values of M, which at low values, can be subject to substantial error.

The analysis of the noise data was terminated at this point for it was felt that even though an up-to-three-ionizations-per-SCR-transit theory would undoubtedly

Reproduced with permission of the copyright owner. Further reproduction prohibited without permission.

yield better agreement between theory and experiment, it would probably offer no new insights into the details of the multiplication mechanism, and, therefore, in view of the algebraic tedium required for its derivation, would not be worthwhile.

Reproduced with permission of the copyright owner. Further reproduction prohibited without permission.

CHAPTER V

CALCULATION OF DC MULTIPLICATION

As has already been mentioned in Chapter III, the calculation of DC multiplication in avalanche diodes has conventionally been done by integrating the electron and hole ionization rates, α and β, over the junction SCR, in accordance with the solution of the differential equation

$$-\frac{dJ_p(x)}{dx} = \frac{dJ_n(x)}{dx} = \alpha(x)J_n(x)+\beta(x)J_p(x) \qquad (5.1)$$

modeling the process. Since this equation incorporates the effect of the threshold energies for ionization implicitly in the ionization rates and, therefore, is not capable of modeling those segments of the carrier trajectories over which multiplication does not occur because the carriers do not have sufficient energy to ionize, it is not applicable to calculation of DC multiplication in low breakdown voltage diodes in which these "inactive" segments of carrier trajectories constitute a very sizeable portion of the diode SCR.

These "inactive" segments could be taken into account in the above equation by incorporating "distance delays," $L_1(x)$ and $L_2(x)$, so that

Reproduced with permission of the copyright owner. Further reproduction prohibited without permission.

$$-\frac{dJ_p(x)}{dx} = \frac{dJ_n(x)}{dx} = \alpha(x)J_n[x-L_1(x)]+\beta(x)J_p[x+L_2(x)] \quad . \tag{5.2}$$

However, if $L_1(x)$ and $L_2(x)$ are taken so that

$$V_e = -q\int_{x-L_1(x)}^{x} E(x)\ dx \tag{5.3}$$

and

$$V_h = -q\int_{x}^{x+L_2(x)} E(x)\ dx \tag{5.4}$$

where V_e and V_h represent, respectively, the threshold potentials for ionization of electrons and holes, then the magnitudes of J_n and J_p must be increased from their actual values at $x\pm L(x)$ since, in general, there will be some carriers with non-zero energies which will not need to travel the full distance $L(x)$ to acquire the necessary threshold energy for ionization. On the other hand, if J_n and J_p are left unaltered, then $L_1(x)$ and $L_2(x)$ need to be evaluated as suitable averages over all carrier energies. Since neither correction is easy to make at the outset, and since the modified differential equation would still need to be solved numerically, the author chose to abandon this approach in favor of a numerical simulation of the multiplication process.

The simulation, whose program listing is given in Appendix C is accomplished as follows. An abrupt junction

Reproduced with permission of the copyright owner. Further reproduction prohibited without permission.

doping profile is assumed, and the electric field triangle is cut into a large number of variable width segments such that the integral of the electric field is the same over each segment. (In the results shown in Figures 47 to 50, $dV = -q\int_{x}^{x+\Delta x} \mathcal{E}(x)\, dx = 0.01V$, so that the electric field triangle was cut into several hundred segments.) The integral of the ionization rates, which represents the probability of an ionization, and the fraction of the tunneling current originating in a given interval are then evaluated approximately for each interval by

$$dP_n(k) = \int_{x_k}^{x_k+\Delta x_k} \alpha(x)\, dx \simeq \frac{1}{2}[\alpha(x_k+\Delta x_k)+\alpha(x_k)]\Delta x_k \quad (5.5)$$

$$dP_h(k) = \int_{x_k}^{x_k+\Delta x_k} \beta(x)\, dx \simeq \frac{1}{2}[\beta(x_k+\Delta x_k)+\beta(x_k)]\Delta x_k \quad (5.6)$$

and

$$dI_t(k) = \frac{\int_{x_k}^{x_k+\Delta x_k} e^{-\frac{s'}{\mathcal{E}(x)}}\, dx}{\int_{0}^{w} e^{-\frac{s'}{\mathcal{E}(x)}}\, dx}$$

$$\simeq \frac{\frac{1}{2}[e^{-\frac{s'}{\mathcal{E}(x_k+\Delta x_k)}} + e^{-\frac{s'}{\mathcal{E}(x_k)}}]\Delta x_k}{\frac{1}{2}\sum_k [e^{-\frac{s'}{\mathcal{E}(x_k+\Delta x_k)}} + e^{-\frac{s'}{\mathcal{E}(x_k)}}]\Delta x_k} \quad (5.7)$$

Reproduced with permission of the copyright owner. Further reproduction prohibited without permission.

where $dP_n(k)$ and $dP_h(k)$ represent, respectively, the probability of ionization for electrons and holes in the k-th interval, and $dI_t(k)$ represents the normalized tunneling current originating in the k-th interval. The multiplication process is then simulated by following the motion of electrons and holes back and forth across the diode SCR, and allowing them to participate in ionizations after they acquire their respective threshold energies, which can be kept track of very easily by counting off the appropriate number of intervals. Thus, the tunneling current originating in the k-th interval becomes a free electron current in the (k+m)-th interval, where $m=\frac{V_g}{dV}$, which may then ionize starting in the $(k+m+n_1)$-th interval, where $n_1=\frac{V_e}{dV}$, and where V_g and V_e denote, respectively, the bandgap potential and the electron threshold potential for ionization. That fraction of the tunneling current which ionizes in a particular interval, and the ionization produced electrons originating in that interval, are then not allowed to ionize again until they have traveled at least another n_1 intervals. The tunneling electrons are traced in this manner across the entire SCR, while the holes produced in ionizations occurring in a given interval are traced in the opposite direction, not being allowed to ionize until they have traveled at least $n_2=\frac{V_h}{dV}$ intervals, where V_h is the hole threshold potential for ionization. The fraction of the hole current ionizing in a particular interval, along with the

Reproduced with permission of the copyright owner. Further reproduction prohibited without permission.

ionization produced holes originating in that interval, are then not allowed to ionize again until they have traversed at least another n_2 intervals. In this manner the hole current is traced across the entire SCR.

This procedure is alternately repeated for electrons and holes, and the contribution to the terminal current due to ionizations on each carrier transit across the SCR is recorded. When the contribution on the p-th transit is less than 0.005 of the contribution on the first transit, the simulation is stopped and the contributions to the terminal current from all transits are added. The same procedure is followed for the multiplication process initiated by the holes left in the valence band when the electrons tunnel to the conduction band. The total multiplication is then the sum of the contributions from the tunneling electron initiated multiplication and the typically much smaller hole initiated multiplication.

The simulation thus circumvents both of the previously discussed difficulties which would be encountered in the differential equation approach to the computation of DC multiplication. It incorporates unambiguously the threshold energies for ionization and, by keeping track of the past history of the carriers, automatically computes the fraction of the total current crossing a given interval which is sufficiently energetic to ionize in that interval. This is equivalent to automatically adjusting the magnitudes of

Reproduced with permission of the copyright owner. Further reproduction prohibited without permission.

$J_n[x-L_1(x)]$ and $J_p[x+L_2(x)]$ to account for the fact that not all carriers need to travel the full distance L(x) in order to acquire the necessary threshold energy for ionization.

Unfortunately, the simulation creates a different problem which, too, is difficult to resolve at the outset. Namely, it assumes that when an ionizing collision occurs the primary carrier and the secondary carriers are scattered in a way which, on the average, does not impart any excess energy to either the primary or the secondary carriers, so that all carriers will be accelerated again essentially from rest. Since the scattering produced by an ionizing collision is probably not isotropic, this assumption may not seem very reasonable. However, in the actual calculations the non-isotropic effects should, at least partially, cancel, for if the scattering favors the direction of the ionizing carrier, then the carriers of the same polarity as the ionizing carriers will not need to accelerate the full distance L(x) to acquire the threshold energy, whereas the carriers of opposite polarity will need to accelerate farther than the distance L(x) to acquire their threshold energy. Since the simulation is performed by alternately tracing the motion of electrons and holes across the SCR, these effects should alternately cancel to some extent. However, without knowing the exact details of the ionization and scattering mechanism, it is difficult to estimate how much cancelling actually takes place.

Reproduced with permission of the copyright owner. Further reproduction prohibited without permission.

Although the simulation program was written especially for computation of DC multiplication occurring in low breakdown voltage diodes, where it is necessary to take the threshold energies for ionization explicitly into account, it may also be used to perform DC multiplication calculations in the conventional manner simply by letting the threshold energies for ionization, and the bandgap energy, approach zero. In actual calculations the bandgap and threshold potentials were set at 0.01 V. The ionization rates employed were those of van Overstraeten and de Man (1970). From the results obtained for diodes 1N750 to 1N752, shown in Figures 47 to 49 under the label of "conventional calculations," it is apparent that the conventional method of performing DC multiplication calculations is inadequate for it predicts much greater multiplication than is experimentally observed, even to the point of predicting finite multiplication when no multiplication actually occurs, as evidenced by the noise data of Figures 15 to 21.

Although, as shown in Figures 47 to 49 under the label of "conventional calculations, including tunneling," the agreement between the experimental and the calculated results improves somewhat when, on the first transit, the bandgap energy for tunneling is taken into account, the calculated values of DC multiplication are still considerably larger than what is experimentally observed, and finite values of multiplication are still calculated when no multiplication actually occurs.

Reproduced with permission of the copyright owner. Further reproduction prohibited without permission.

When the threshold energies for ionization are finally taken into account, the calculated values of DC multiplication do go to zero when no multiplication is observed in the noise data, but the predicted magnitudes of the DC multiplication are smaller than those experimentally observed. This, however, is understandable for the integral of the ionization rates over a given distance represents, by definition, the probability of ionization over that distance. Therefore, eliminating large portions of the diode SCR from integration by explicitly taking the threshold energies for ionization into account, but employing conventional ionization rates derived from integration over the entire SCR, reduces the calculated ionization probabilities and, therefore, the calculated DC multiplication factor. It, therefore, seems appropriate to increase the ionization rates to compensate for this shortening of the ionization rates' integration region. Unfortunately, this is not a trivial matter since the functional dependence of the ionization rates on the electric field implicitly reflects, along with other parameters, the influence of the threshold energies for ionization on the ionization rates, and, therefore, should probably be modified when the threshold energies for ionization are explicitly taken into account. Since there exists no theoretical groundwork to indicate how this should be accomplished, the author chose not to modify the functional dependence of the ionization rates, but merely introduce scaling constants c_1 and c_2 so that

Reproduced with permission of the copyright owner. Further reproduction prohibited without permission.

the adjusted ionization rates α' and β' are given by $\alpha' = c_1\alpha$ and $\beta' = c_2\beta$, where α and β are the "reference", conventional ionization rates given by van Overstraeten and de Man (1970). The constants c_1 and c_2 are adjusted to give the best possible agreement between the calculated and the experimentally obtained values of DC multiplication.

Since the adjusted ionization coefficients would be useless if c_1 and c_2 were determined individually for each diode, the author chose to adjust c_1 and c_2 on diode 1N752, whose DC calculations are most sensitive to the values of c_1 and c_2 because they need to attain the largest values of DC multiplication without diverging. Once this was done, calculations were performed on the remaining diodes, using their respective values of the threshold energies for ionization, as determined in Chapter IV. The results of these calculations are shown in Figures 47 to 49 under the label of "calculated". The discrepancy between the calculated and the experimental values of DC multiplication occurring for low values of M is attributed to the triangle approximation for the junction electric field, which gets progressively worse with decreasing reverse voltage since the diode SCR narrows and gets progressively closer to the changing doping densities of the junction metallurgical transition region. In that region the triangle approximation predicts stronger electric fields than are actually present. This, in turn, leads to larger

Reproduced with permission of the copyright owner. Further reproduction prohibited without permission.

calculated values of ionization probabilities and, hence, larger than observed values of DC multiplication. In spite of this discrepancy, the DC calculations performed by explicitly taking the threshold energies for ionization into account and employing the adjusted ionization rates are in considerably better agreement with the experimental data than are the results obtained by conventional calculations.

The values obtained for c_1 and c_2 are quite reasonable also: $c_1=3$, $c_2=5$. In fact, it was on the basis of the magnitude of c_2 that the author dismissed as unlikely the 2.85 ± 0.2 eV value for the hole threshold energy for ionization, for when this value was employed in the DC calculations it was not possible to obtain reasonable agreement between the calculated and the experimental values of DC multiplication for values of c_2 as large as twenty.

It was also observed that when the best agreement between the theoretical and experimental results was obtained, the electron and hole ionization contributions to the DC multiplication decreased monotonically on successive transits, as shown in Figure 43. Since the ratio of successive terms remained essentially constant regardless of which terms were picked (with the exception of the beginning few) this implies that the ionization probabilities for electrons and holes were essentially

Reproduced with permission of the copyright owner. Further reproduction prohibited without permission.

the same. This information is used in Appendix B to simplify the derivation of the expressions for the magnitude of the low frequency spectral density of noise current produced in a multiplication process resulting from no more than two ionizations per carrier transit across the diode SCR.

Reproduced with permission of the copyright owner. Further reproduction prohibited without permission.

CHAPTER VI

CONCLUSIONS

The principal result of this study is a detailed understanding of the mechanism of reverse conduction transition from tunneling to impact ionization multiplication in low breakdown voltage silicon p-n junctions. It is concluded that the transition occurs when the energy of the tunneling electrons exceeds the electron threshold energy for ionization.

If the DC multiplication factor is redefined by $M = (I_r/I_t)-1$, and the functional form of the expression for the magnitude of the noise current spectral density is changed to $S_i = 2qI_t[1+f(M)]$, then the electron and hole threshold energies may be obtained from slope transitions in the plots of log f(M) vs. log M. The electron threshold energy for ionization determined in this manner is found to be in excellent agreement with the value of 1.8±0.1 eV found by Moll and van Overstraeten (1963). However, the hole threshold energy of 1.9±0.15 eV disagrees with their value of 2.4±0.1 eV. Moreover, it is found that the threshold energy for ionization is not constant, but increases slightly with increasing junction width.

The noise data may also be used to estimate the average minimum distance between ionizing collisions. This is

Reproduced with permission of the copyright owner. Further reproduction prohibited without permission.

accomplished by obtaining the junction width at the reverse voltage corresponding to the onset of the transition from no more than two to no more than three ionizing collisions per electron or hole transit across the diode SCR, and dividing that distance by three. The results are:

Diode type	Average min. distance for electron ionizing collisions	Average min. distance for hole ionizing collisions
1N749	192 A	199 A
1N750	213 A	224 A
1N751	223 A	234 A
1N752	242 A	250 A

When the threshold energies for ionization, the total potential at the onset of carrier multiplication, and the value of $(N_A-N_D)N_D/N_A$ are interpreted in terms of the transition model (Figure 35), the values of N_A and N_D can be determined. The doping densities on both sides of a step junction may thus be evaluated from diode noise and C-V measurements. This technique could be used in some cases for the evaluation of impurity solubilities in silicon.

Conversely, when the junction doping profile and the threshold energies for ionization are known, the transition model may be used to predict the reverse potential for the onset of impact ionization multiplication. This furnishes a method for distinguishing the tunneling section from the multiplication section of the diode reverse V-I characteristics.

Reproduced with permission of the copyright owner. Further reproduction prohibited without permission.

Besides determining the onset of carrier multiplication, the threshold energies for ionization dominate the mechanism of the multiplication process. Because they allow no more than two or three ionizations per carrier transit across the diode SCR, theyrender Tager's (1965) and McIntyre's (1966) theories of noise in avalanche diodes inapplicable to the diodes of this study. This is amply demonstrated by the severe discrepancies between their theoretical results and the experimental data, and by the considerable improvement in agreement between the data and the theoretical results obtained when an upper limit of two ionizations per carrier transit across the SCR is explicitly imposed. Indeed, for low multiplication values, a noise theory based on the explicit constraint of no more than one ionization per carrier transit across the diode SCR gives considerably better agreement with the experimental data than do the theories of Tager (1965) or McIntyre (1966).

Moreover, unless the effect of threshold energies for ionization is explicitly taken into account, a finite value of DC multiplication is calculated when no multiplication is experimentally observed. This discrepancy does not arise when a simulation program incorporating the threshold energies for ionization is used for calculating the DC multiplication.

The many details of the transition mechanism thus lead to the conclusion that the conventional treatment of carrier multiplication phenomena, based on the equation

Reproduced with permission of the copyright owner. Further reproduction prohibited without permission.

$$-\frac{dJ_p(x)}{dx} = \frac{dJ_n(x)}{dx} = \alpha(x)J_n(x)+\beta(x)J_p(x) \qquad (6.1)$$

is not applicable to carrier multiplication in low breakdown voltage diodes.

Reproduced with permission of the copyright owner. Further reproduction prohibited without permission.

CHAPTER VII

RECOMMENDATIONS FOR FURTHER STUDY

The first undertaking in further work on this topic should be the removal of the triangular electric field approximation from the DC multiplication simulation program. The electric field should be obtained from the Poisson equation and the impurity doping profile. If this correction does not remove the discrepancy between the experimental and the calculated values of DC multiplication at low reverse voltages, the cause of the discrepancy should be investigated.

When good agreement between the experimental and the calculated values of DC multiplication is obtained, the calculations should be extended to a case of greater practical importance: the reverse breakdown characteristics of base-emitter junctions of bipolar transistors. Because of the very heavy doping densities encountered in base-emitter junctions, it will probably be necessary to take bandgap narrowing into account. Moreover, if the reverse DC V-I characteristics of the base-emitter junctions or of the low breakdown voltage diodes are to be calculated directly from impurity doping profiles, it will also be necessary to refine the theory of tunneling breakdown (Chynoweth et al., 1960; Tyagi, 1968).

Reproduced with permission of the copyright owner. Further reproduction prohibited without permission.

Furthermore, the program should be modified to calculate carrier multiplication resulting from a single pass across the space charge region. This would permit calculation of carrier multiplication in short channel FET's and other small devices in which one carrier type is somehow removed so that it does not participate in the multiplication process.

Since the threshold energies for ionization play an important role in the simulation program, accurate calculations of DC multiplication in structures of arbitrary lengths and arbitrary impurity doping profiles will require accurate knowledge of the threshold energies under these conditions. Consequently, it will be necessary to carry out additional DC and noise studies to establish means of predicting the threshold energies for ionization in such structures.

The effect of different junction widths and different electric field profiles could be investigated further with the aid of the recently developed replacement series for the 1N746 to 1N752 diodes employed in this study. The new series of diodes, manufactured by alloying aluminum onto the lightly doped p layer of a $p\text{-}n^+$ diode, break down more abruptly than their older counterparts. The more abrupt breakdown is obtained from the resulting $p^+\text{-}p\text{-}n^+$ doping profile (author's conjecture!), which, for any given reverse voltage, widens the space charge region and lowers the peak electric field. The lower peak electric field decreases the tunneling current

Reproduced with permission of the copyright owner. Further reproduction prohibited without permission.

and the wider junction sets up a more favorable environment for impact ionization. Thus, when impact ionization multiplication finally sets in, it occurs more abruptly than in the conventional p^+-n^+ alloy diodes employed in this study. Since the new diodes should, for a given value of DC multiplication, exhibit more noise than their older counterparts, this conjecture should not be difficult to verify.

Moreover, it would be possible to fabricate narrower junctions by employing stronger p-type material, such as boron doped aluminum (Chynoweth et al., 1960). The electric field profiles in such p^{++}-n^+ diodes would be more asymmetrical, which should permit impact ionization multiplication at lower reverse voltages. This should reduce the likelihood of multiple ionizations per carrier transit across the space charge region, and make the noise data more amenable to interpretation in terms of the already developed noise theory.

Due to phonon involvement in the carrier transport and energy balance mechanisms, the threshold energies for ionization should also be determined as function of temperature. Low temperature measurements might also shed some light on the mechanism of phonon collision involvement in the ionization and multiplication processes. Tunnel diode DC V-I characteristics measured at 4.2°K revealed structure which reflected the cooperation of different energy phonons in the tunneling process (Chynoweth et al., 1962; Logan and Chynoweth, 1963; Logan et al., 1964). Such structure might also be observed in the DC or noise data of these diodes.

Reproduced with permission of the copyright owner. Further reproduction prohibited without permission.

In conjunction with the experimental work, the noise theory should be extended to the case of a multiple, but finite number of ionizing collisions per carrier transit across the diode space charge region. This might be possible by combining the author's method with the approach employed by van Vliet in the derivation of avalanche photodetector noise (van Vliet, 1967). Incorporating the quantum efficiency and the Boson factor in the primary current would also make the theory useful for evaluating avalanche photodetector performance.

Finally, the improved multiple ionization noise theory could be used to extract from the noise data information on the ionization probabilities. This would be of considerable help in undertaking a theoretical study of the adjusted ionization coefficients. Such a study might also lead to new approaches to the treatment of other aspects of carrier transport in small devices for which the conventional, differential equations approach, with its implicit assumption of unlimited scattering, is not valid.

Reproduced with permission of the copyright owner. Further reproduction prohibited without permission.

APPENDIX A

MULTIPLICATION NOISE RESULTING FROM NO MORE THAN ONE IONIZATION PER CARRIER TRANSIT ACROSS DIODE SCR

The derivation of expressions for the magnitude of the low frequency spectral density of noise current produced in impact ionization multiplication resulting from no more than one ionization per carrier transit across the diode space charge region proceeds as follows. As indicated in Chapter IV, the total number of carriers, N, collected at the diode terminals in one second is given by

$$N = \sum_{i=0}^{\infty} n_i$$

where n_0 is the number of electrons tunneling in one second, and n_i, i=1, 2, 3, ... is the number of hole-electron pairs produced in one second on the i-th carrier transit across the diode SCR.

If it is assumed that $\bar{n}_1=\bar{a}\bar{n}_0$, $\bar{n}_2=\bar{b}\bar{n}_1=\bar{a}\bar{b}\bar{n}_0$, $\bar{n}_3=\bar{a}\bar{n}_2=\bar{a}^2\bar{b}\bar{n}_0$, etc., where the $\bar{}$ denotes averages and $\bar{a}$ and $\bar{b}$ represent the ionization probabilities of electrons and holes, respectively, then

$$\bar{N} = \bar{n}_0(1+\bar{a}+\bar{a}\bar{b}+\bar{a}^2\bar{b}+\bar{a}^2\bar{b}^2+\ldots)$$

and the DC multiplication factor, $M = \bar{N}/\bar{n}_0-1$ becomes

$$M = \frac{\bar{a}(1+\bar{b})}{1-\bar{a}\bar{b}} \quad .$$

Reproduced with permission of the copyright owner. Further reproduction prohibited without permission.

The low frequency spectrum of the current fluctuations can be obtained from

$$S_N = 2\text{var } N$$

where S_N denotes the magnitude of the spectrum of N, the number of events occurring per unit time interval (van der Ziel, 1970). Since $I_r = qN$,

$$S_{I_r} = 2q^2 \text{var } N$$

$$= 2q^2(\overline{N^2} - \bar{N}^2)$$

$$= 2q^2\{\overline{(\sum_{i=0}^{\infty} n_i)^2} - \overline{(\sum_{i=0}^{\infty} n_i)}^2\}$$

$$= 2q^2\{\sum_{i=0}^{\infty}\sum_{j=0}^{\infty}(\overline{n_i n_j} - \bar{n}_i \bar{n}_j)\} \quad .$$

To evaluate $\overline{n_i n_j}$, it is necessary to have explicit expressions for n_i and n_j. These may be obtained as follows. If the emission of tunneling electrons is pictured as a sequence of 1's, then the terms n_j, j=0, 1, 2, ... can be pictured as

n_0:	1	1	1	1	1	1	1	1	...	1	...	1
n_1:	0	1	1	0	1	0	0	1	...	a_{1r}	...	1
n_2:	0	1	1	0	1	0	0	0	...	$a_{1r}b_{2r}$	...	0
n_3:	0	1	0	0	1	0	0	0	...	$a_{1r}b_{2r}a_{3r}$	...	0
n_4:	0	1	0	0	0	0	0	0	...	$a_{1r}b_{2r}a_{3r}b_{4r}$	...	0

. . .

etc.

Reproduced with permission of the copyright owner. Further reproduction prohibited without permission.

where 1_{jk} j=1, 2, 3, ..., k=1, 2, 3, ... n_0, denotes the occurrence of an ionizing collision on the j-th transit, initiated by the k-th tunneling electron, and where the 0's denote the absence of ionizing collisions. The transitions from 1 to 0 occur independently and at random. From the above tabulation, it is apparent that n_j is given by

$$n_j = \sum_{r=1}^{n_0} a_{1r}b_{2r}a_{3r}b_{4r} \cdots \begin{matrix} a_{jr} \text{ ; j odd} \\ \text{or} \\ b_{jr} \text{ ; j even} \end{matrix}$$

where a_{jk} and b_{jk}, j=1, 2, 3, ... , k=1, 2, 3, ... n_0 are 1 or 0, for eventhough a_{jk} and b_{jk} are allowed to fluctuate independently and at random, $\prod_{k=1}^{j} a_{kr}b_{kr}$ retains the two essential features of the above table, namely, that (i) if all preceding entries in the k-th column are 1, then the next entry can be 1 or 0, and (ii) that if any of the preceding entries is 0, then the next succeeding entry must be 0. The average

$$\overline{n_i n_j} = \left(\sum_{r=1}^{n_0} a_{1r}b_{2r} \cdots \begin{matrix} a_{ir} \\ \text{or} \\ b_{ir} \end{matrix} \right)\left(\sum_{p=1}^{n_0} a_{1p}b_{2p} \cdots \begin{matrix} a_{jp} \\ \\ b_{jp} \end{matrix} \right)$$

may now be evaluated by ensemble averaging. Averaging over the m_N subensembles containing $n_0 = N$ elements

$$\overline{n_i n_j}^N = \frac{1}{m_N} \sum_{m=1}^{m_N} \left\{ \left(\sum_{r=1}^{N} a_{1r}b_{2r} \cdots \begin{matrix} a_{ir} \\ \text{or} \\ b_{ir} \end{matrix} \right)\left(\sum_{p=1}^{N} a_{1p}b_{2p} \cdots \begin{matrix} a_{jp} \\ \text{or} \\ b_{jp} \end{matrix} \right) \right\}$$

$$= \frac{1}{m_N} \sum_{m=1}^{m_N} \left\{ \sum_{r=1}^{N} a_{1r}^2 b_{2r}^2 \cdots \begin{matrix} a_{ir}^2 & b_{(i+1)r} \cdots \begin{matrix} a_{jr} \\ \text{or} \\ b_{jr} \end{matrix} \\ \text{or} & \\ b_{ir}^2 & a_{(i+1)r} \cdots a_{jr} \end{matrix} \right\}$$

Reproduced with permission of the copyright owner. Further reproduction prohibited without permission.

$$+\frac{1}{m_N}\sum_{m=1}^{m_N}\Big\{\sum_{\substack{r=1\\ r\neq p}}^{N}\sum_{p=1}^{N}(a_{1r}b_{2r}\cdots\overset{a_{ir}}{\underset{b_{ir}}{\text{or}}})(a_{1p}b_{2p}\cdots\overset{a_{jp}}{\underset{b_{jp}}{\text{or}}})\Big\}\ .$$

Since all $\bar{a}$'s and $\bar{b}$'s are equal, then if both i and j are even

$$\overline{\underset{j>i}{n_i n_j}}^{N} = N(\overline{a^2})^{(\frac{i}{2})}(\overline{b^2})^{(\frac{i}{2})}(\bar{a})^{(\frac{j-i}{2})}(\bar{b})^{(\frac{j-i}{2})}$$

$$+N(N-1)(\bar{a})^{(\frac{i+j}{2})}(\bar{b})^{(\frac{i+j}{2})}\ .$$

Moreover, since a and b are 1 or 0, $\overline{a^2}=\bar{a}$ and $\overline{b^2}=\bar{b}$. Therefore,

$$\overline{\underset{j>i}{n_i n_j}}^{N} = N\bar{a}^{(\frac{j}{2})}\bar{b}^{(\frac{j}{2})} + N(N-1)\bar{a}^{(\frac{i+j}{2})}\bar{b}^{(\frac{i+j}{2})}\ .$$

Finally, averaging over all subensembles

$$\overline{\underset{j>i}{n_i n_j}} = \overline{n_0}\bar{a}^{(\frac{j}{2})}\bar{b}^{(\frac{j}{2})} + (\overline{n_0^2}-\overline{n_0})\bar{a}^{(\frac{i+j}{2})}\bar{b}^{(\frac{i+j}{2})}\ .$$

Thus,

$$\overline{\underset{j>i}{n_i n_j}}-\bar{n}_i\bar{n}_j = \overline{n_0}\bar{a}^{(\frac{j}{2})}\bar{b}^{(\frac{j}{2})} + (\overline{n_0^2}-\bar{n}_0)a^{(\frac{i+j}{2})}\bar{b}^{(\frac{i+j}{2})}$$

$$-\bar{n}_0^2\bar{a}^{(\frac{i+j}{2})}b^{(\frac{i+j}{2})}$$

$$= \bar{n}_0\bar{a}^{(\frac{j}{2})}\bar{b}^{(\frac{j}{2})} + [(\overline{n_0^2}-\bar{n}_0^2)-\bar{n}_0]\bar{a}^{(\frac{i+j}{2})}\bar{b}^{(\frac{i+j}{2})}\ .$$

However, since the tunneling electrons have a Poisson distribution, for which var $n_0 = \bar{n}_0$

$$(\overline{\underset{j>i}{n_i n_j}}-\bar{n}_i\bar{n}_j) = \bar{n}_0\bar{a}^{(\frac{j}{2})}\bar{b}^{(\frac{j}{2})}\ ;\quad i,j \text{ even}\ .$$

Reproduced with permission of the copyright owner. Further reproduction prohibited without permission.

The same expression is obtained if j is even and i is odd.

If j is odd and i is odd or even,

$$(\overline{n_i n_j} - \bar{n}_i \bar{n}_j) = \bar{n}_0 \bar{a}^{(\frac{j+1}{2})} \bar{b}^{(\frac{j-1}{2})} \quad .$$

If $i \geq j$, the above expressions hold provided j is replaced by i.

Consequently,

$$\text{var } N = \sum_{i=0}^{\infty} \sum_{j=0}^{\infty} (\overline{n_i n_j} - \bar{n}_i \bar{n}_j)$$

$$= \sum_{i=0}^{\infty} (\overline{n_i^2} - \bar{n}_i^2) + 2 \sum_{i=0}^{\infty} \sum_{\substack{j=0 \\ j>i}}^{\infty} (\overline{n_i n_j} - \bar{n}_i \bar{n}_j)$$

$$= \bar{n}_0 (1+\bar{a}+\bar{a}\bar{b}+\bar{a}^2\bar{b}+\bar{a}^2\bar{b}^2+ \ldots$$

$$+2\bar{n}_0 (\bar{a}+\bar{a}\bar{b}+\bar{a}^2\bar{b}+\bar{a}^2\bar{b}^2+ \ldots$$

$$+\bar{a}\bar{b}+\bar{a}^2\bar{b}+\bar{a}^2\bar{b}^2+ \ldots$$

$$+\bar{a}^2\bar{b}+\bar{a}^2\bar{b}^2+ \ldots$$

$$+\bar{a}^2\bar{b}^2+ \ldots$$

$$\vdots \qquad)$$

$$= \bar{n}_0 \{ \frac{1+\bar{a}}{1-\bar{a}\bar{b}} + 2 [\frac{\bar{a}(1+\bar{b})}{(1-\bar{a}\bar{b})^2} + \frac{\bar{a}\bar{b}(1+\bar{a})}{(1-\bar{a}\bar{b})^2}] \}$$

$$= \bar{n}_0 \{ \frac{1+3\bar{a}+3\bar{a}\bar{b}+\bar{a}^2\bar{b}}{(1-\bar{a}\bar{b})^2} \} \quad .$$

Reproduced with permission of the copyright owner. Further reproduction prohibited without permission.

Therefore,

$$S_{I_r} = 2q^2 \text{var } N$$

$$= 2q^2 \bar{n}_0 \{\frac{1+3\bar{a}+3\bar{a}\bar{b}+\bar{a}^2\bar{b}}{(1-\bar{a}\bar{b})^2}\}$$

$$= 2qI_t \{\frac{1+3\bar{a}+3\bar{a}\bar{b}+\bar{a}^2\bar{b}}{(1-\bar{a}\bar{b})^2}\} \quad .$$

If $\bar{a}=\bar{b}$

$$S_{I_r} = 2qI_t \frac{(1+\bar{a})}{(1-\bar{a})^2}$$

and

$$M = \frac{\bar{a}}{(1-\bar{a})} \quad .$$

Therefore,

$$S_{I_r} = 2qI_t (1+3M+2M^2) \quad .$$

If, however, the probability of ionizing collision on the first transit, $\bar{a}_1$, is not equal to $\bar{a}$, the probability of ionizing collision on succeeding transits, then

$$(\overline{n_i n_j} - \bar{n}_i \bar{n}_j) = \bar{n}_0 \bar{a}_1 \bar{a}^{(j-1)} \quad ; \; j>i$$

$$(\overline{n_i n_j} - \bar{n}_i \bar{n}_j) = \bar{n}_0 \bar{a}_1 \bar{a}^{(i-1)} \quad ; \; j<i$$

and

$$(\overline{n_0^2} - \bar{n}_0^2) = \overline{n_0} \quad .$$

Reproduced with permission of the copyright owner. Further reproduction prohibited without permission.

Consequently,

$$\text{var } N = \sum_{i=0}^{\infty} \sum_{j=0}^{\infty} (\overline{n_i n_j} - \bar{n}_i \bar{n}_j)$$

$$= \bar{n}_0 \{ \frac{(1+\bar{a})^2 + \bar{a}_1 (1-\bar{a}) + 2\bar{a}_1}{(1-\bar{a})^2} \}$$

and

$$M = \frac{\bar{a}_1}{(1-\bar{a})} \quad .$$

Therefore, if $\frac{\bar{a}_1}{\bar{a}} = r$

$$S_{I_r} = 2qI_t (1+3M+\frac{2M^2}{r}) \quad .$$

Reproduced with permission of the copyright owner. Further reproduction prohibited without permission.

APPENDIX B

MULTIPLICATION NOISE RESULTING FROM NO MORE THAN TWO IONIZATIONS PER CARRIER TRANSIT ACROSS DIODE SCR

The derivation of expressions for the magnitude of the low frequency spectral density of noise current produced in impact ionization multiplication resulting from no more than two ionizations per carrier transit across the diode space charge region proceeds as follows.

It is assumed that carrier multiplication taking place during one transit across the diode SCR is, in general, of the form

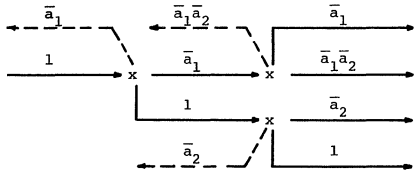

where "1" denotes the "primary" carrier initiating the multiplication process, "x" denotes an ionizing collision, $\bar{a}_1$ and $\bar{a}_2$ denote the probabilities of the first and second ionizing collision, and the dashed lines indicate carriers of opposite charge to the "primary" carriers.

If the above diagram is extended to include several transits across the diode SCR, it takes on the appearance

Reproduced with permission of the copyright owner. Further reproduction prohibited without permission.

of a "tree" from which it becomes apparent that the multiplication process can be decomposed into an infinite number of "branches" of the form

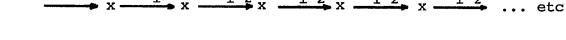

which is precisely the up to <u>one</u> ionization per carrier transit across the SCR process for the case of unequal probabilities for holes and electrons. (It should be observed, however, that in this analysis, the ionization probabilities for electrons and holes <u>are</u> assumed to be the same. The evidence supporting this assumption is discussed in Chapter V. Even if this assumption were not strictly valid, however, Figure 40 indicates that the results obtained for unequal ionization probabilities do not differ substantially from the result obtained for equal ionization probabilities in the one ionization per carrier transit case. And since the up to two ionizations per carrier transit across the SCR case is a composition of the one ionization per carrier transit cases, the final result should not be very sensitive to the difference in ionization probabilities for holes and electrons.)

To reduce the number of "branches" that need to be considered, it will also be assumed that $\bar{a}_2 << \bar{a}_1$, so that branches beginning with $\bar{a}_{11}\bar{a}_1^{j-k}\bar{a}_2^k$, $k \geq 2$, will be neglected. This assumption is justified in Appendix C . Moreover,

Reproduced with permission of the copyright owner. Further reproduction prohibited without permission.

since the probability of ionizing collision is smaller on the first transit than it is on succeeding transits, the probability of the first ionizing collision on the first transit across the diode SCR will be denoted by $\bar{a}_{11}$. According to the conduction model of Figure 35, the probability of the second ionizing collision on the first transit, $\bar{a}_{21}$, for the range of voltages where the up to two ionizations per transit across the SCR theory may be considered valid, is zero. This follows from equation 3.13, with 1.8 ± 0.1 replaced by $2V_e$. The results of this calculation are

Diode type	Reverse voltage for which $\bar{a}_{21}>0$
1N749	4.89-5.06
1N750	4.85-5.00
1N751	4.90-5.06
1N752	4.95-5.10

The reverse voltages given above are greater than the voltages corresponding to the first slope transition in Figures 36 to 39, thus confirming the contention that for the range of voltages where the up to two ionizing collisions per carrier transit theory is valid, $\bar{a}_{21}=0$.

Under the condition stipulated, the "tree" for this multiplication process is given in Figure 50. The heavy arrows denote electron ionizations, the light arrows denote hole ionizations, and the $\boxed{ki}$ denote "branch" numbers. To avoid excessive clutter, only the beginnings of each "branch" are indicated. Thus, "branch" $\boxed{11}$ is the branch given by

Reproduced with permission of the copyright owner. Further reproduction prohibited without permission.

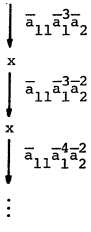

All branches, therefore, continue vertically downward, and their continuation is indicated by dashed arrows. The beginning of each new branch is indicated by a horizontal translation to the right, followed by the downward arrows of that branch.

The analysis of this multiplication process proceeds as follows. Let N be the total number of carriers collected at the diode terminals as a result of multiplication initiated by n_0 tunneling electrons. Then,

$$N = \sum_i^{\infty} m_i$$

where m_i denotes the number of carriers produced by the i-th branch. Hence,

$$\operatorname{var} N = \sum_i \operatorname{var} m_i + 2 \sum_i \sum_{j>i} (\overline{m_i m_j} - \bar{m}_i \bar{m}_j)$$

Reproduced with permission of the copyright owner. Further reproduction prohibited without permission.

But

$$m_i = \sum_{k=0}^{\infty} n_{ik}$$

where n_{ik} is the number of carriers produced in the i-th branch, on the k-th transit across the SCR. Following the procedure of Appendix A, n_{ik} is, in turn, represented by

$$n_{ik} = \sum_{r=1}^{n_0} (\text{product of } a_{11}, a_1\text{'s and } a_2\text{'s})_r$$

where a_{11}, a_1's and a_2's are 1 or 0, and the product function of a_{11}, a_1's, and a_2's reflects the past history of the r-th primary carrier, in the i-th branch, on the k-th transit across the diode SCR. Thus the problem of up to two ionizing collisions per carrier transit across the SCR is reduced to a sum of an infinite number of up to one ionization per carrier transit analyses.

To obtain the expression for M, the branch contributions are summed as follows:

$$\bar{N} = \sum_i m_i = m_{10} + \sum_{j=1}^{\infty} m_{1j} + \sum_{j=0}^{\infty} m_{0j0}$$

$$+ \sum_{i=2}^{\infty} \sum_{j=1}^{\infty} m_{0ij} + \sum_{j=2}^{\infty} m_{j0} + \sum_{i=2}^{\infty} \sum_{j=1}^{\infty} m_{ij}$$

resulting in

Reproduced with permission of the copyright owner. Further reproduction prohibited without permission.

$$\bar{N} = \bar{n}_0[1 + \bar{a}_{11}(\frac{1+\bar{a}_1}{1-\bar{a}_1\bar{a}_2}) + \frac{\bar{a}_{11}\bar{a}_1^3\bar{a}_2(1+\bar{a}_2)}{(1-\bar{a}_1\bar{a}_2)(1-\bar{a}_1)}$$

$$+ \frac{\bar{a}_{11}\bar{a}_1^4\bar{a}_2(1+\bar{a}_2)}{(1-\bar{a}_1\bar{a}_2)(1-\bar{a}_1)^2} + \frac{\bar{a}_{11}\bar{a}_1^3\bar{a}_2(1+\bar{a}_2)}{(1-\bar{a}_1\bar{a}_2)(1-\bar{a}_1)^2}$$

$$+ \frac{\bar{a}_{11}\bar{a}_1^2(1+\bar{a}_2)}{(1-\bar{a}_1\bar{a}_2)(1-\bar{a}_1)} + \frac{\bar{a}_{11}\bar{a}_1^4\bar{a}_2(1+\bar{a}_2)}{(1-\bar{a}_1\bar{a}_2)(1-\bar{a}_1)^2}] \quad .$$

Hence, $M = \frac{\bar{N}}{\bar{n}_0} - 1$ becomes

$$M = \bar{a}_{11}[(1+\frac{\bar{a}_1\bar{a}_2}{1-\bar{a}_1})(\frac{1+\bar{a}_1}{1-\bar{a}_1\bar{a}_2}) + \frac{\bar{a}_1^2(1-\bar{a}_1+2\bar{a}_1\bar{a}_2)(1+\bar{a}_2)}{(1-\bar{a}_1)^2(1-\bar{a}_1\bar{a}_2)}] \quad .$$

To calculate the results for var N, the procedure of Appendix A is duplicated to obtain

$$\text{var } m_1 = 1 + \frac{\bar{a}_{11}(3+5\bar{a}_1+\bar{a}_1\bar{a}_2-\bar{a}_1^2\bar{a}_2)}{(1-\bar{a}_1\bar{a}_2)^2}$$

and the variances of the branches b_1 and b_2 whose averages are given by

$$b_1: \quad 1+\bar{a}_1+\bar{a}_1\bar{a}_2+\bar{a}_1^2\bar{a}_2+\bar{a}_1^2\bar{a}_2^2+\ldots$$

and

$$b_2: \quad \bar{a}_1+\bar{a}_1\bar{a}_2+\bar{a}_1^2\bar{a}_2+\bar{a}_1^2\bar{a}_2^2+\ldots \quad .$$

Reproduced with permission of the copyright owner. Further reproduction prohibited without permission.

They are, respectively,

$$\text{var } b_1 = \frac{1+3\bar{a}_1+3\bar{a}_1\bar{a}_2+\bar{a}_1{}^2\bar{a}_2}{(1-\bar{a}_1\bar{a}_2)^2}$$

and

$$\text{var } b_2 = \frac{\bar{a}_1(1+3\bar{a}_2+3\bar{a}_1\bar{a}_2+\bar{a}_1\bar{a}_2{}^2)}{(1-\bar{a}_1\bar{a}_2)^2} \quad .$$

Observing that the variances of branches whose averages are represented by

$$\bar{a}_{11}\bar{a}_1{}^j\bar{a}_2{}^k(1+\bar{a}_1+\bar{a}_1\bar{a}_2+\bar{a}_1{}^2\bar{a}_2+ \ldots)$$

or

$$\bar{a}_{11}\bar{a}_1{}^j\bar{a}_2{}^k(\bar{a}_1+\bar{a}_1\bar{a}_2+\bar{a}_1{}^2\bar{a}_2+\bar{a}_1{}^2\bar{a}_2{}^2+ \ldots)$$

are given, respectively, by

$$\bar{a}_{11}\bar{a}_1{}^j\bar{a}_2{}^k \text{ var } b_1$$

or

$$\bar{a}_{11}\bar{a}_1{}^j\bar{a}_2{}^k \text{ var } b_2$$

and repeating the summation performed to obtain $\bar{N} = \sum_i m_i$

Reproduced with permission of the copyright owner. Further reproduction prohibited without permission.

$$\sum_i \text{var } m_i = 1 + \frac{\bar{a}_{11}(3+5\bar{a}_1+\bar{a}_1\bar{a}_2-\bar{a}_1^2\bar{a}_2)}{(1-\bar{a}_1\bar{a}_2)^2}$$

$$+ \frac{\bar{a}_{11}\bar{a}_1\bar{a}_2}{(1-\bar{a}_1)}\left[\frac{1+3\bar{a}_1+3\bar{a}_1\bar{a}_2+\bar{a}_1^2\bar{a}_2}{(1-\bar{a}_1\bar{a}_2)^2}\right.$$

$$+ \frac{\bar{a}_{11}\bar{a}_1^2(1-\bar{a}_1+2\bar{a}_1\bar{a}_2)}{(1-\bar{a}_1)^2}\left[\frac{1+3\bar{a}_2+3\bar{a}_1\bar{a}_2+\bar{a}_1\bar{a}_2^2}{(1-\bar{a}_1\bar{a}_2)^2}\right] .$$

It, therefore, remains to compute $2\sum_i \sum_{j>i} (\overline{m_i m_j} - \bar{m}_i \bar{m}_j)$.

Fortunately, it is necessary to compute only seven $(\overline{m_i m_j} - \bar{m}_i \bar{m}_j)$'s, since the remaining can be obtained by inspection. The procedure employed in calculating these is illustrated for the case of $(\overline{m_{10} m_{11}} - \bar{m}_{10}\, \bar{m}_{11})$:

$$(\overline{m_{10} m_{11}} - \bar{m}_{10}\bar{m}_{11}) = \sum_{i=1}^{\infty} \sum_{j=1}^{\infty} (\overline{n_{10i} n_{11j}} - \overline{n_{10i}}\,\overline{n_{11j}})$$

where

$$n_{10i} = \sum_{r=1}^{n_0} (\overline{1 \underbrace{a_{11}\, a_1\, a_2\, a_1\, a_2\, a_1 \ldots}_{i \text{ terms}}})_r$$

and

$$n_{11j} = \sum_{s=1}^{n_0} \overline{[1 - a_{11}\, a_1\, a_2\, a_1 \underbrace{(a_1\, a_2\, a_1 \ldots)}_{j \text{ terms}}]}_s \quad .$$

Reproduced with permission of the copyright owner. Further reproduction prohibited without permission.

Here, $\underline{\quad}$ denotes identically the same factor in n_{10i} and n_{11j}, and the factors bracketed by $\overline{\quad\quad}$ are to be treated as one, since they correspond to i=1 or j=1. Since this approach is identical to that employed in Appendix A, it may be observed there that

$$(\overline{n_{10i}n_{11j}}-\overline{n_{10i}}\,\overline{n_{11j}}) = \overline{(n_{10i}n_{11j})}\big|_{r=s} \quad ,$$

since $\overline{n_0^2}-\bar{n}_0^2=\bar{n}_0$.

Moreover, when r=s, $\underline{a_{11}^2}=\overline{a_{11}}$, $\underline{a_1^2}=\overline{a_1}$, and $\underline{a_2^2}=\overline{a_2}$. Consequently,

$$(\overline{m_{10}m_{11}}-\overline{m_{10}}\,\overline{m_{11}}) = \sum_{i=1}^{\infty}\sum_{j=1}^{\infty}(\overline{n_{10i}n_{11j}})\big|_{r=s}$$

$$= \bar{n}_0\frac{\bar{a}_{11}\bar{a}_1^3\bar{a}_2(1+\bar{a}_2)(5+\bar{a}_2-4\bar{a}_1\bar{a}_2)}{(1-\bar{a}_1\bar{a}_2)^2} \quad .$$

The other six $(\overline{m_i m_j}-\overline{m}_i\overline{m}_j)$'s of importance are

$$(\overline{m_{11}m_{12}}-\overline{m_{11}}\,\overline{m_{12}}) = \bar{a}_{11}\bar{a}_1^4\bar{a}_2(\frac{1+\bar{a}_2}{1-\bar{a}_1\bar{a}_2})^2$$

$$(\overline{m_{10}m_{020}}-\overline{m_{10}}\,\overline{m_{020}}) = \frac{\bar{a}_{11}\bar{a}_1\bar{a}_2(1+\bar{a}_1)}{(1-\bar{a}_1\bar{a}_2)}[3+\frac{\bar{a}_2(1+\bar{a}_1)}{(1-\bar{a}_1\bar{a}_2)}]$$

$$(\overline{m_{10}m_{021}}-\overline{m_{11}}\,\overline{m_{021}}) = \bar{a}_{11}\bar{a}_1^3\bar{a}_2(\frac{1+\bar{a}_2}{1-\bar{a}_1\bar{a}_2})[2+\frac{(1+\bar{a}_2)}{(1-\bar{a}_1\bar{a}_2)}]$$

Reproduced with permission of the copyright owner. Further reproduction prohibited without permission.

$$(\overline{m_{11}m_{020}}-\bar{m}_{11}\bar{m}_{020}) = \frac{\bar{a}_{11}\bar{a}_1^3\bar{a}_2^2(1+\bar{a}_1)(1+\bar{a}_2)}{(1-\bar{a}_1\bar{a}_2)^2}$$

$$(\overline{m_{020}m_{021}}-\bar{m}_{020}\bar{m}_{021}) = \bar{a}_{11}\bar{a}_1^3\bar{a}_2\left(\frac{1+\bar{a}_2}{1-\bar{a}_1\bar{a}_2}\right)\left(1+\frac{1+\bar{a}_2}{1-\bar{a}_1\bar{a}_2}\right)$$

$$(\overline{m_{20}m_{21}}-\bar{m}_{20}\bar{m}_{21}) = \bar{a}_{11}\bar{a}_1^4\bar{a}_2\left(\frac{1+\bar{a}_2}{1-\bar{a}_1\bar{a}_2}\right)\left(2+\frac{1+\bar{a}_2}{1-\bar{a}_1\bar{a}_2}\right) .$$

All other $(\overline{m_i m_j}-\bar{m}_i\bar{m}_j)$'s may be obtained from these by observing that, for example,

$$(\overline{m_{1i}m_{1j}}-\overline{m}_{1i}\overline{m}_{1j}) = \bar{a}_1(\overline{m_{1i}m_{1(j-1)}}-\overline{m}_{1i}\overline{m}_{1(j-1)}) \quad .$$
$$i\geq 1,\ j\geq 3$$

Generating additional $(\overline{m_i m_j}-\bar{m}_i\bar{m}_j)$'s in this manner and adding the results

Reproduced with permission of the copyright owner. Further reproduction prohibited without permission.

A: $$\sum_{i=0}^{\infty}\sum_{\substack{j=1\\ j>i}}^{\infty}(\overline{m_{1i}m_{1j}}-\overline{m_{1i}}\,\overline{m_{1j}}) = \frac{\bar{n}_0\bar{a}_{11}\bar{a}_1^3\bar{a}_2(1+\bar{a}_2)(5+\bar{a}_2-4\bar{a}_1\bar{a}_2)}{(1-\bar{a}_1)(1-\bar{a}_1\bar{a}_2)^2}$$

$$+\frac{\bar{n}_0\bar{a}_{11}\bar{a}_1^4\bar{a}_2}{(1-\bar{a}_1)^2}\left(\frac{1+\bar{a}_2}{1-\bar{a}_1\bar{a}_2}\right)^2$$

B: $$\sum_{j=0}^{\infty}(\overline{m_{10}m_{02j}}-\overline{m_{10}}\,\overline{m_{02j}}) = \frac{\bar{n}_0\bar{a}_{11}\bar{a}_1^3\bar{a}_2(1+\bar{a}_2)(3+\bar{a}_2-2\bar{a}_1\bar{a}_2)}{(1-\bar{a}_1)(1-\bar{a}_1\bar{a}_2)^2}$$

$$+\frac{\bar{n}_0\bar{a}_{11}\bar{a}_1\bar{a}_2(1+\bar{a}_1)(3-2\bar{a}_1\bar{a}_2+\bar{a}_2)}{(1-\bar{a}_1\bar{a}_2)^2}$$

C: $$\sum_{i=1}^{\infty}\sum_{j=0}^{\infty}(\overline{m_{1i}m_{02j}}-\overline{m_{1i}}\,\overline{m_{02j}}) = \frac{\bar{n}_0\bar{a}_{11}\bar{a}_1^3\bar{a}_2^2(1+\bar{a}_1)(1+\bar{a}_2)}{(1-\bar{a}_1)(1-\bar{a}_1\bar{a}_2)^2}$$

$$+\frac{\bar{n}_0\bar{a}_{11}\bar{a}_1^5\bar{a}_2^2}{(1-\bar{a}_1)^2}\left(\frac{1+\bar{a}_2}{1-\bar{a}_1\bar{a}_2}\right)^2$$

D: $$\sum_{i=0}^{\infty}(\overline{m_{10}m_{2j}}-\overline{m_{10}}\,\overline{m_{2j}}) = \frac{\bar{n}_0\bar{a}_{11}\bar{a}_1^2(1+\bar{a}_2)(3+\bar{a}_2-2\bar{a}_1\bar{a}_2)}{(1-\bar{a}_1)(1-\bar{a}_1\bar{a}_2)^2}$$

$$\cdot\frac{(1-\bar{a}_1+\bar{a}_1^2\bar{a}_2)}{(1-\bar{a}_1)(1-\bar{a}_1\bar{a}_2)^2}$$

E: $$\sum_{i=1}^{\infty}\sum_{j=0}^{\infty}(\overline{m_{1i}m_{2j}}-\overline{m_{1i}}\,\overline{m_{2j}}) = \frac{\bar{n}_0\bar{a}_{11}\bar{a}_1^4\bar{a}_2(1-\bar{a}_1+\bar{a}_1^2\bar{a}_2)}{(1-\bar{a}_1)^2}\left(\frac{1+\bar{a}_2}{1-\bar{a}_1\bar{a}_2}\right)^2$$

Reproduced with permission of the copyright owner. Further reproduction prohibited without permission.

F: $$\sum_{i=1}^{\infty}\sum_{\substack{j=0\\ j>i}}^{\infty}(\overline{m_{02i}m_{02j}}-\overline{m_{02i}}\,\overline{m_{02j}}) = \frac{\bar{n}_0\bar{a}_{11}\bar{a}_1^3\bar{a}_2(1+\bar{a}_2)(2+\bar{a}_2-\bar{a}_1\bar{a}_2)}{(1-\bar{a}_1)(1-\bar{a}_1\bar{a}_2)^2}$$

$$+\frac{\bar{n}_0\bar{a}_{11}\bar{a}_1^4\bar{a}_2}{(1-\bar{a}_1)^2}\left(\frac{1+\bar{a}_2}{1-\bar{a}_1\bar{a}_2}\right)^2$$

G: $$\sum_{i=0}^{\infty}\sum_{\substack{j=1\\ j>i}}^{\infty}(\overline{m_{2i}m_{2j}}-\overline{m_{2i}}\,\overline{m_{2j}}) = \frac{\bar{n}_0\bar{a}_{11}\bar{a}_1^4\bar{a}_2}{(1-\bar{a}_1)}\left(\frac{1+\bar{a}_2}{1-\bar{a}_1\bar{a}_2}\right)\left(2+\frac{1+\bar{a}_2}{1-\bar{a}_1\bar{a}_2}\right)$$

$$+\frac{\bar{n}_0\bar{a}_{11}\bar{a}_1^5\bar{a}_2}{(1-\bar{a}_1)^2}\left(\frac{1+\bar{a}_2}{1-\bar{a}_1\bar{a}_2}\right)^2$$

H: $$\sum_{j=0}^{\infty}(\overline{m_{20}m_{02j}}-\overline{m_{20}}\,\overline{m_{02j}}) = \frac{\bar{n}_0\bar{a}_{11}\bar{a}_1^2\bar{a}_2(1+\bar{a}_1)(1+\bar{a}_2)}{(1-\bar{a}_1\bar{a}_2)^2}$$

$$+\frac{\bar{n}_0\bar{a}_{11}\bar{a}_1^4\bar{a}_2}{(1-\bar{a}_1)}\left(\frac{1+\bar{a}_2}{1-\bar{a}_1\bar{a}_2}\right)^2$$

I: $$\sum_{i=1}^{\infty}\sum_{j=0}^{\infty}(\overline{m_{2i}m_{02j}}-\overline{m_{2i}}\,\overline{m_{02j}}) = \frac{\bar{n}_0\bar{a}_{11}\bar{a}_1^{4-2}(1+\bar{a}_1)(1+\bar{a}_2)}{(1-\bar{a}_1)(1-\bar{a}_1\bar{a}_2)^2}$$

$$+\frac{\bar{n}_0\bar{a}_{11}\bar{a}_1^{6-2}\bar{a}_2}{(1-\bar{a}_1)^2}\left(\frac{1+\bar{a}_2}{1-\bar{a}_1\bar{a}_2}\right)^2$$

Reproduced with permission of the copyright owner. Further reproduction prohibited without permission.

J: $$\sum_{j=0}^{\infty}(\overline{m_{020}m_{03j}}-\overline{m_{020}}\,\overline{m_{03j}}) = \bar{n}_0\bar{a}_{11}\bar{a}_1^2\bar{a}_2^2\left(\frac{1+\bar{a}_1}{1-\bar{a}_1\bar{a}_2}\right) + \frac{\bar{n}_0\bar{a}_{11}\bar{a}_1^4\bar{a}_2^2(1+\bar{a}_1)(1+\bar{a}_2)}{(1-\bar{a}_1)(1-\bar{a}_1\bar{a}_2)^2}$$

K: $$\sum_{i=1}^{\infty}\sum_{j=1}^{\infty}(\overline{m_{02i}m_{03j}}-\overline{m_{02i}}\,\overline{m_{03j}}) = \frac{\bar{n}_0\bar{a}_{11}\bar{a}_1^4\bar{a}_2^2(1+\bar{a}_1)(1+\bar{a}_2)}{(1-\bar{a}_1)(1-\bar{a}_1\bar{a}_2)^2} + \frac{\bar{n}_0\bar{a}_{11}\bar{a}_1^6\bar{a}_2^2}{(1-\bar{a}_1)^2}\left(\frac{1+\bar{a}_2}{1-\bar{a}_1\bar{a}_2}\right)^2$$

L: $$\sum_{j=0}^{\infty}(\overline{m_{020}m_{3j}}-\overline{m_{020}}\,\overline{m_{3j}}) = \frac{\bar{n}_0\bar{a}_{11}\bar{a}_1^3\bar{a}_2(1+\bar{a}_1)(1+\bar{a}_2)(1-\bar{a}_1+\bar{a}_1^2\bar{a}_2)}{(1-\bar{a}_1)(1-\bar{a}_1\bar{a}_2)^2}$$

M: $$\sum_{i=1}^{\infty}\sum_{j=0}^{\infty}(\overline{m_{02i}m_{3j}}-\overline{m_{02i}}\,\overline{m_{3j}}) = \frac{\bar{n}_0\bar{a}_{11}\bar{a}_1^5\bar{a}_2(1-\bar{a}_1+\bar{a}_1^2\bar{a}_2)}{(1-\bar{a}_1)^2}\cdot\left(\frac{1+\bar{a}_2}{1-\bar{a}_1\bar{a}_2}\right)^2$$

N: $$\sum_{j=0}^{\infty}(\overline{m_{20}m_{03j}}-\overline{m_{20}}\,\overline{m_{03j}}) = \frac{\bar{n}_0\bar{a}_{11}\bar{a}_1^2\bar{a}_2(1+\bar{a}_1)(1+\bar{a}_2)}{(1-\bar{a}_1\bar{a}_2)^2} + \frac{\bar{n}_0\bar{a}_{11}\bar{a}_1^4\bar{a}_2}{(1-\bar{a}_1)}\left(\frac{1+\bar{a}_2}{1-\bar{a}_1\bar{a}_2}\right)^2$$

Reproduced with permission of the copyright owner. Further reproduction prohibited without permission.

O: $$\sum_{i=1}^{\infty}\sum_{j=0}^{\infty}(\overline{m_{2i}m_{03j}}-\overline{m_{2i}}\,\overline{m_{03j}}) = \frac{\bar{n}_0\bar{a}_{11}\bar{a}_1^2\bar{a}_2(1+\bar{a}_1)(1+\bar{a}_2)}{(1-\bar{a}_1\bar{a}_2)^2}$$

$$+\frac{\bar{n}_0\bar{a}_{11}\bar{a}_1^4\bar{a}_2}{(1-\bar{a}_1)}\left(\frac{1+\bar{a}_2}{1-\bar{a}_1\bar{a}_2}\right)^2$$

P: $$\sum_{j=0}^{\infty}(\overline{m_{20}m_{3i}}-\overline{m_{20}}\,\overline{m_{3j}}) = \frac{\bar{n}_0\bar{a}_{11}\bar{a}_1^3(1-\bar{a}_1+\bar{a}_1\bar{a}_2)}{(1-\bar{a}_1)}\left(\frac{1+\bar{a}_2}{1-\bar{a}_1\bar{a}_2}\right)^2$$

Q: $$\sum_{i=1}^{\infty}\sum_{j=0}^{\infty}(m_{2i}m_{3j}-m_{2i}m_{3j}) = \frac{\bar{n}_0\bar{a}_{11}\bar{a}_1^5\bar{a}_2(1-\bar{a}_1+\bar{a}_1\bar{a}_2)}{(1-\bar{a}_1)^2}$$

$$\cdot\left(\frac{1+\bar{a}_2}{1-\bar{a}_1\bar{a}_2}\right)^2$$

Finally,

$$2\sum_{j>i}\sum_{i}(\overline{m_i m_j}-\overline{m_i}\,\overline{m_j}) = 2\left[A+\frac{1}{1-\bar{a}_1}(B+C+D+E+F+G+H+I)\right.$$

$$\left.+\frac{1}{(1-\bar{a}_1)^2}(J+K+L+M+N+O+P+Q)\right] .$$

After $\overline{a_{11}}$, $\overline{a_1}$, and $\overline{a_2}$ are calculated using the DC multiplication program of Appendix C, the above results are evaluated, and (var N) - 1 is plotted vs. M in Figures 44 to 46.

Reproduced with permission of the copyright owner. Further reproduction prohibited without permission.

APPENDIX C

DC MULTIPLICATION SIMULATION PROGRAM

The DC multiplication simulation program performs calculations of carrier multiplication resulting from impact ionization in p-n step junctions. Its input variables are:

NSETS : number of diodes whose DC V-I characteristics will be calculated

NVREV : number of reverse voltages for which the DC multiplication will be calculated

XNA : $N_A - N_D$ = net doping density on p-side (cm^{-3})

XND : N_D = net doping density on n-side (cm^{-3})

ALPHA1, B1 : electron ionization rate constants: adjusted ionization rate is given by $\alpha' = \text{ALPHA1}\ e^{-\frac{B1}{E}}$

ALPHA2, B2 : hole ionization rate constants: adjusted ionization rate for $E \leq 4 \times 10^5$ V/cm is given by $\beta_1' = \text{ALPHA2}\ e^{-\frac{B2}{E}}$

ALPHA3, B3 : hole ionization rate constants: adjusted ionization rate for $E > 4 \times 10^5$ V/cm is given by $\beta_2' = \text{ALPHA3}\ e^{-\frac{B3}{E}}$

PHI : ϕ, junction built-in potential

DV : $dV = -q \int_{x_k}^{x_k+\Delta x_k} E(x)\, dx$, where Δx_k is the length of the k-th interval in the $E(x)$ vs. x diagram

Reproduced with permission of the copyright owner. Further reproduction prohibited without permission.

TV : tunneling potential

EV : electron threshold potential for ionization

HV : hole threshold potential for ionization

SLOPE : the tunneling current, I_t, is given by

$$I_t = I_o e^{-\frac{SLOPE}{\sqrt{V_r + \phi}}}$$

VREV : reverse voltage for which DC multiplication will be calculated

The different portions for the program perform the following computations. Statements 29 to 66 divide the p and n sides of the electric field triangle into equipotential intervals, DXN(K), DXP(K), and compute the electric field values, EN(K), EP(K), at the end points of the intervals. Statements 67 to 95 number these quantities consecutively, starting on the p side with the first interval and the first electric field value. Statements 96 to 164 compute the approximate values of the ionization probabilities for electrons and holes, $dP_n(k)$ = XINTN(K) and $dP_n(k)$ = XINTP(K), in each interval, DX(K). The spatial distribution of the tunneling current, $dI_t(k)$ = TI(K), is computed in statements 173 to 219.

The electron initiated multiplication is calculated in statements 220 to 241, 251 to 266, and 276 to 287. Statements 220 to 225 shift the tunneling current by $\frac{TV}{DV}$ intervals to obtain the free electron current. (In "conventional calculations" TV is set to one DV.) The book-

Reproduced with permission of the copyright owner. Further reproduction prohibited without permission.

keeping algorithms which trace the electrons and holes back and forth across the SCR and compute the DC multiplication on each transit are contained in statements 237 to 241 and 262 to 266. (If the available storage is sufficiently large, the encremental increase in current, DIE(N) and DIH(N), resulting from carrier multiplication in each interval can be replaced by DI(K,N), where K is the transit number and N is the interval number. Combining Σ_k DI(K,N) with the interval number as function of distance then yields the distribution of carrier multiplication as function of distance across the SCR.)

Statements 242 to 250 and 267 to 275 retrieve and save the electron multiplication in each interval on the 10-th and 12-th transits, and the hole multiplication on the 11-th and 13-th transits. These quantities are used later in the program to compute the values of $\bar{a}_1$, $\bar{a}_2$, and $\bar{a}_3$, the first, second, and third ionization probabilities. (There is nothing special about these transits. Any other corresponding set of transits for which the multiplication has achieved a steady state condition would do as well.)

The multiplication initiated by holes left in the valence band when electrons tunnel to the conduction band is calculated in statements 293 to 338. They are essentially mirror images of the statements handling the electron initiated multiplication. The total DC multiplication is then the sum of the electron initiated and the hole initiated multi-

Reproduced with permission of the copyright owner. Further reproduction prohibited without permission.

plication. It is denoted by SUM and computed in statement 342. This ends the DC multiplication simulation.

The remainder of the program is devoted to the calculation of the ionization probabilities, $\bar{a}_1$, $\bar{a}_2$, $\bar{a}_3$, and to the evaluation of the final results of the up to two ionization per SCR transit noise theory.

The electron ionization probabilities are computed in statements 345 to 421. The probability of the first ionization, $\bar{a}_1$, is computed by taking the multiplication due to holes on the 11-th and 13-th transits and calculating the electron ionizations on the 12-th and 14-th transits, allowing no more than one ionization. This is performed in statements 345 to 356 and 379 to 390. The square root of the ratio of the first electron ionizations on the 14-th transit, E1, to the first electron ionizations on the 12-th transit, D1, is $\bar{a}_1$. If this calculation is repeated starting with the first electron ionizations on the 12-th and 14-th transits (the results of the computation just completed), as done in statements 358 to 367 and 391 to 401, $\bar{a}_2$ is obtained. Repeating the calculations once more in statements 368 to 378 and 402 to 412 leads to $\bar{a}_3$.

The corresponding hole ionization probabilities are computed in the same manner, but starting with the electron multiplication on 10-th and 12-th transits. These calculations are carried out in statements 452 to 519.

Reproduced with permission of the copyright owner. Further reproduction prohibited without permission.

Because the two ionizations noise theory does not distinguish between electron and hole ionization probabilities, it is now necessary to evaluate the "average" ionization probabilities to be used in the noise theory. They are simply the square root of the product of the electron and hole ionization probabilities, as given in statements 558 to 560.

According to Appendix B, the probability of the second ionization on the first transit is zero for all reverse voltages for which the probability of the third ionization is zero. Hence, $\bar{a}_{11} = S(2)$, the probability of ionization on the first transit.

Now, that the ionization probabilities $\bar{a}_{11}$, $\bar{a}_1$ and $\bar{a}_2$ are known, the theoretical expressions for noise resulting from up to two ionizations per carrier transit across the SCR may be evaluated. This is performed in statements 561 to 577. This completes the program.

The calculations described above yield the following ionization probabilities for the 1N751 diode:

Diode reverse voltage	$\bar{a}_{11}$	$\bar{a}_1$	$\bar{a}_2$
5.05	0.485	0.909	0.114
5.0	0.474	0.897	0.107
4.95	0.462	0.886	0.0994
4.9	0.451	0.874	0.0926
4.8	0.428	0.851	0.0796
4.7	0.403	0.829	0.0676

Reproduced with permission of the copyright owner. Further reproduction prohibited without permission.

Diode reverse voltage	$\bar{a}_{11}$	$\bar{a}_1$	$\bar{a}_2$
4.6	0.378	0.807	0.0567
4.5	0.353	0.786	0.0469
4.4	0.327	0.766	0.0381
4.3	0.299	0.746	0.0304
4.2	0.273	0.728	0.0237
4.1	0.245	0.710	0.0180
4.0	0.218	0.693	0.0133
3.9	0.190	0.677	0.0094
3.8	0.163	0.661	0.0064

The range and functional dependence of the above values are typical of the other diodes employed in this study. Consequently, the approximation that $\bar{a}_2 << \bar{a}_1$, invoked in the derivation of the up to two ionizations per SCR transit noise theory, is justified.

Reproduced with permission of the copyright owner. Further reproduction prohibited without permission.

```
      DIMENSION  XN(600),VN(600),EMAX(600),DXN(600),EN(600),DXP(600),
     1XP(600),VP(600),EP(600),E( 900),XINTN( 900),XINTP( 900),DX( 900),
     2VREV(30),TI(900),                S(301),SDIN(900),SDI(900),SSDI(900),
     3DIE(1200),DIM(1200)
      READ 13, NSETS,NVREV
   13 FORMAT(2I2)
      DO 1000 NS=1,NSETS
      READ10, XNA,XND,ALPHA1,B1,ALPHA2,B2,ALPHA3,B3
   10 FORMAT(2E9.2,6E7.3)
      READ 11, PHI,DV,TV,EV,HV,SLOPE
   11 FORMAT(5F5.3,F10.7)
      READ 12, (VREV(I),I=1,NVREV)
   12 FORMAT(16F5.3)
      PRINT 14,(VREV(I),I=1,NVREV)
   14 FORMAT('1VREV'  ',I4(1X,F5.3,2X))
      EPSREL=11.7
      EPSO=8.86E-14
      G=1.6E-19
      W1=SQRT((2.*EPSREL*EPSO/G)*((XNA+XND)/(XNA*XND)))
      DO 1000 NV=1,NVREV
      W=W1*SQRT(PHI+VREV(NV))
      G=2.*SLOPE/W1
      EMAXX=(2.*SQRT(PHI+VREV(NV)))/W1
      IF(EMAXX.GE. 1.2E4) GO TO 98
      PRINT 97
   97 FORMAT(1X,'MAXIMUM FIELD VALUE TOO SMALL')
      STOP
   98 XNN=(XNA/(XNA+XND))*W
      XPP=W-XNN
      VNN=(XNA/(XNA+XND))*(PHI+VREV(NV))
      VPP=PHI+VREV(NV)-VNN
C     COMPUTE DX AND E FOR N SIDE
      XN(1)=XNN
      VN(1)=VNN
      EMAX(1)=EMAXX
      K=VNN/DV
      IF (K-1) 101,99,99
   99 DO 100 II=1,K
      JJ=II+1
      DXN(II)=XN(II)*(1.-SQRT(1.-DV/VN(II)))
      EN(II)=EMAX(II)*(1.-DXN(II)/XN(II))
      VN(JJ)=VN(II)-DV
      XN(JJ)=XN(II)-DXN(II)
      EMAX(JJ)=EN(II)
  100 CONTINUE
      DXN(K+1)=2.*(VNN-K*DV)/EN(K)
      GO TO 102
  101 CONTINUE
      JJ=1
      DXN(JJ)=2.*VNN/EMAXX
C     COMPUTE DX AND E FOR P SIDE
  102 XP(1)=XPP
      VP(1)=VPP
      EMAX(1)=EMAXX
      H=VPP/DV
      IF (H-1) 201,199,199
  199 DO 200 I=1,H
      J=I+1
      DXP(I)=XP(I)*(1.-SQRT(1.-DV/VP(I)))
      EP(I)=EMAX(I)*(1.-DXP(I)/XP(I))
      VP(J)=VP(I)-DV
      XP(J)=XP(I)-DXP(I)
      EMAX(J)=EP(I)
  200 CONTINUE
      GO TO 202
  201 J=1
      DXP(J)=2.*VPP/EMAXX
      GO TO 203
  202 CONTINUE
      DXP(H+1)=2.*(VPP-H*DV)/EP(H)
  203 CONTINUE
C     RENUMBER DX
      JN=H+1
      II=H+1
      DO 300 N=1,II
      DX(N)=DXP(JN)
```

Reproduced with permission of the copyright owner. Further reproduction prohibited without permission.

```
0071                 JN=JN-1
0072          300    CONTINUE
0073                 JJJ=M+K+2
0074                 JA=M+2
0075                 JI=1
0076                 DO 310 N=JA,JJJ
0077                 DX(N)=DXN(JI)
0078                 JI=JI+1
0079          310    CONTINUE
              C      RENUMBER E
0080                 IF (M  ) 321,321,319
0081          319    JN=M
0082                 JN=M
0083                 DO 320 NE=1,JG
0084                 E(NE)=EP(JN)
0085                 JN=JN-1
0086          320    CONTINUE
0087          321    E(M+1)=EMAXX
0088                 IF (K  ) 330,330,322
0089          322    JE=M+2
0090                 JEE=M+K+1
0091                 JP=1
0092                 DO 330 NE=JE,JEE
0093                 E(NE)=EN(JP)
0094                 JP=JP+1
0095          330    CONTINUE
              C      COMPUTE IONIZATION SUBINTEGRALS FOR ELECTRONS
              CCC    COMPUTE START AND STOP POINTS FOR TRAPEZOID METHOD OF APPROXIMATING
              C      SUBINTEGRALS
0096                 B=AMAX1(B1,B2,B3)
0097                 II=M+1
0098                 IJJ=M+1
0099          331    DO 340 I=1,II
0100                 KESTAR=I
0101                 BOE=B/E(I)
0102                 IF(BOE.LE.100.) GO TO 341
0103          340    CONTINUE
0104          341    DO 342 I=1,IIJ
0105                 KESTOP=JJJ-I
0106                 BOE=B/E(KESTOP)
0107                 IF(BOE.LE.100.) GO TO 343
0108          342    CONTINUE
              C      SET XINTN'S AND XINTP'S TO ZERO FOR FIELD VALUES WHICH ARE TOO SMALL
0109          343    II=KESTAR-1
0110                 IF(II.LE.0) GO TO 345
0111                 KK=I-1
0112                 DO 344 I=1,KK
0113                 XINTN(I)=0
0114                 XINTP(I)=0
0115                 II=II-1
0116                 IF(II.LE.0) GO TO 345
0117          344    CONTINUE
0118          345    II=KESTOP+2
0119                 IF(JJJ-KESTOP-1 .LE.0) GO TO 347
0120                 KK=K+1
0121                 DO 346 I=1,KK
0122                 XINTN(I)=0
0123                 XINTP(I)=0
0124                 II=II+1
0125                 IF(JJJ-II.LT.0) GO TO 347
0126          346    CONTINUE
              C      TRIANGLE APPROXIMATION FOR FIRST AND LAST NON ZERO XINTN.
0127          347    XINTN(KESTAR)=(DX(KESTAR)*ALPHA1*EXP(-B1/E(KESTAR)))/2.
0128                 XINTN(KESTOP+1)=(DX(KESTOP+1)*ALPHA1*EXP(-B1/E(KESTOP+1)))/2.
              C      TRAPEZOID METHOD USED FOR REMAINING  XINTN'S
0129                 IF(KESTOP-KESTAR .LT. 1) GO TO 401
0130                 II=KESTOP-1
0131                 DO 400 I=KESTAR,II
0132                 J=I+1
0133                 XINTN(J)=DX(J)*ALPHA1*(EXP(-B1/E(I))+EXP(-B1/E(J)))/2.
0134          400    CONTINUE
              C      COMPUTE FIRST NON ZERO XINTP
0135          401    IF(E(KFSTAR).LE. 0.65) GO TO 402
0136                 XINTP(KESTAR)=(DX(KESTAR)*ALPHA3*EXP(-B3/E(KESTAR)))/2.
0137                 GO TO 403
0138          402    XINTP(KESTAR)=(DX(KESTAR)*ALPHA2*EXP(-B2/E(KESTAR)))/2.
```

Reproduced with permission of the copyright owner. Further reproduction prohibited without permission.

```
C     COMPUTE LAST NON ZERO XINTP
403   IF(E(KESTOP+1) .LE. 4.E5) GO TO 404
      XINTP(KESTOP+1)=(DX(KESTOP+1)*ALPHA3*EXP(-B3/E(KESTOP)))/2.
      GO TO 412
404   XINTP(KESTOP+1)=(DX(KESTOP+1)*ALPHA2*EXP(-B2/E(KESTOP)))/2.
C     USE TRAPEZOID APPROXIMATION FOR REMAINING XINTP'S WHILE CONSIDERING FIELD
C     VALUES.
412   IF(KESTOP - KESTAR .LT. 1) GO TO 501
      II=KESTOP -1
      DO 500 I=KESTAR,II
      J=I+1
      IF(E(I) .LE. 4.E5) GO TO 451
450   XINTP(J)=DX(J)*ALPHA3*(EXP(-B3/E(I))+EXP(-B3/E(J)))/2.
      GO TO 500
451   XINTP(J)=DX(J)*ALPHA2*(EXP(-B2/E(I))+EXP(-B2/E(J)))/2.
500   CONTINUE
501   CONTINUE
      PRINT 19, VREV(NV)
19    FORMAT('1',T2,'VREV = ',F5.3)
      PRINT 15, XNA,XND,ALPHA1,B1,ALPHA2,B2,ALPHA3,B3
15    FORMAT(/T4,'XNA',T19,'XND',T32,'ALPHA',T49,'BETA',/4(1X,E10.4,4X)/
     1T32,2(E10.4,5X)/T32,2(E10.4,5X))
      PRINT 16, PHI,DV,TV,EV,HV
16    FORMAT(/1X,'PHI = ',F5.3,5X,'DV = ',F5.3,5X,'TV = ',F5.3,5X,'EV =
     1',F5.3,5X,'HV = ',F5.3)
      PRINT 18, M
18    FORMAT(/,1X,'M = ',I3)
      PRINT 17, EMAXX
17    FORMAT(/,1X,'PEAK FIELD IN JUNCTION = ',E10.4,3X,'VOLTS/CM')
      PRINT 32,W
32    FORMAT(/,1X,'JUNCTION WIDTH = ',E10.4,3X,'CM')
C     PRINT STATEMENT FOR DX,XINTN,XINTP,AND E GOES HERE
      NTO=TV/DV+1.
      NTT=NTO+1
      NFO=EV/DV+1.
      NET=NEO+1
      NHO=HV/DV+1.
      JHO=JJJ+NHO
      JMO=JJJ-1
      JMHO=JJJ-NHO
C     COMPUTE DISTRIBUTION OF TUNNELING PROBABILITY
C     COMPUTE START AND STOP POINTS FOR TRAPEZOID METHOD OF APPROX SUBINTEGRALS
      II=M+1
      IIJ=K+1
      DO 502 I=1,II
      KESTAR=I
      BOE=G/E(I)
      IF (BOE.LE.50.) GO TO 503
502   CONTINUE
503   DO 504 I=1,IIJ
      KESTOP=JJJ-I
      BOE=G/E(KESTOP)
      IF (BOE.LE.50.) GO TO 505
504   CONTINUE
C     SET TUNNELING PROBABILITY TO ZERO FOR SMALL FIELD VALUES
505   II=KESTAR-1
      IF(II.LE.0) GO TO 507
      KK=M+1
      DO 506 I=1,KK
      TI(II)=0.
      II=II-1
      IF (II.LE.0) GO TO 507
506   CONTINUE
507   CONTINUE
      II=KESTOP+2
      IF (JMO-KESTOP.LE.0) GO TO 509
      KK=K+1
      DO 508 I=1,KK
      TI(II)=0.
      II=II+1
      IF (JJJ-II.LT.0) GO TO 509
508   CONTINUE
509   CONTINUE
C     TRIANGLE APPROXIMATION FOR FIRST AND LAST TUNNELING SUBINTEGRAL
      TI(KESTAR)=(DX(KESTAR)*EXP(-G/E(KESTAR)))/2.
      TI(KESTOP+1)=(DX(KESTOP+1)*EXP(-G/E(KESTOP)))/2.
```

Reproduced with permission of the copyright owner. Further reproduction prohibited without permission.

```
                C       TRAPEZOID APPROX FOR REMAINING SUBINTEGRALS
0205                    IF (KESTOP-KESTAR,LT,1) GO TO 511
0206                    II=KESTOP+1
0207                    DO 510 I=KESTAR,II
0208                    J=I+1
0209                    TI(I)=(DX(J)*(EXP(-G/E(I))+EXP(-G/E(J))))/2.
0210            510     CONTINUE
0211            511     CONTINUE
                C       NORMALIZE TUNNELING PROBABILITY FOR EACH SUBINTERVAL
0212                    SUMTP=0.
0213                    DO 512 I=1,JJJ
0214                    SUMTP=SUMTP+TI(I)
0215            512     CONTINUE
0216                    II=KESTOP+1
0217                    DO 513 I=KESTAR,II
0218                    TI(I)=TI(I)/SUMTP
0219            513     CONTINUE
                C       TUNNELING PROBABILITY PRINT STATEMENTS GO HERE
                C       ELECTRON INITIATED MULTIPLICATION
                C       SHIFT TUNNELING PROBABILITY TO OBTAIN TUNNELING CURRENT
0220                    DO 550 N=1,NTO
0221                    DIE(N)=0.
0222            550     CONTINUE
0223                    DO 551 N=NTT,JJJ
0224                    DIE(N) =TI(N-NTO)
0225            551     CONTINUE
0226                    S(1)=0.
0227                    DO 552 N=NTT,JJJ
0228                    S(1)=S(1)+DIE(N)
0229            552     CONTINUE
                C       COMPUTE ELECTRON INITIATED MULTIPLICATION
0230                    DO 580 K=2,200,2
0231                    KK=K
0232                    KM=K-1
0233                    DO 560 N=1,NEO
0234                    DIM(N)=0.
0235            560     CONTINUE
0236                    RI=0.
0237                    DO 561 N=NET,JJJ
0238                    XI=RI+DIE(N-NEO)+2.*DIM(N-NEO)
0239                    DIM(N) =XINTN(N)*XI
0240                    RI=XI-DIM(N)
0241            561     CONTINUE
0242                    IF (K-10) 563,520,522
0243            520     DO 521 N=1,JJJ
0244                    VM(N)=DIM(N)
0245            521     CONTINUE
0246                    GO TO 563
0247            522     IF (K-12) 563,523,563
0248            523     DO 524 N=1,JJJ
0249                    VP(N)=DIM(N)
0250            524     CONTINUE
0251            563     S(K)=0.
0252                    DO 562 N=NET,JJJ
0253                    S(K)=S(K)+DIM(N)
0254            562     CONTINUE
0255                    IF(S(K),LE.1.E-9) GO TO 581
0256                    KP=K+1
0257                    KK=KP0
0258                    DO 570 N=JMHO,JJJ
0259                    DIE(N)=0.
0260            570     CONTINUE
0261                    RI=0.
0262                    DO 571 N=NNO,JMO
0263                    XI=RI+DIM(JMO-N)+2.*DIE(JMO-N)
0264                    DIE(JJJ-N)   =XINTP(JJJ-N)*XI
0265                    RI=XI-DIE(JJJ-N)
0266            571     CONTINUE
0267                    IF(K-10) 586,587,589
0268            587     DO 588 N=1,JJJ
0269                    XN(N)=DIE(N)
0270            588     CONTINUE
0271                    GO TO 586
0272            589     IF(K-12) 586,590,586
0273            590     DO 591 N=1,JJJ
0274                    XP(N)=DIE(N)
```

Reproduced with permission of the copyright owner. Further reproduction prohibited without permission.

```
0275          591   CONTINUE
0276          586   S(KPO)=0.
0277                DO 572 N=1,JMHO
0278                S(KPO)=S(KPO)+DIE(N)
0279          572   CONTINUE
0280                IF(S(KPO)/S(2).LT.0.002)GO TO 581
0281          580   CONTINUE
0282          581   CONTINUE
0283                STEST=S(2)
0284                A11=S(2)
0285                SN=0.
0286                DO 585 N=2,KK
0287                SN=SN+S(N)
0288          585   CONTINUE
0289                PRINT 21, SN
0290          21    FORMAT(///,1X,'ELFCTRON INITIATED MULTIPLICATION',///,T2,
                   1'SN = ',E10.4)
0291                PRINT 20, (N, S(N),          N=1,KK)
0292          20    FORMAT(//(T2,'S(',I3,') = ',E10.4))
              C     HOLE INITIATED MULTIPLICATION
              C     TRANSFER TUNNELING PROBABILITY TO DIH(N)
0293                DO 600 N=1,JJJ
0294                DIH(N) =TI(N)
0295          600   CONTINUE
0296                S(1)=0.
0297                DO 601 N=1,JJJ
0298                S(1)=S(1)+DTH(N)
0299          601   CONTINUE
              C     COMPUTE HOLE INITIATED MULTIPLICATION
0300                DO 640 K=2,100,2
0301                KK=K
0302                KMO=K-1
0303                DO 610 N=JMHO,JJJ
0304                DIE(N)=0.
0305          610   CONTINUE
0306                RI=1.
0307                DO 611 N=NMHO,JMO
0308                XI=RI+DTH(JMO-N)+2.*DIE(JMO-N)
0309                DIE(JJJ-N) =XINTP(JJJ-N)*XI
0310                RI=XI-DIE(JJJ-N)
0311          611   CONTINUE
0312                S(K)=0.
0313                DO 612 N=1,JMHO
0314                S(K)=S(K)+DIE(N)
0315          612   CONTINUE
0316                IF(S(K).LE.1.E-5) GO TO 641
0317                KPO=K+1
0318                KKE=KPO
0319                DO 620 N=1,NEO
0320                DIH(N)=0.
0321          620   CONTINUE
0322                RI=0.
0323                DO 621 N=NFET,JJJ
0324                XI=RI+DIE(N-NEO)+2.*DTH(N-NEO)
0325                DTH(N)   =XINTN(N)*XI
0326                RI=XI-DTH(N)
0327          621   CONTINUE
0328                S(KPO)=0.
0329                DO 622 N=NFET,JJJ
0330                S(KPO)=S(KPO)+DTH(N)
0331          622   CONTINUE
0332                IF(S(KPO)/STEST.LT.0.01) GO TO 641
0333          640   CONTINUE
0334          641   CONTINUE
0335                SP=0.
0336                DO 650 N=2,KK
0337                SP=SP+S(N)
0338          650   CONTINUE
0339                PRINT 24, SP
0340          24    FORMAT(///,1X,'HOLE INITIATED MULTIPLICATION',///,T2,'SP = ',E10.4)
0341                PRINT 20, (N,S(N),          N=1,KK)
0342                SUM=SN+SP
0343                PRINT 26, SUM
0344          26    FORMAT(//////,T2,'SUM = SN + SP = ',E10.4)
0345                DO 730 N=1,JJJ
0346                DIE(N)=XN(N)
```

Reproduced with permission of the copyright owner. Further reproduction prohibited without permission.

```
      DIH(N)=0.
720   CONTINUE
721   RI=0.
      D1=0.
      DO 730 N=NET,JJJ
      XI=RI+DIE(N-NEO)
      DIH(N)=XINTN(N)*XI
      RI=XI-DIH(N)
      D1=D1+DIH(N)
730   CONTINUE
      DO 731 N=1,JJJ
      DIE(N)=0.
731   CONTINUE
      RI=0.
      D2=0.
      DO 740 N=NET,JJJ
      XI=RI+DIH(N-NEO)
      DIE(N)=XINTN(N)*XI
      RI=XI-DIE(N)
      D2=D2+DIE(N)
740   CONTINUE
      DO 741 N=1,JJJ
      DIH(N)=0.
741   CONTINUE
      RI=0.
      D3=0.
      DO 750 N=NET,JJJ
      XI=RI+DIE(N-NEO)
      DIH(N)=XINTN(N)*XI
      RI=XI-DIH(N)
      D3=D3+DIH(N)
750   CONTINUE
      DO 760 N=1,JJJ
      DIE(N)=XP(N)
      DIH(N)=0.
760   CONTINUE
      RI=0.
      E1=0.
      DO 770 N=NET,JJJ
      XI=RI+DIE(N-NEO)
      DIH(N)=XINTN(N)*XI
      RI=XI-DIH(N)
      E1=E1+DIH(N)
770   CONTINUE
      DO 771 N=1,JJJ
      DIE(N)=0.
771   CONTINUE
      RI=0.
      E2=0.
      DO 780 N=NET,JJJ
      XI=RI+DIH(N-NEO)
      DIE(N)=XINTN(N)*XI
      RI=XI-DIE(N)
      E2=E2+DIE(N)
780   CONTINUE
      DO 781 N=1,JJJ
      DIH(N)=0.
781   CONTINUE
      RI=0.
      E3=0.
      DO 790 N=NET,JJJ
      XI=RI+DIE(N-NEO)
      DIH(N)=XINTN(N)*XI
      RI=XI-DIH(N)
      E3=E3+DIH(N)
790   CONTINUE
      RATIO1=D2/D1
      RATIO2=D3/D1
      RATIO3=E2/E1
      RATIO4=E3/E1
      A1=SQRT(E1/D1)
      R1=A1
      A2=RATIO1*A1
      R2=A2
      RATIO5=A11/A1
      PRINT 789
```

Reproduced with permission of the copyright owner. Further reproduction prohibited without permission.

```
0423          789   FORMAT(//,1X,'NOISE PARAMETERS COMPUTED FROM ELECTRON IONIZATION')
0424                PRINT 799,A11
0425          799   FORMAT(/,1X,'A11= ',E10.4)
0426                PRINT 800,D1
0427          800   FORMAT(/,1X,'D1 = ',E10.4)
0428                PRINT 801,D2
0429          801   FORMAT(/,1X,'D2 = ',E10.4)
0430                PRINT 802,D3
0431          802   FORMAT(/,1X,'D3 = ',E10.4)
0432                PRINT 803,E1
0433          803   FORMAT(/,1X,'E1 = ',E10.4)
0434                PRINT 804,E2
0435          804   FORMAT(/,1X,'E2 = ',E10.4)
0436                PRINT 805,E3
0437          805   FORMAT(/,1X,'E3 = ',E10.4)
0438                PRINT 806,RATIO1
0439          806   FORMAT(/,1X,'D2/D1 = ',E10.4)
0440                PRINT 807,RATIO2
0441          807   FORMAT(/,1X,'D3/D1 = ',E10.4)
0442                PRINT 808,RATIO3
0443          808   FORMAT(/,1X,'E2/E1 = ',E10.4)
0444                PRINT 809,RATIO4
0445          809   FORMAT(/,1X,'E3/E1 = ',E10.4)
0446                PRINT 810,A1
0447          810   FORMAT(/,1X,'A1 = ',E10.4)
0448                PRINT 811,A2
0449          811   FORMAT(/,1X,'A2 = ',E10.4)
0450                PRINT 812,RATIO5
0451          812   FORMAT(/,1X,'A11/A1= ',E10.4)
0452                DO 830 N=1,JJJ
0453                DIE(N)=VP(N)
0454                DIH(N)=0.
0455          830   CONTINUE
0456                RI=0.
0457                QI=0.
0458                DO 831 N=NHO,JMO
0459                XI=RI+DIE(JHO-N)
0460                DIH(JJJ-N)=XINTP(JJJ-N)*XI
0461                RI=XI-DIH(JJJ-N)
0462                QI=QI+DIH(JJJ-N)
0463          831   CONTINUE
0464                DO 832 N=1,JJJ
0465                DIE(N)=0.
0466          832   CONTINUE
0467                RI=0.
0468                Q2=0.
0469                DO 840 N=NHO,JMO
0470                XI=RI+DIH(JHO-N)
0471                DIE(JJJ-N)=XINTP(JJJ-N)*XI
0472                RI=XI-DIE(JJJ-N)
0473                Q2=Q2+DIE(JJJ-N)
0474          840   CONTINUE
0475                DO 841 N=1,JJJ
0476                DIH(N)=0.
0477          841   CONTINUE
0478                RI=0.
0479                Q3=0.
0480                DO 850 N=NHO,JMO
0481                XI=RI+DIE(JHO-N)
0482                DIH(JJJ-N)=XINTP(JJJ-N)*XI
0483                RI=XI-DIH(JJJ-N)
0484                Q3=Q3+DIH(JJJ-N)
0485          850   CONTINUE
0486                DO 860 N=1,JJJ
0487                DIE(N)=VP(N)
0488                DIH(N)=0.
0489          860   CONTINUE
0490                RI=0.
0491                T1=0.
0492                DO 870 N=NHO,JMO
0493                XI=RI+DIE(JHO-N)
0494                DIH(JJJ-N)=XINTP(JJJ-N)*XI
0495                RI=XI-DIH(JJJ-N)
0496                T1=T1+DIH(JJJ-N)
0497          870   CONTINUE
0498                DO 871 N=1,JJJ
```

Reproduced with permission of the copyright owner. Further reproduction prohibited without permission.

```
      DIE(N)=0.
  871 CONTINUE
      RI=0.
      T2=0.
      DO 880 N=NHO,JHO
      XI=RI+DIE(JHO-N)
      DIE(JJJ-N)=XINTP(JJJ-N)*XI
      RI=XI-DIE(JJJ-N)
      T2=T2+DIE(JJJ-N)
  880 CONTINUE
      DO 881 N=1,JJJ
      DIH(N)=0.
  881 CONTINUE
      RI=0.
      T3=0.
      DO 890 N=NHO,JHO
      XI=RI+DIE(JHO-N)
      DIH(JJJ-N)=XINTP(JJJ-N)*XI
      RI=XI-DIH(JJJ-N)
      T3=T3+DIH(JJJ-N)
  890 CONTINUE
      PRINT 891
  891 FORMAT(//,1X,'NOISE PARAMETERS COMPUTED FROM HOLE IONIZATION')
      PRINT 900,Q1
  900 FORMAT(/,1X,'Q1 = ',E10.4)
      PRINT 901,Q2
  901 FORMAT(/,1X,'Q2 = ',E10.4)
      PRINT 902,Q3
  902 FORMAT(/,1X,'Q3 = ',E10.4)
      PRINT 903,T1
  903 FORMAT(/,1X,'T1 = ',E10.4)
      PRINT 904,T2
  904 FORMAT(/,1X,'T2 = ',E10.4)
      PRINT 905,T3
  905 FORMAT(/,1X,'T3 = ',E10.4)
      RAT1=Q2/Q1
      PRINT 906, RAT1
  906 FORMAT(/,1X,'Q2/Q1 = ',E10.4)
      RAT2=Q3/Q1
      PRINT 907,RAT2
  907 FORMAT(/,1X,'Q3/Q1 = ',E10.4)
      RAT3=T2/T1
      PRINT 908,RAT3
  908 FORMAT(/,1X,'T2/T1 = ',E10.4)
      RAT4=T3/T1
      PRINT 909,RAT4
  909 FORMAT(/,1X,'T3/T1 = ',E10.4)
      A1=SQRT(E1/T1)
      PRINT 910,A1
  910 FORMAT(/,1X,'A1 = ',E10.4)
      A2=RAT1*A1
      PRINT 911,A2
  911 FORMAT(/,1X,'A2 = ',E10.4)
      RATIO5=A11/A1
      PRINT 912,RATIO5
  912 FORMAT(/,1X,'A11/A1= ',E10.4)
      PRINT 913
  913 FORMAT(///,1X,'AVERAGED NOISE PARAMETERS')
      PRINT 799,A11
      A1=SQRT(R1*A1)
      PRINT 810,A1
      A2=SQRT(R2*A2)
      PRINT 811,A2
      X=A11
      Y=A1
      Z=A2
      B=1.+Y
      C=1.+Z
      D=1.-Y
      F=1.-Y*Z
      G=C/F
      H=B/F
      XMULT=(X/D**2)*(D*(D+Y*Z)*H+Y**2*(D+2.*Y*Z)*G)
      F20=(2.*X*Y**2*Z*G*H/D**3)*(D**2+D*B*(1.+Y*Z)+Y**2*Z*(3.+Y))
      F21=(2.*X*Y**2*G**2/D**4)*(D**3+D**2*(Y+Y*Z*(2.+5.*Y))+
     1Y**2*Z*D*(B+Y)*(3.-F)+2.*Y**4*Z**2*B)
```

Reproduced with permission of the copyright owner. Further reproduction prohibited without permission.

```
0574            F22=(2.*X*Y**2*G/(D**2*F))*(2.*D*F+Y*Z*(F*(3.*B+Y)+D*(C+4.*F)))
0575            F23=(2.*X*Y*Z*M/D**2)*(3.*D+Z*M)
0576            F24=(X/(D**2*F**2))*(D**2*(3.*G*Y+Y*Z*D)+Y*Z*(1.+3.*Y*C+Y**2*Z)+
               1Y**2*(1.+3.*Z*B+Y*Z**2)*(D+2.*Y*Z))
0577            XNOISE=F20+F21+F22+F23+F24
0578            PRINT 820,XMULT
0579      820   FORMAT(/,1X,'DC MULTIPLICATION FROM NOISE PARAMETERS = ',E10.4)
0580            PRINT 821,XNOISE
0581      821   FORMAT(/,1X,'NOISE MULTIPLICATION FACTOR = ',E10.4)
0582     1000   CONTINUE
0583            STOP
0584            END
```

Reproduced with permission of the copyright owner. Further reproduction prohibited without permission.

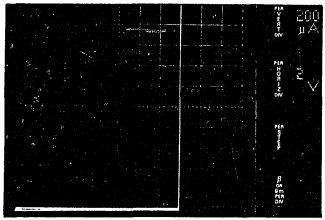

a. Dickson 1N3025

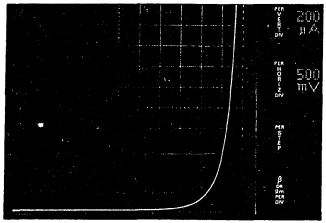

b. CDC 1N752

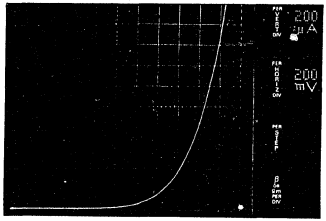

c. TI 1N4372

Figure 1. Typical voltage-current characteristics of commercially available diodes

Reproduced with permission of the copyright owner. Further reproduction prohibited without permission.

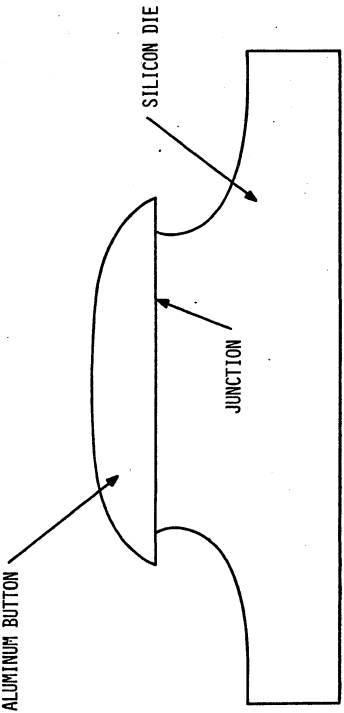

Figure 2. Diode vertical cross section

Reproduced with permission of the copyright owner. Further reproduction prohibited without permission.

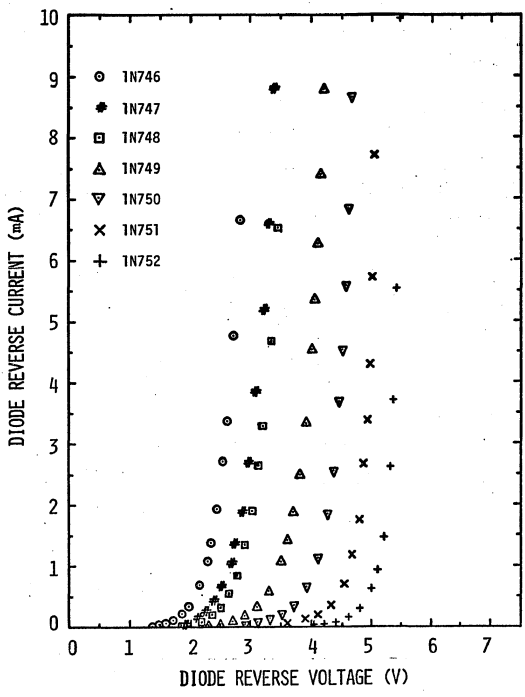

Figure 3. DC V-I characteristics of diodes employed in this study

Reproduced with permission of the copyright owner. Further reproduction prohibited without permission.

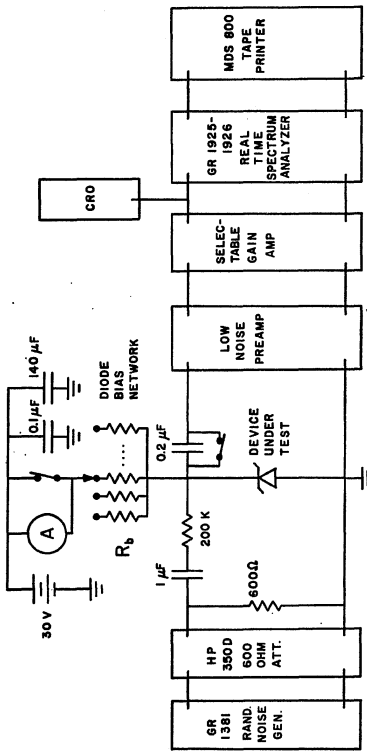

Figure 4. Diode noise measurement system

Reproduced with permission of the copyright owner. Further reproduction prohibited without permission.

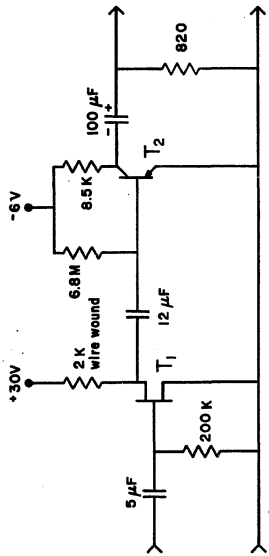

Figure 5. Low noise preamplifier

Reproduced with permission of the copyright owner. Further reproduction prohibited without permission.

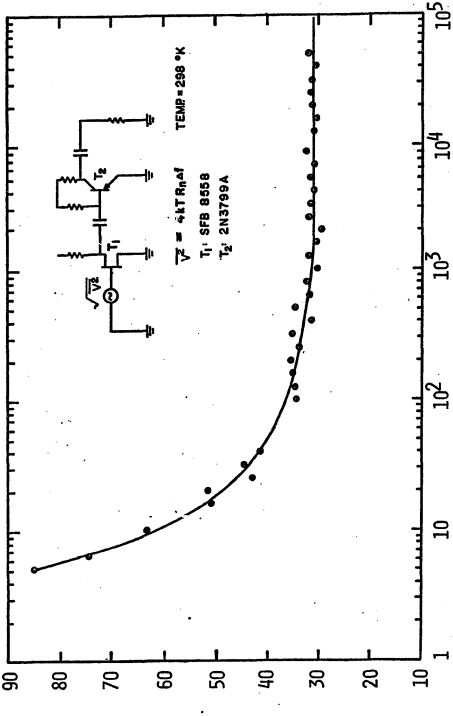

Figure 6. Preamplifier equivalent noise resistance

Reproduced with permission of the copyright owner. Further reproduction prohibited without permission.

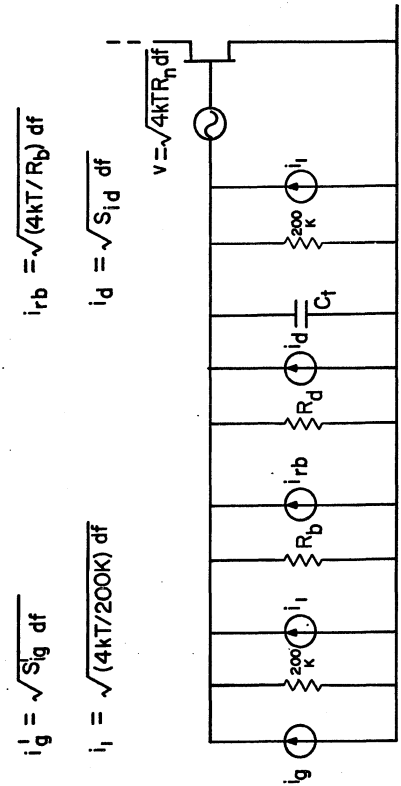

Figure 7. Noise measurement system equivalent input circuit

Reproduced with permission of the copyright owner. Further reproduction prohibited without permission.

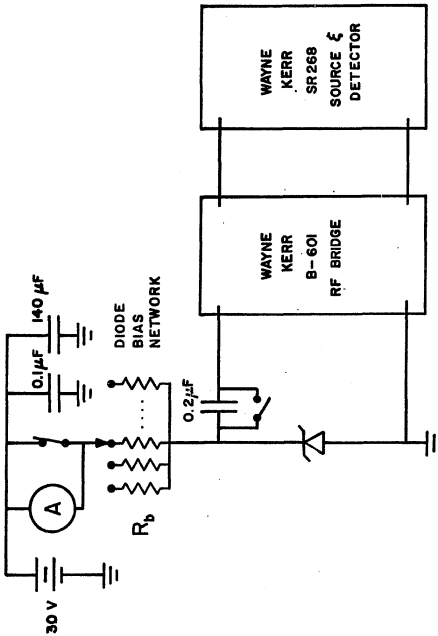

Figure 8. Diode dynamic impedance measurement setup

Reproduced with permission of the copyright owner. Further reproduction prohibited without permission.

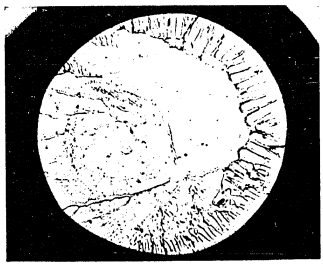

Scale: 1 cm = 3.13 x10^5 A

Figure 9. Typical alloy junction surface (diode 1N749)

Reproduced with permission of the copyright owner. Further reproduction prohibited without permission.

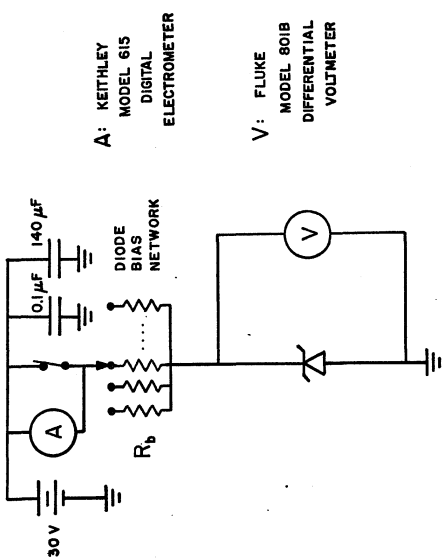

Figure 10. Diode DC V-I measurement setup

Reproduced with permission of the copyright owner. Further reproduction prohibited without permission.

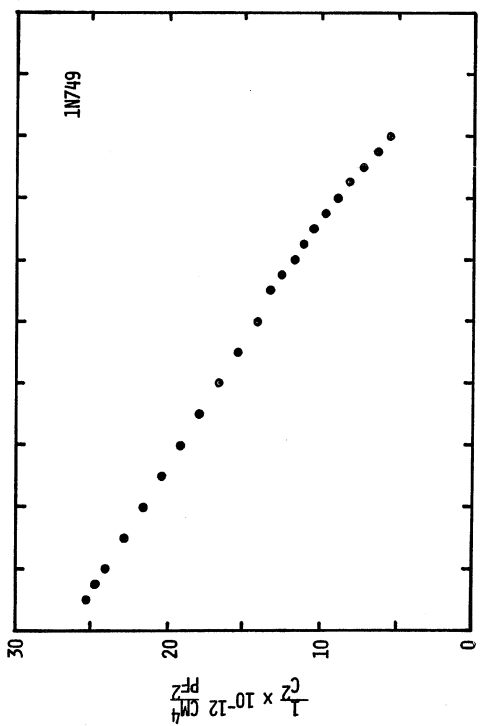

Figure 11. Junction capacitance: diode 1N749

Reproduced with permission of the copyright owner. Further reproduction prohibited without permission.

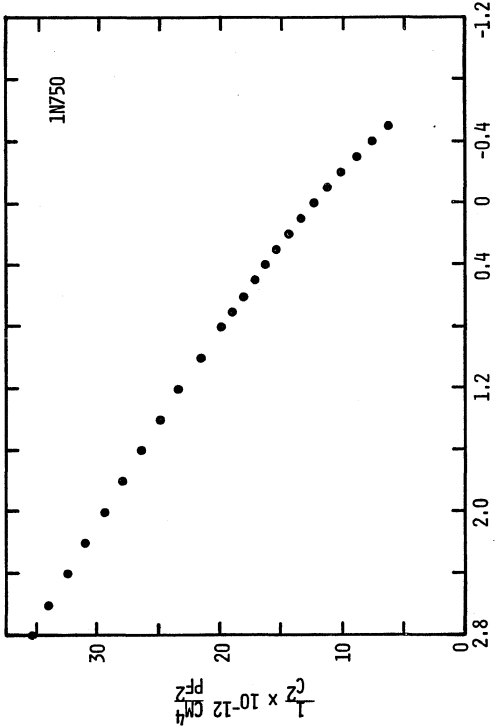

Figure 12. Junction capacitance: diode 1N750

Reproduced with permission of the copyright owner. Further reproduction prohibited without permission.

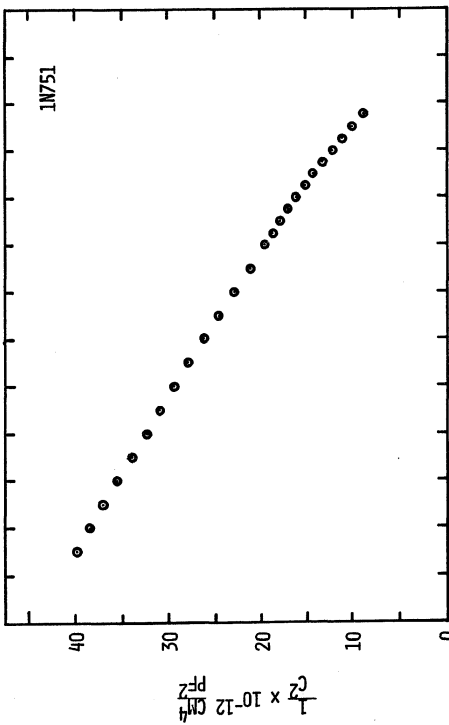

Figure 13. Junction capacitance: diode 1N751

Reproduced with permission of the copyright owner. Further reproduction prohibited without permission.

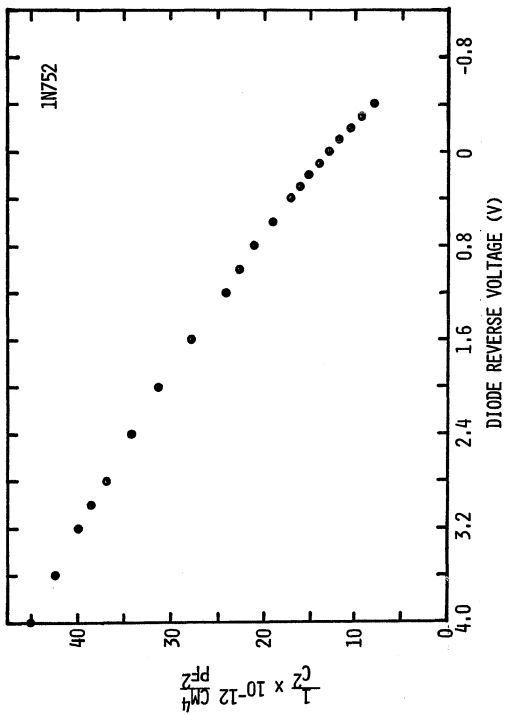

Figure 14. Junction capacitance: diode 1N752

Reproduced with permission of the copyright owner. Further reproduction prohibited without permission.

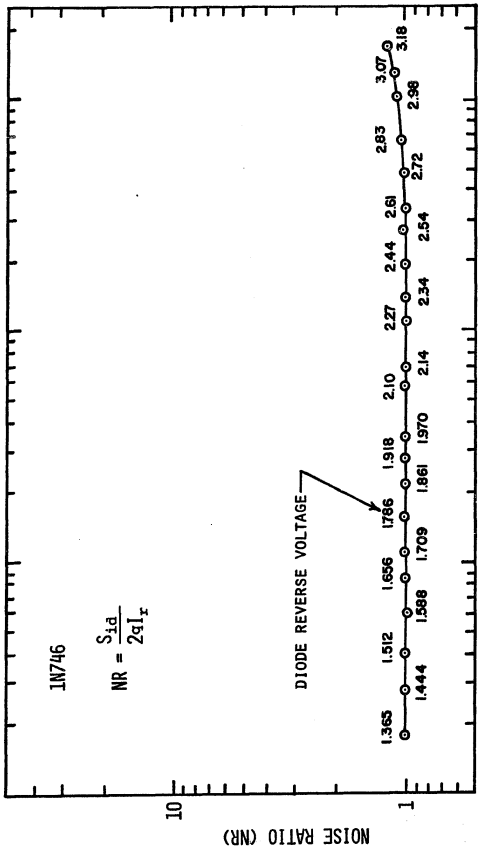

Figure 15. Noise ratio: diode 1N746

Reproduced with permission of the copyright owner. Further reproduction prohibited without permission.

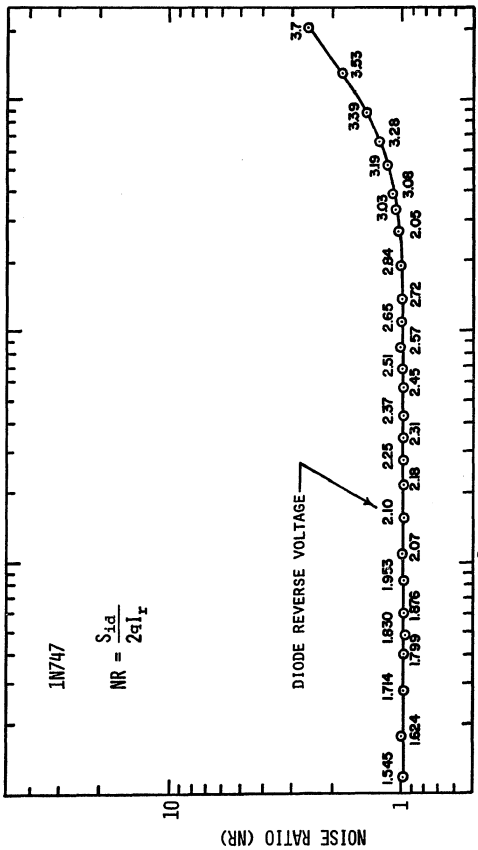

Figure 16. Noise ratio: diode 1N747

Reproduced with permission of the copyright owner. Further reproduction prohibited without permission.

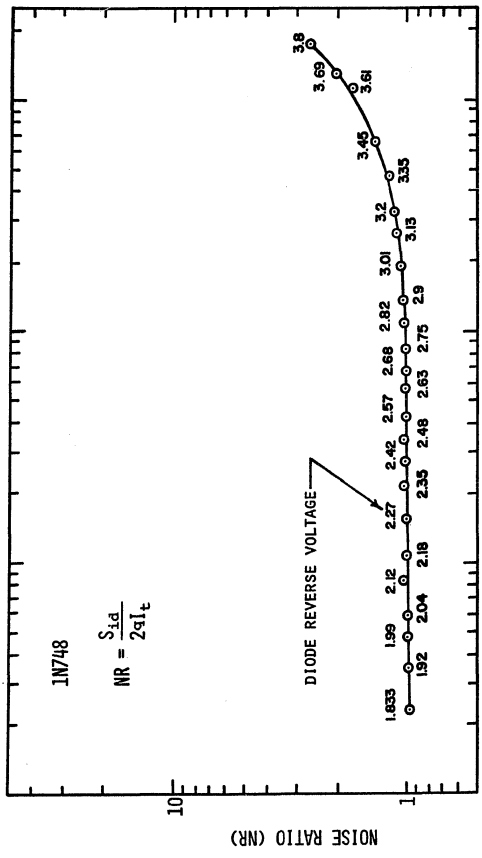

Figure 17. Noise ratio: diode 1N748

Reproduced with permission of the copyright owner. Further reproduction prohibited without permission.

Reproduced with permission of the copyright owner. Further reproduction prohibited without permission.

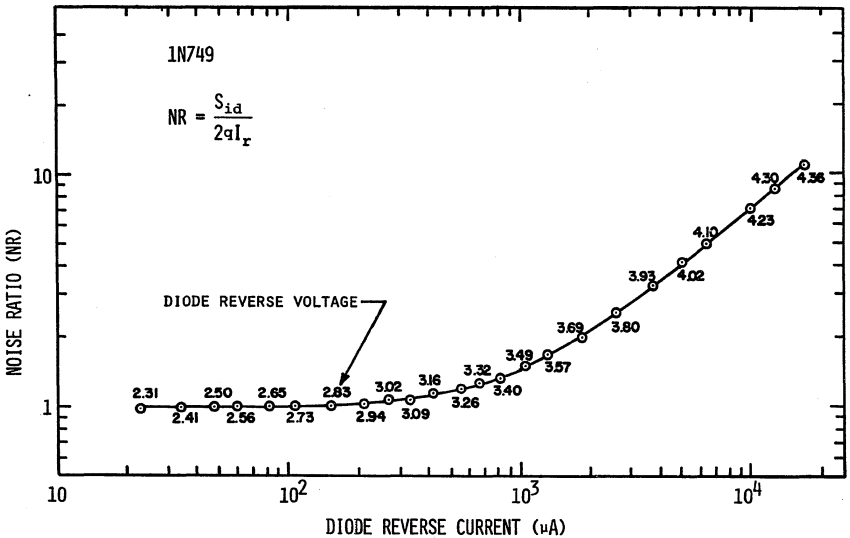

Figure 18. Noise ratio: diode 1N749

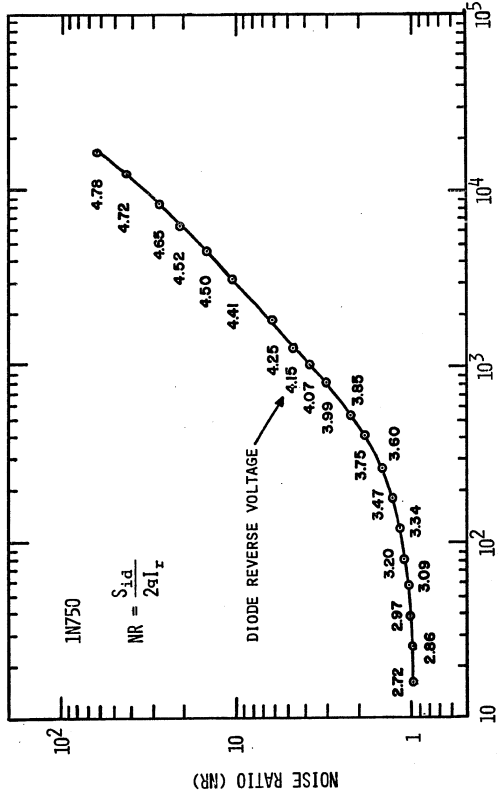

Figure 19. Noise ratio: diode 1N750

Reproduced with permission of the copyright owner. Further reproduction prohibited without permission.

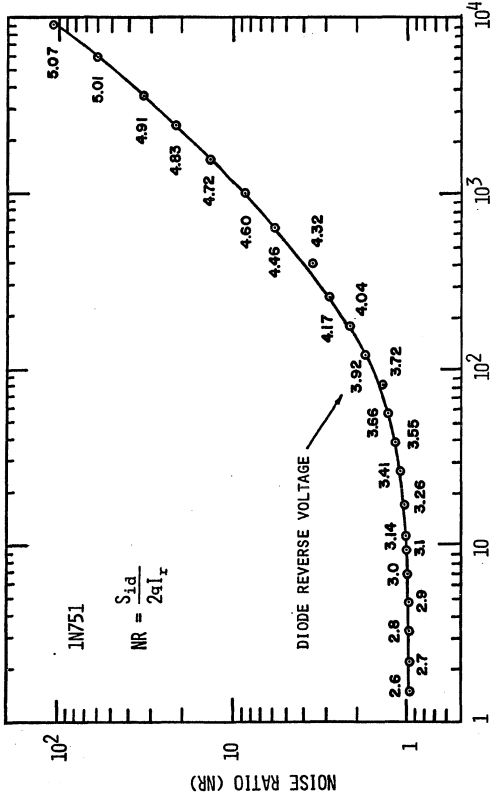

Figure 20. Noise ratio: diode 1N751

Reproduced with permission of the copyright owner. Further reproduction prohibited without permission.

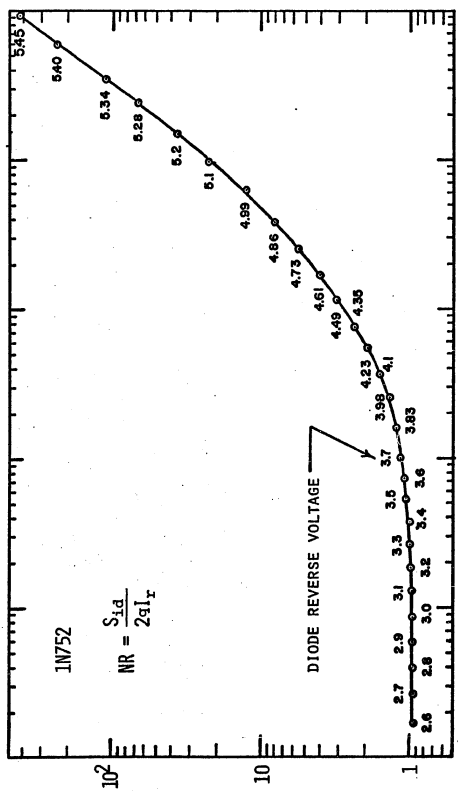

Figure 21. Noise ratio: diode 1N752

Reproduced with permission of the copyright owner. Further reproduction prohibited without permission.

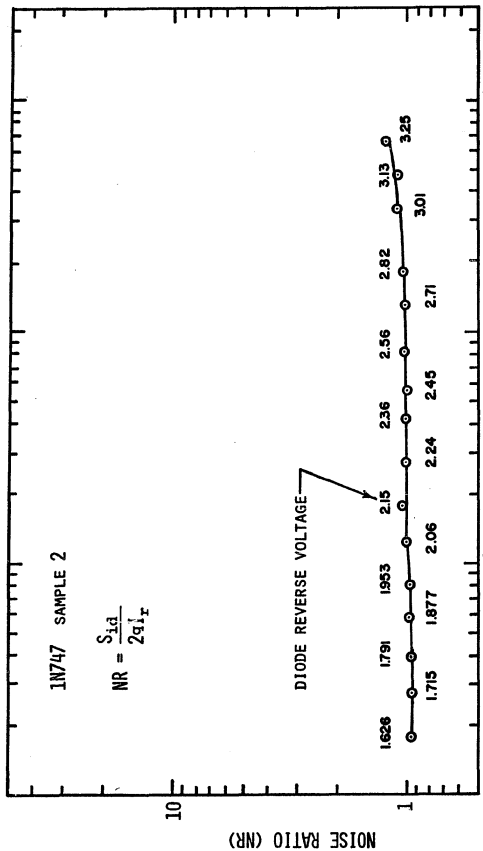

Figure 21a. Noise ratio: diode 1N747, sample 2

Reproduced with permission of the copyright owner. Further reproduction prohibited without permission.

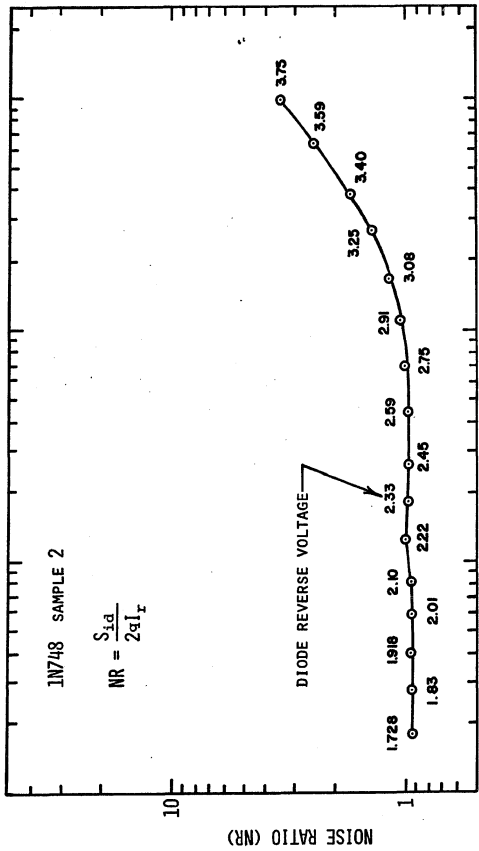

Figure 21b. Noise ratio: diode 1N748, sample 2

Reproduced with permission of the copyright owner. Further reproduction prohibited without permission.

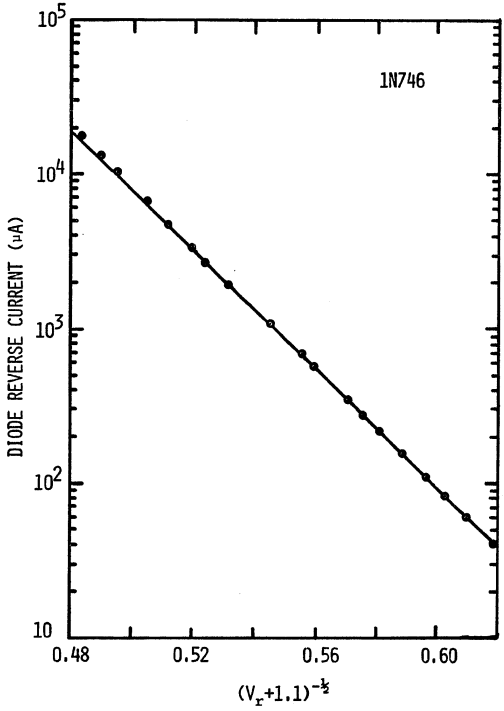

Figure 22. Reverse V-I characteristic: diode 1N746

Reproduced with permission of the copyright owner. Further reproduction prohibited without permission.

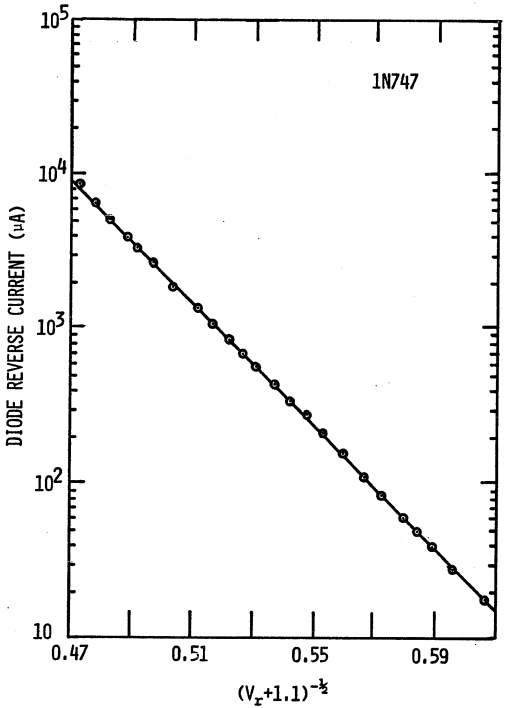

Figure 23. Reverse V-I characteristic: diode 1N747

Reproduced with permission of the copyright owner. Further reproduction prohibited without permission.

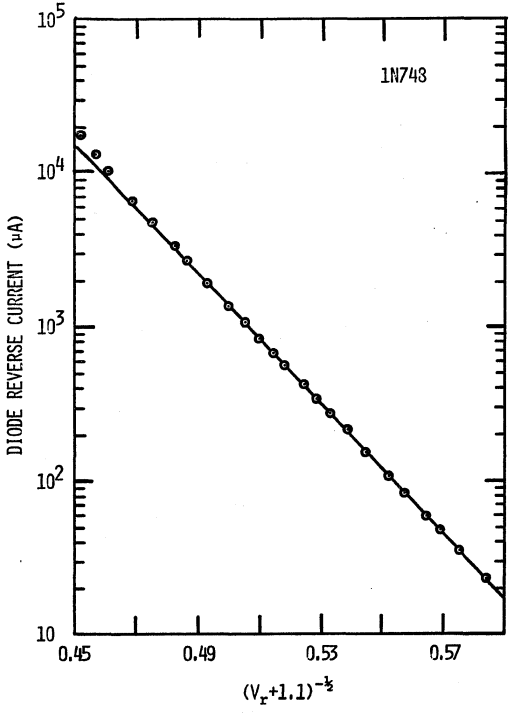

Figure 24. Reverse V-I characteristic: diode 1N748

Reproduced with permission of the copyright owner. Further reproduction prohibited without permission.

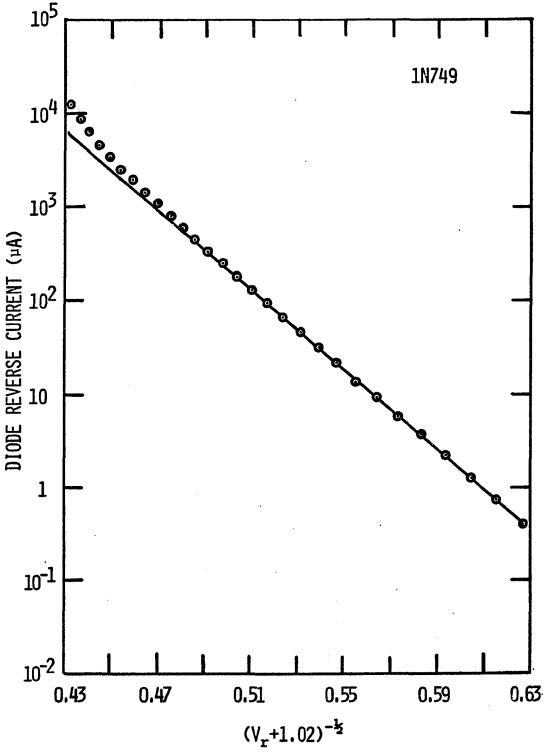

Figure 25. Reverse V-I characteristic: diode 1N749

Reproduced with permission of the copyright owner. Further reproduction prohibited without permission.

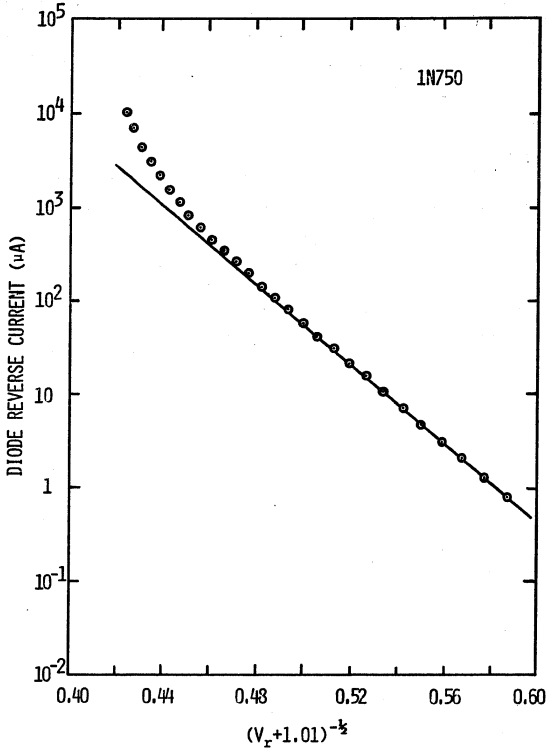

Figure 26. Reverse V-I characteristic: diode 1N750

Reproduced with permission of the copyright owner. Further reproduction prohibited without permission.

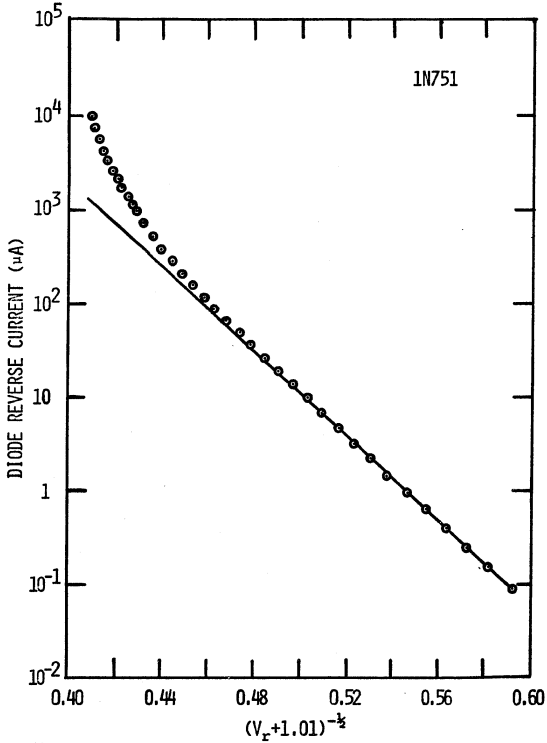

Figure 27. Reverse V-I characteristic: diode 1N751

Reproduced with permission of the copyright owner. Further reproduction prohibited without permission.

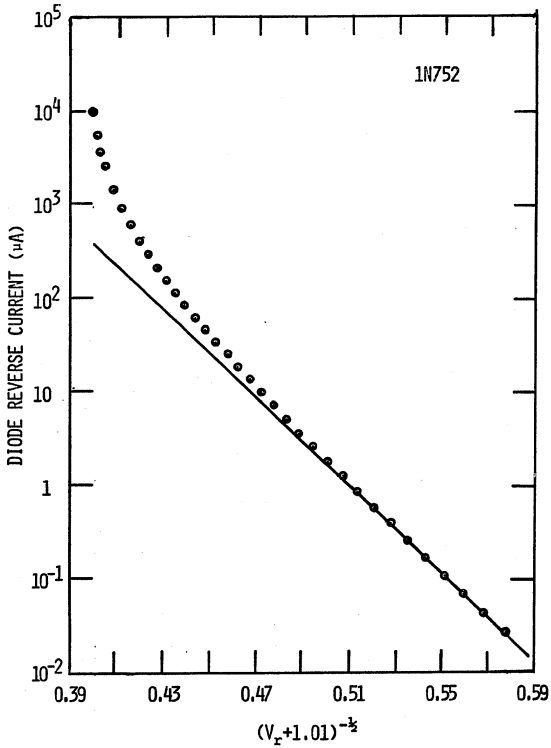

Figure 28. Reverse V-I characteristic: diode 1N752

Reproduced with permission of the copyright owner. Further reproduction prohibited without permission.

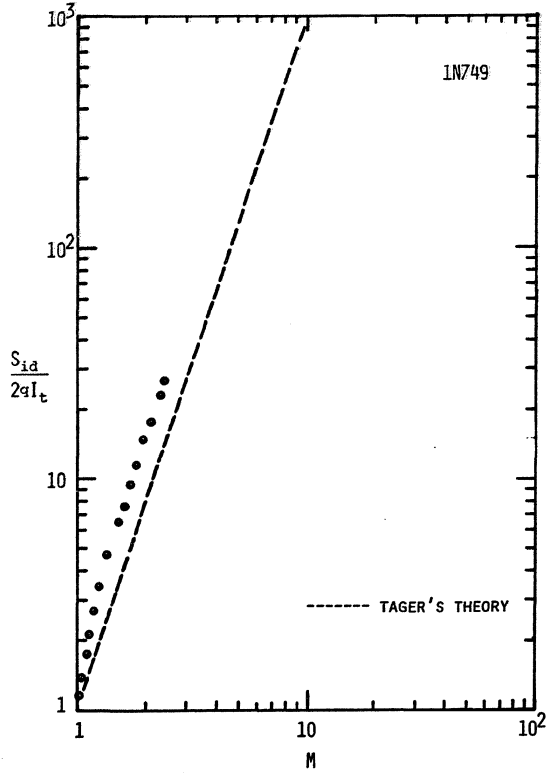

Figure 29. Comparison of Tager's theory with data: diode 1N749

Reproduced with permission of the copyright owner. Further reproduction prohibited without permission.

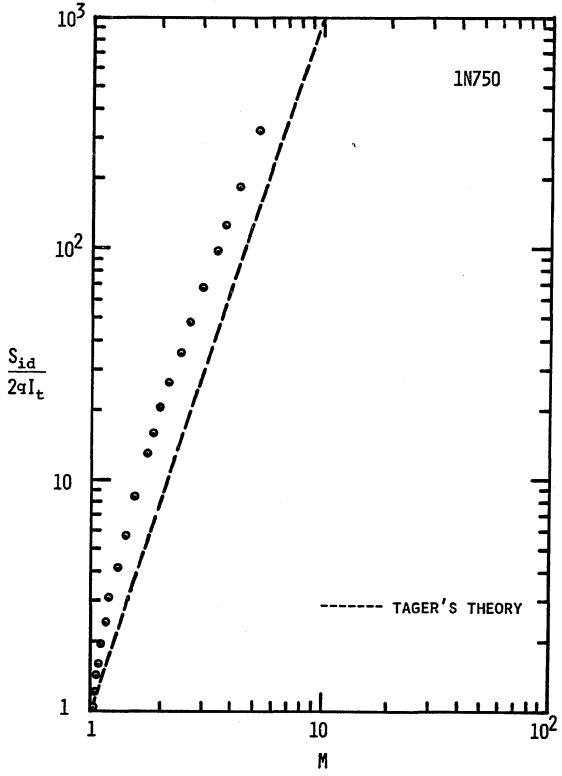

Figure 30. Comparison of Tager's theory with data: diode 1N750

Reproduced with permission of the copyright owner. Further reproduction prohibited without permission.

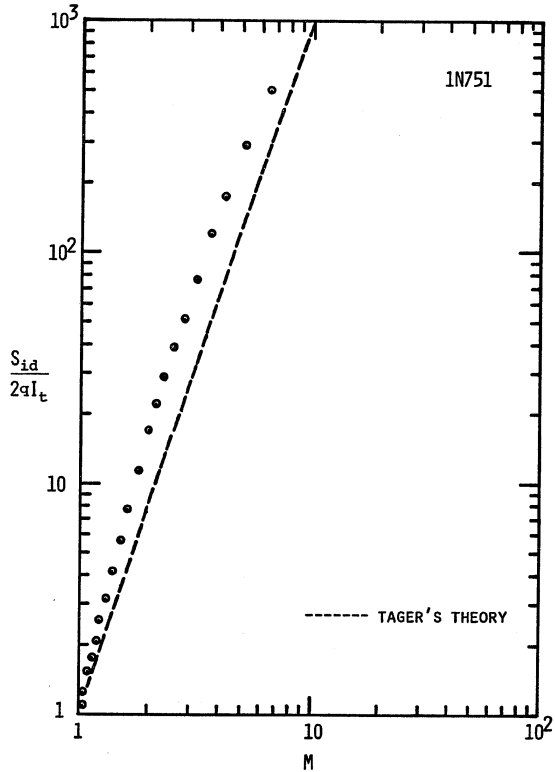

Figure 31. Comparison of Tager's theory with data: diode 1N751

Reproduced with permission of the copyright owner. Further reproduction prohibited without permission.

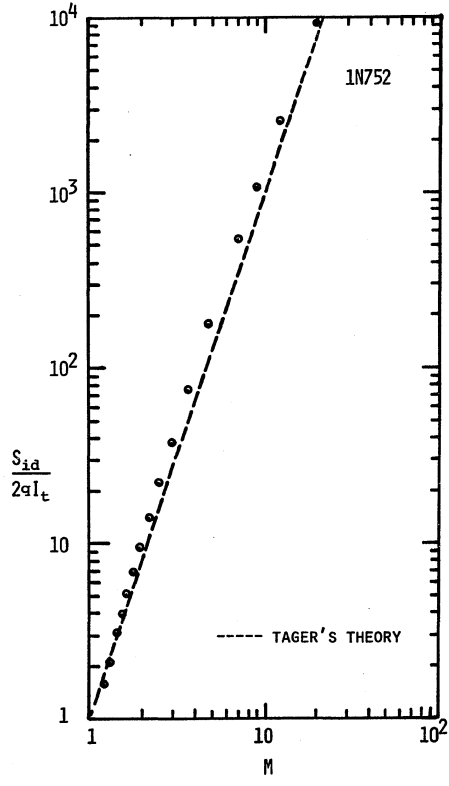

Figure 32. Comparison of Tager's theory with data: diode 1N752

Reproduced with permission of the copyright owner. Further reproduction prohibited without permission.

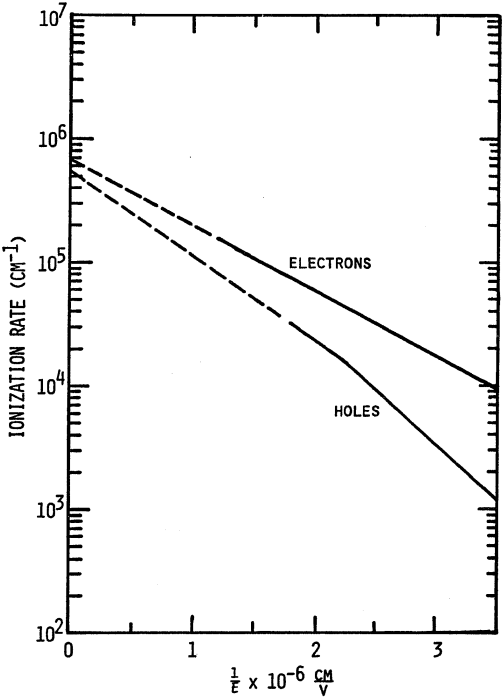

Figure 33. Ionization rates in silicon
[after van Overstraeten and de Man (1970)]

Reproduced with permission of the copyright owner. Further reproduction prohibited without permission.

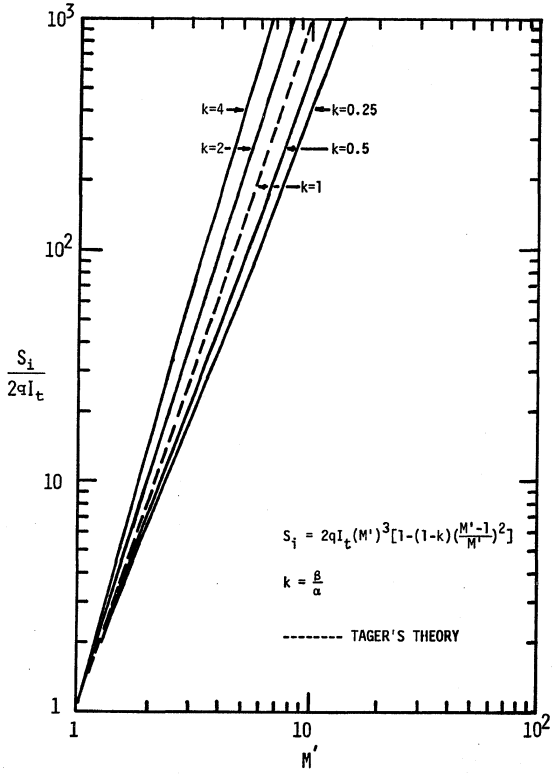

Figure 34. McIntyre's theory

Reproduced with permission of the copyright owner. Further reproduction prohibited without permission.

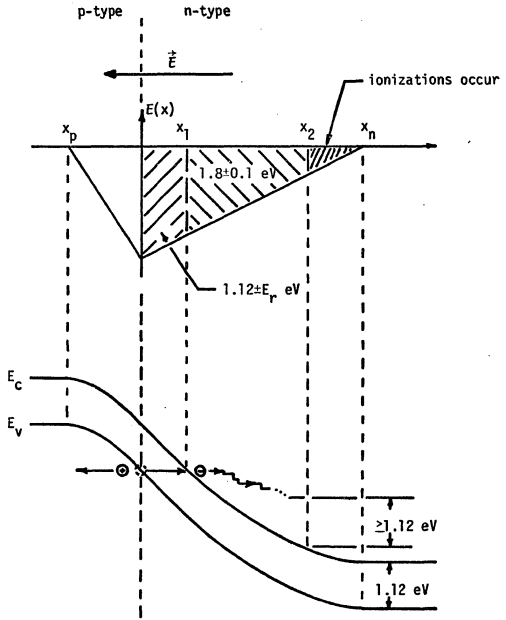

Figure 35. Multiplication threshold model

Reproduced with permission of the copyright owner. Further reproduction prohibited without permission.

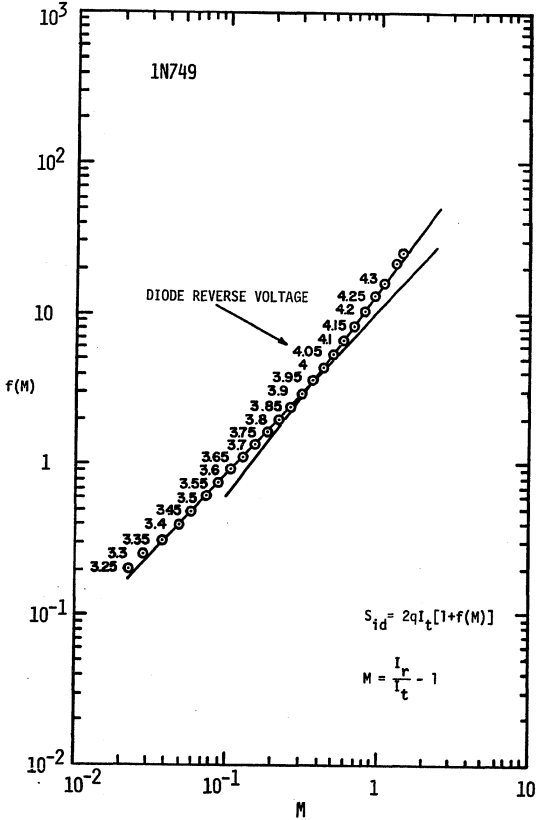

Figure 36. Multiplication noise: diode 1N749

Reproduced with permission of the copyright owner. Further reproduction prohibited without permission.

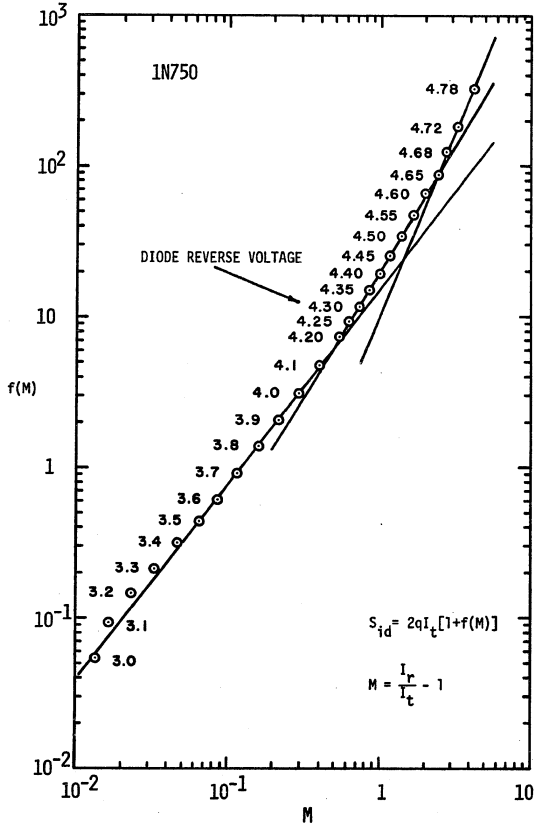

Figure 37. Multiplication noise: diode 1N750

Reproduced with permission of the copyright owner. Further reproduction prohibited without permission.

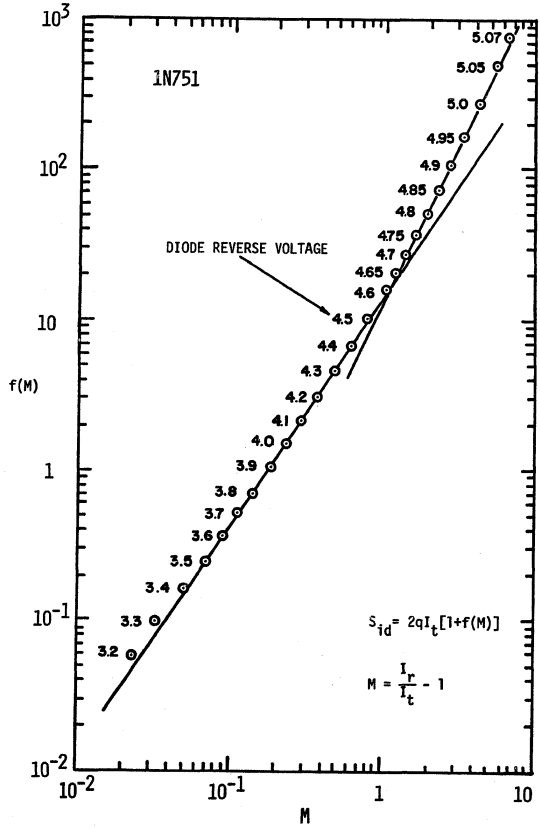

Figure 38. Multiplication noise: diode 1N751

Reproduced with permission of the copyright owner. Further reproduction prohibited without permission.

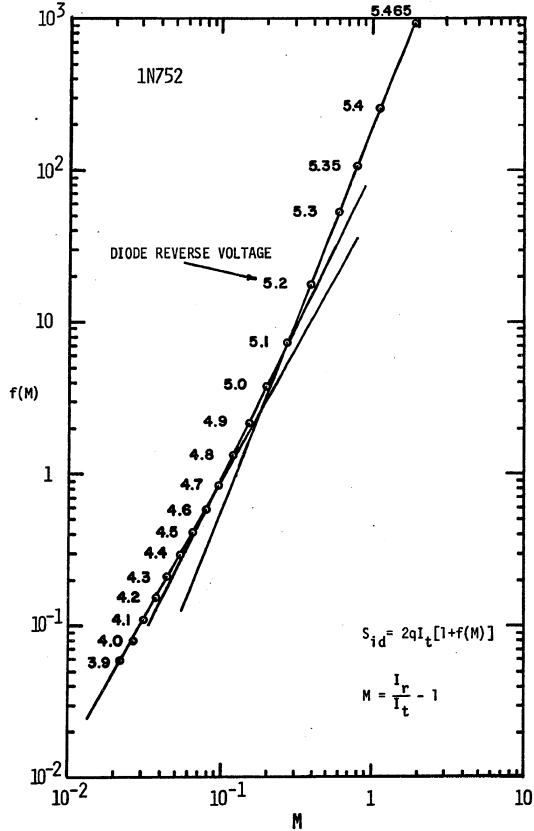

Figure 39. Multiplication noise: diode 1N752

Reproduced with permission of the copyright owner. Further reproduction prohibited without permission.

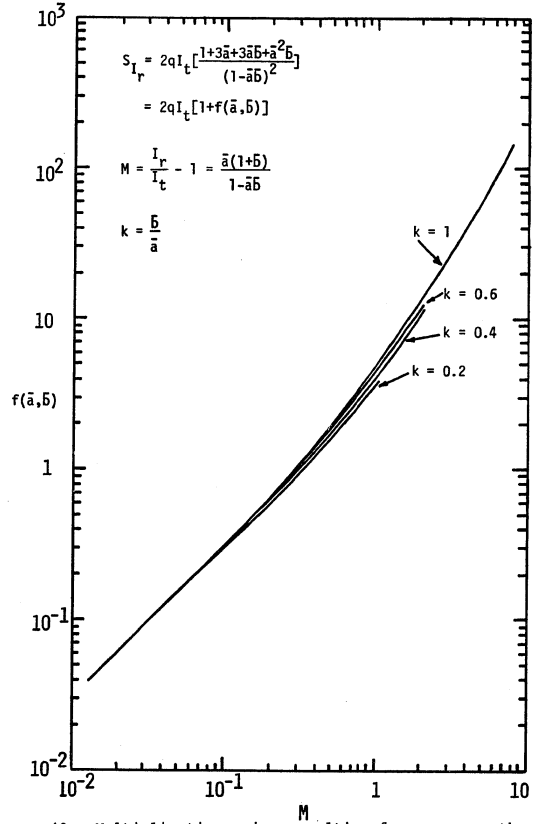

Figure 40. Multiplication noise resulting from no more than one ionization per carrier transit across SCR

Reproduced with permission of the copyright owner. Further reproduction prohibited without permission.

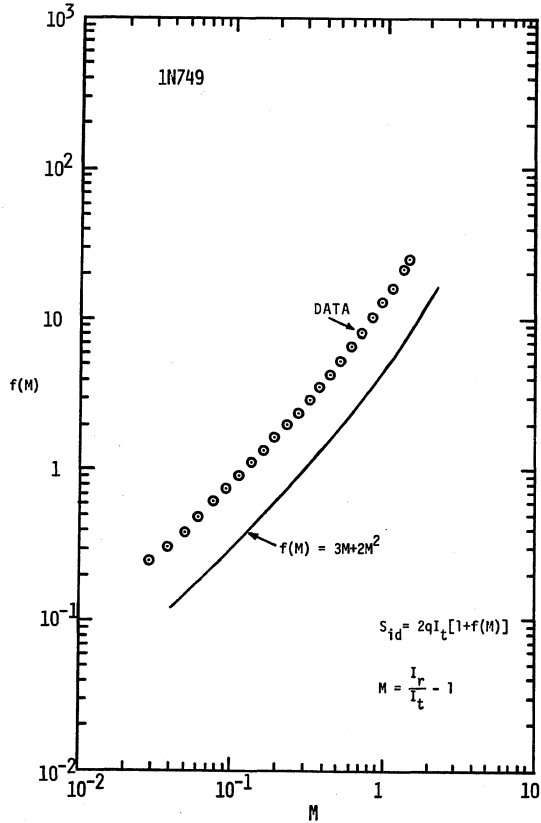

Figure 41. Comparison of one ionization per SCR transit noise theory with data: diode 1N749

Reproduced with permission of the copyright owner. Further reproduction prohibited without permission.

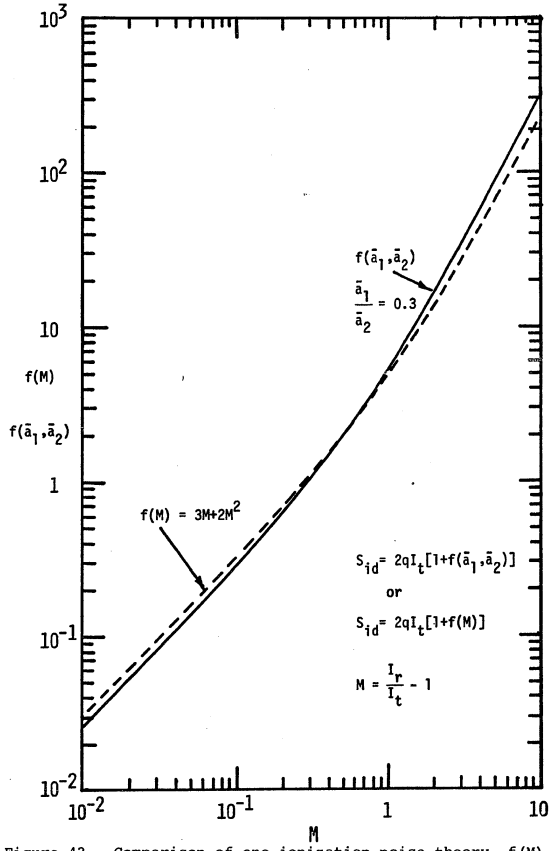

Figure 42. Comparison of one ionization noise theory, f(M), with two ionizations noise theory, $f(\bar{a}_1,\bar{a}_2)$

Reproduced with permission of the copyright owner. Further reproduction prohibited without permission.

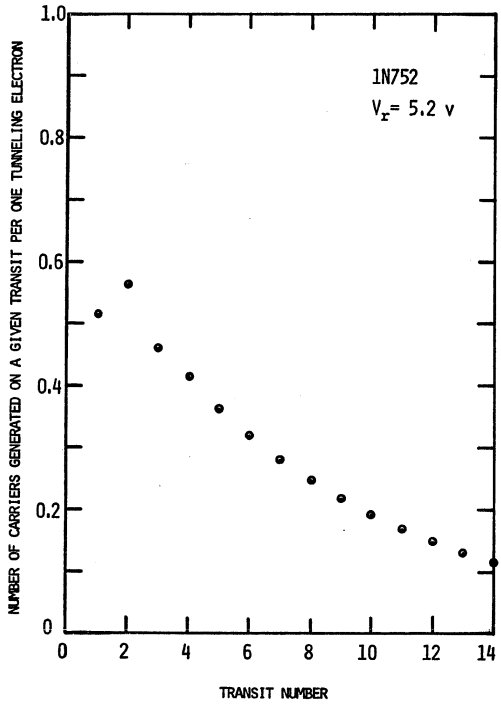

Figure 43. Contribution to multiplication on n-th carrier transit across the diode SCR

Reproduced with permission of the copyright owner. Further reproduction prohibited without permission.

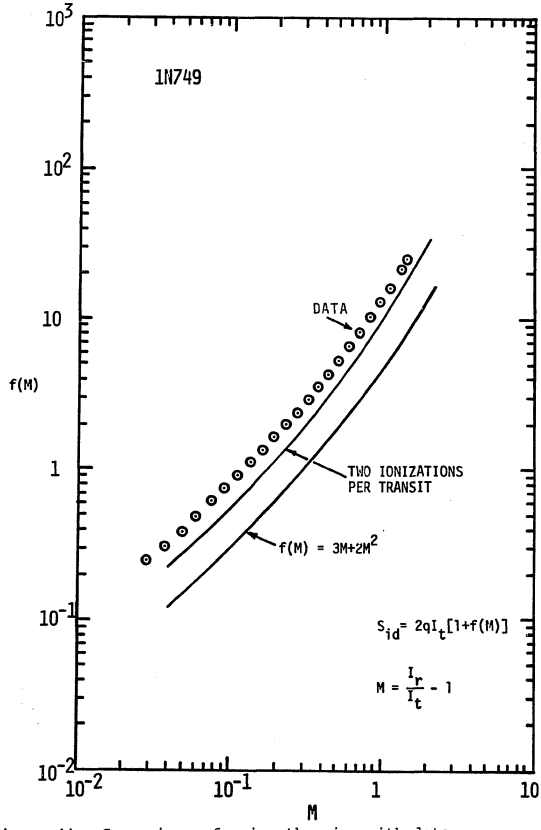

Figure 44. Comparison of noise theories with data: diode 1N749

Reproduced with permission of the copyright owner. Further reproduction prohibited without permission.

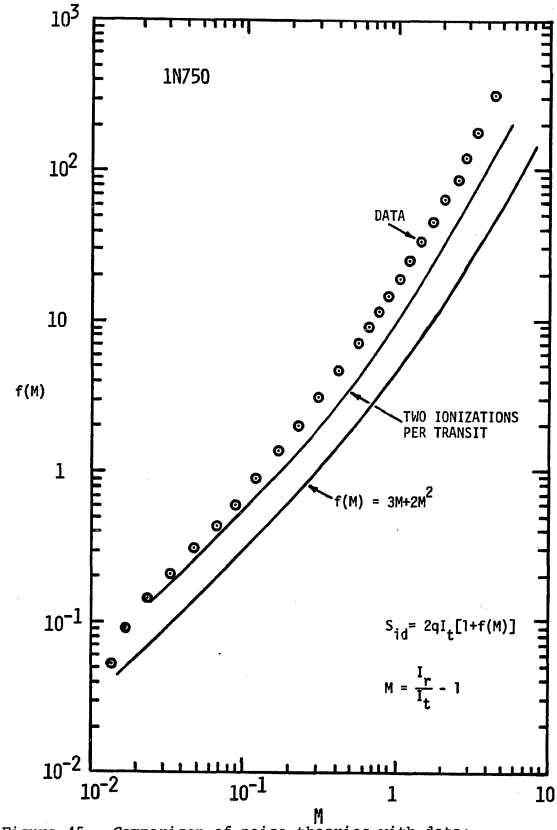

Figure 45. Comparison of noise theories with data: diode 1N750

Reproduced with permission of the copyright owner. Further reproduction prohibited without permission.

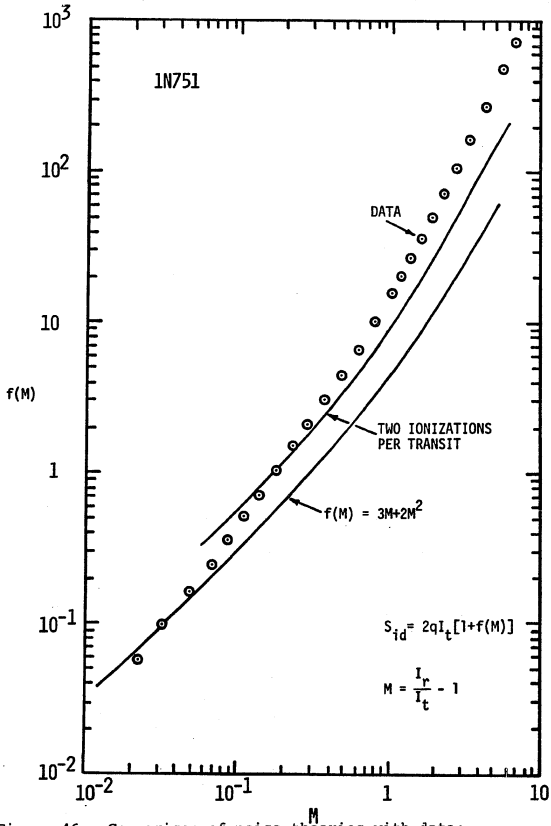

Figure 46. Comparison of noise theories with data: diode 1N751

Reproduced with permission of the copyright owner. Further reproduction prohibited without permission.

Reproduced with permission of the copyright owner. Further reproduction prohibited without permission.

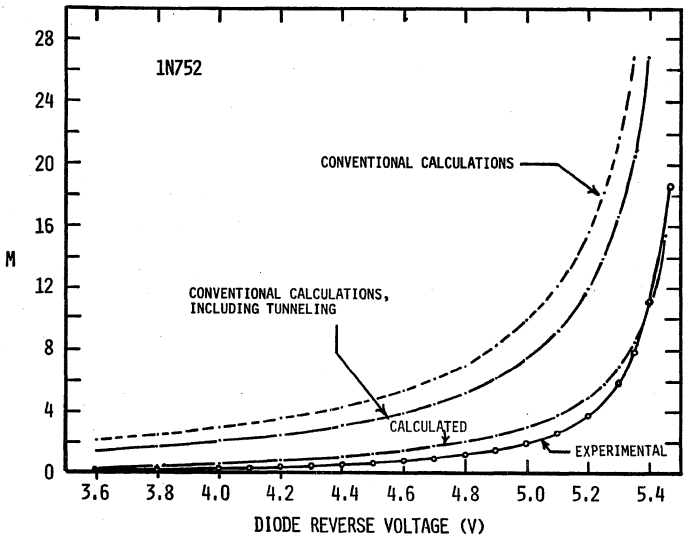

Figure 47. DC multiplication calculations: diode 1N752

Reproduced with permission of the copyright owner. Further reproduction prohibited without permission.

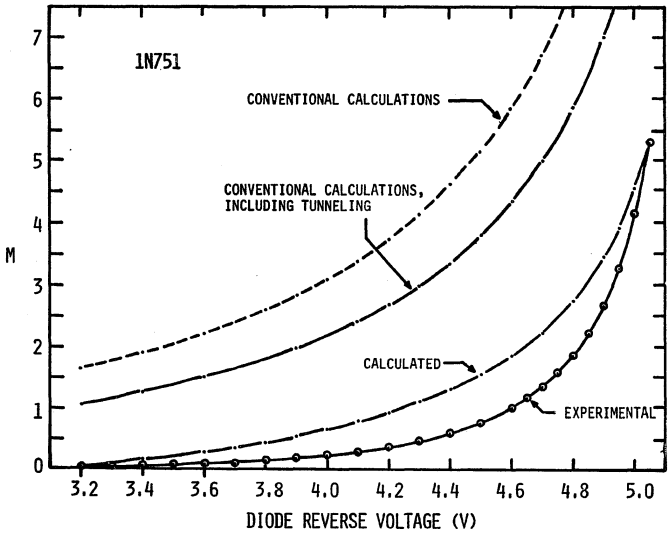

Figure 48. DC multiplication calculations: diode 1N751

Reproduced with permission of the copyright owner. Further reproduction prohibited without permission.

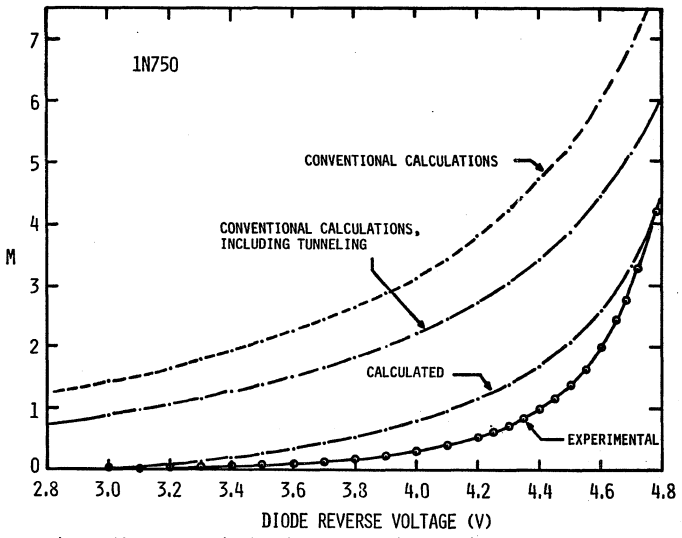

Figure 49. DC multiplication calculations: diode 1N750

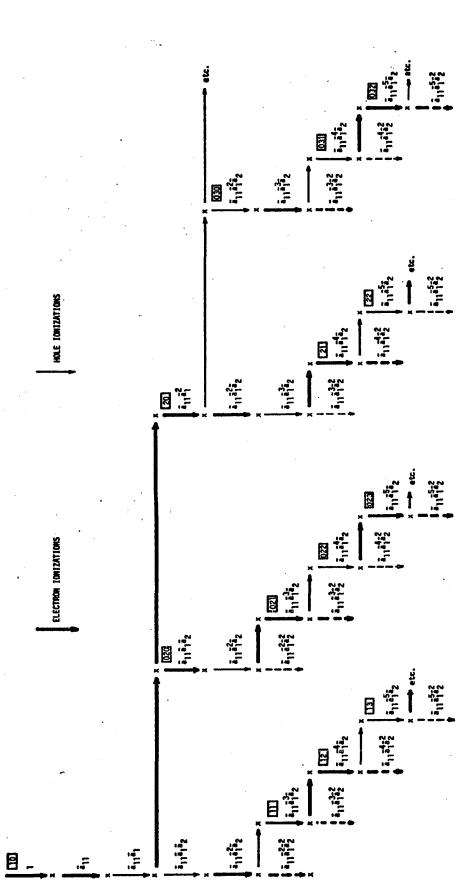

Figure 50. Multiplication process resulting from no more than two ionizations per carrier transit across diode SCR

Reproduced with permission of the copyright owner. Further reproduction prohibited without permission.

BIBLIOGRAPHY

Baertsch, R. D., "Low Frequency Noise Measurements in Silicon Avalanche Photodiodes," IEEE Trans. Electron Devices, Vol. ED-13, pp. 383-385, March 1966.

Baertsch, R. D., "Noise and Ionization Rate Measurements in Silicon Photodiodes," IEEE Trans. Electron Devices, Vol. ED-13, p. 987, December 1966.

Baertsch, R. D., "Noise and Multiplication Measurements in InSb Avalanche Photodiodes," J. Appl. Phys., Vol. 38, pp. 4267-4274, October 1967.

Chynoweth, A. G., Feldmann, W. L., Lee, C. A., Logan, R. A., Pearson, G. L., and Aigrain, P., "Internal Field Emission at Narrow Silicon and Germanium p-n Junctions," Phys. Rev., Vol. 118, No. 2, pp. 425-434, April 15, 1960.

Chynoweth, A. G., Logan, R. A., and Thomas, D. E., "Phonon-Assisted Tunneling in Silicon and Germanium Esaki Junctions," Phys. Rev., Vol. 125, No. 3, pp. 877-881, February 1, 1962.

Gummel, H. K., and Blue, J. L., "Small-Signal Theory of Avalanche Noise in IMPATT Diodes," IEEE Trans. Electron Devices, Vol. ED-14, No. 9, September 1967.

Haitz, R. H., "Controlled Noise Generation with Avalanche Diodes-I. Low Pulse Rate Design," IEEE Trans. Electron Devices, Vol. ED-12, pp. 198-207, April 1965.

Haitz, R. H., "Controlled Noise Generation with Avalanche Diodes-II. High Pulse Rate Design," IEEE Trans. Electron Devices, Vol. ED-13, pp. 342-346, March 1966.

Haitz, R. H., "Mechanisms Contributing to the Noise Pulse Ratio of Avalanche Diodes," J. Appl. Phys., Vol. 36, pp. 3123-3131, October 1965.

Reproduced with permission of the copyright owner. Further reproduction prohibited without permission.

Haitz, R. H. and Voltmer, F. W., "Noise of Self-Sustaining Avalanche Discharge in Silicon: Studies at Microwave Frequencies," J. Appl. Phys., Vol. 39, pp. 3379-3384, June 1968.

Hines, M. E., "Noise Theory for the Read Type Avalanche Diode," IEEE Trans. Electron Devices, Vol. ED-13, No. 1, pp. 158-163, January 1966.

Kumo, H. F., Collard, J. R. and Golat, A. R., "Low-Noise Epitaxial GaAs Avalanche Diode Amplifier," 1968 IEEE International Electron Devices Meeting (Washington, D. C.), p. 104, October 23-25.

Lauritzen, P. O., "Ionization Threshold Observed in Noise from Silicon Zener Diodes," J. Appl. Phys., Vol. 37, No. 1, pp. 463-464, January 1966.

Lee, C. A., Logan, R. A., Batdorf, R. L., Kleimack, J. J., and Wiegmann, W., "Ionization Rates of Holes and Electrons in Silicon," Phys. Rev., Vol. 134, No. 3A, pp. A761-A773, May 4, 1964.

Logan, R. A. and Chynoweth, A. G., "Effect of Degenerate Semiconductor Band Structure on Current-Voltage Characteristics of Silicon Tunnel Diodes," Phys. Rev., Vol. 131, No. 1, pp. 89-95, July 1, 1963.

Logan, R. A., Rowell, J. M., and Trumbore, F. A., "Phonon Spectra of Ge-Si Alloys," Phys. Rev., Vol. 136, No. 6A, pp. A1751-A1755, December 14, 1964.

Logan, R. A., "Phonon-Assisted Semiconductor Tunneling," in Tunneling Phenomena in Solids (ed. by Burstein, E., and Lundqvist, S.) Plenum Press, New York, 1969.

McIntyre, R. J., "Multiplication Noise in Uniform Avalanche Diodes," IEEE Trans. Electron Devices, Vol. ED-13, No. 1, pp. 164-168, January 1966.

McIntyre, R. J., "The Distribution of Gains in Uniformly Multiplying Avalanche Photodiodes: Theory," IEEE Trans. Electron Devices, Vol. ED-19, No. 6, pp. 703-713, June 1973.

Moll, J. L. and van Overstraeten, R., "Charge Multiplication in Silicon p-n Junctions," Solid State Electronics, Vol. 6, pp. 147-157, 1963.

Reproduced with permission of the copyright owner. Further reproduction prohibited without permission.

Shockley, W., "Problems Related to p-n Junctions in Silicon," Solid State Electronics, Vol. 2, No. 1, pp. 35-67, 1961.

Tager, A. S., "Current Fluctuations in a Semiconductor (Dielectric) Under the Condition of Impact Ionization and Avalanche Breakdown," Soviet Physics-Solid State, Vol. 6, No. 8, pp. 1919-1925, February 1965.

Tyagi, M. Singh, "Zener and Avalanche Breakdown in Silicon Alloyed p-n Junctions-I, II," Solid State Electronics, Vol. 11, pp. 99-128, 1968.

van der Ziel, A., Noise: Sources, Characterization, Measurement, Prentice-Hall, Inc., Englewood Cliffs, New Jersey, p. 15, 1970.

van Overstraeten, R., and de Man, H., "Measurement of the Ionization Rates in Diffused Silicon p-n Junctions," Solid State Electronics, Vol. 13, pp. 583-608, 1970.

van Vliet, K. M., "Noise Limitations in Solid State Photodetectors," Applied Optics, Vol. 6, No. 7, pp. 1145-1169, July 1967.

Reproduced with permission of the copyright owner. Further reproduction prohibited without permission.

BIOGRAPHICAL SKETCH

Wieslaw A. Lukaszek was born in Lutcza, Poland, on May 18, 1946, and emigrated to the United States on August 25, 1959. As a recipient of the New Jersey State and Essex Electrical League Scholarships, he attended Newark College of Engineering, graduating with a BSEE in June 1969. A National Science Foundation Graduate Trainee, he has been pursuing studies towards the Ph.D. in electrical engineering at the University of Florida since September, 1969.

During the summers of 1967 to 1970 he worked at the Johns-Manville Research and Engineering Center, the RCA Missile and Surface Radar Division, and the Bell Telephone Laboratories.

His professional interests are primarily in physical electronics. He is a member of Eta Kappa Nu, Tau Beta Pi, Sigma Xi, and IEEE.

Reproduced with permission of the copyright owner. Further reproduction prohibited without permission.

I certify that I have read this study and that in my opinion it conforms to acceptable standards of scholarly presentation and is fully adequate, in scope and quality, as a dissertation for the degree of Doctor of Philosophy.

Aldert van der Ziel, Chairman
Graduate Research Professor of
Electrical Engineering

I certify that I have read this study and that in my opinion it conforms to acceptable standards of scholarly presentation and is fully adequate, in scope and quality, as a dissertation for the degree of Doctor of Philosophy.

Eugene R. Chenette, Co-Chairman
Chairman of Electrical Engineering

I certify that I have read this study and that in my opinion it conforms to acceptable standards of scholarly presentation and is fully adequate, in scope and quality, as a dissertation for the degree of Doctor of Philosophy.

Charles V. Shaffer
Professor of Electrical Engineering

Reproduced with permission of the copyright owner. Further reproduction prohibited without permission.

I certify that I have read this study and that in my opinion it conforms to acceptable standards of scholarly presentation and is fully adequate, in scope and quality, as a dissertation for the degree of Doctor of Philosophy.

Samuel B. Trickey
Associate Professor of Physics

This dissertation was submitted to the Graduate Faculty of the College of Engineering and to the Graduate Council, and was accepted as partial fulfillment of the requirements for the degree of Doctor of Philosophy.

August, 1974

Wayne H. Chen
Dean, College of Engineering

Dean, Graduate School

Reproduced with permission of the copyright owner. Further reproduction prohibited without permission.